

November 2017

## Physical Layer Algorithms for Reliability and Spectral Efficiency in Wireless Communications

Zekeriyya Esat Ankarali  
*University of South Florida*, zekeriyya@mail.usf.edu

Follow this and additional works at: <https://digitalcommons.usf.edu/etd>



Part of the [Electrical and Computer Engineering Commons](#)

---

### Scholar Commons Citation

Ankarali, Zekeriyya Esat, "Physical Layer Algorithms for Reliability and Spectral Efficiency in Wireless Communications" (2017). *USF Tampa Graduate Theses and Dissertations*.  
<https://digitalcommons.usf.edu/etd/6996>

This Dissertation is brought to you for free and open access by the USF Graduate Theses and Dissertations at Digital Commons @ University of South Florida. It has been accepted for inclusion in USF Tampa Graduate Theses and Dissertations by an authorized administrator of Digital Commons @ University of South Florida. For more information, please contact [digitalcommons@usf.edu](mailto:digitalcommons@usf.edu).

Physical Layer Algorithms for Reliability and Spectral Efficiency in Wireless Communications

by

Zekeriyya Esat Ankaralı

A dissertation submitted in partial fulfillment  
of the requirements for the degree of  
Doctor of Philosophy  
Department of Electrical Engineering  
College of Engineering  
University of South Florida

Major Professor: Hüseyin Arslan, Ph.D.  
Richard D. Gitlin, Sc.D.  
Nasir Ghani, Ph.D.  
Yao Liu, Ph.D.  
Mohamed M. Abdallah, Ph.D.

Date of Approval:  
September 28, 2017

Keywords: 5G, Interference Alignment, OFDM, OOB, PAPR, Physical Layer Security, Radio  
Access Technologies, Waveform, WBANs

Copyright © 2017, Zekeriyya Esat Ankaralı

## DEDICATION

To my wife, my family, my country and  
Şehitlerimize.

## ACKNOWLEDGMENTS

First, I extend my thanks to Allah (swt) for everything that He granted me in this life. I would like to thank my advisor Dr. Hüseyin Arslan for his guidance, encouragement, and support throughout my study. I wish to thank Dr. Richard D. Gitlin, Dr. Nasir Ghani, Dr. Mohamed Abdallah, Dr. Yao Liu and Dr. Dimitry Goldgof for serving on my committee. I also thank all the USF College of Engineering staff for their sincere assistance whenever I need.

It has been a great privilege to be a member of the Wireless Communications and Signal Processing (WCSP) group. This group did not only provide a perfect research environment with very valuable collaborations but had me witness a real model of friendship. I would like to thank my friends Dr. Ali Görçin, Dr. Sadia Ahmed, Dr. M. Bahadır Çelebi, Dr. Anas Tom, Murat Karabacak, Dr. M. Harun Yılmaz, Dr. Ertugrul Güvenkaya, Ali Fatih Demir, Mohammad Hafez, Berker Pekoz, Furkan Kucuk, Mohammed Elkourdi, Dr. Orhun Aras Uzun, Ismail Uluturk and Dr. Emre Seyyal for their support as friends and productive discussions as colleagues. I also thank InterDigital, Inc. team; Dr. Rui Yang, Dr. Erdem Bala, and special thanks to Dr. Alphan Şahin for long hours of fruitful discussions and collaboration during this period. His dedication to research has always inspired me.

I wish to thank the members of my family in law, Nizamettin Tekin and Fatma Tekin, my sisters in law Büşra and Melike, and my brother in law Tahsin Esad for all the moral support and prayers throughout this process.

I have always been grateful to my parents Fatma Ankaralı, Dr. Arif Ankaralı, my dear brothers Sadullah, Hüsnü Abdulaziz and my lovely sister Erva for their unconditional support throughout all these challenging years. I learned how the parenthood should be and how precious the brotherhood is within this great family, and I have always felt lucky to be a member of them.

Last, but by no means least, my deepest gratitude goes to my wife for her immense sacrifice, support and great patience. She was the one who left many things behind her just to be with me on this path. I could never thank her enough, but I want her to know that I am always grateful to

the God for having such a great soul mate. I couldn't carry this out without her and my lovely son,  
Feyzullah Zahid.

## TABLE OF CONTENTS

LIST OF TABLES	iii
LIST OF FIGURES	iv
ABSTRACT	vii
CHAPTER 1: INTRODUCTION	1
1.1 Introduction	1
1.2 An Overview on Various Waveform Schemes Alternative to OFDM	2
1.2.1 FBMC	3
1.2.2 UFMC	3
1.2.3 GFDM	4
1.3 Improvements in Waveform Characteristics of OFDM	4
1.3.1 OOB Leakage Suppression	5
1.3.2 PAPR Mitigation	8
1.4 Numerology	10
1.5 Security	12
1.6 Dissertation Outline	13
CHAPTER 2: JOINT TIME/FREQUENCY ALIGNMENT FOR SUPPRESSING OOBE AND PAPR OF OFDM-BASED WAVEFORMS	15
2.1 Introduction	15
2.2 System Model	16
2.3 Joint Time-Frequency Alignment for Joint OOBE and PAPR Suppression	18
2.4 Numerical Results	20
2.5 Conclusion	22
2.6 Acknowledgment	23
CHAPTER 3: STATIC CP ALIGNMENT	26
3.1 Introduction	26
3.2 System Model	29
3.3 Static CP Alignment	32
3.4 Practical Issues	34
3.4.1 Design of Alignment Filter	34
3.4.2 Complexity	36
3.5 Numerical Results	37
3.6 Conclusion	40

CHAPTER 4: FLEXIBLE RADIO ACCESS BEYOND 5G: A FUTURE PROJECTION ON WAVEFORM, NUMEROLOGY AND FRAME DESIGN PRINCIPLES	43
4.1 Introduction	43
4.2 A Historical Overview on Flexible Signaling and Radio Access Schemes	47
4.3 Flexibility in Waveform Design	48
4.3.1 OFDM	50
4.3.2 FBMC	52
4.4 Flexibility in Numerology Design	54
4.5 Flexibility in Frame Design	60
4.5.1 Single Waveform Numerology-based Frame Design	61
4.5.2 Hybrid Waveform Numerology-based Frame Design	65
4.6 Conclusion	67
4.7 Acknowledgement	67
 CHAPTER 5: CYCLIC FEATURE SUPPRESSION FOR PHYSICAL LAYER SECURITY	 68
5.1 Blind Parameter Estimation, Synchronization and Equalization with CP	71
5.2 Cyclic Feature Concealing CP Selection	72
5.2.1 OFDM	76
5.2.2 SC-FDE	77
5.3 Cyclic Feature Suppressing Symbol Time Randomization	77
5.3.1 PAPR Mitigation for OFDM	79
5.3.2 Sidelobe Suppression for OFDM	79
5.4 Numerical Results	80
5.5 Conclusion	84
5.6 Acknowledgment	87
 CHAPTER 6: PHYSICAL LAYER SECURITY FOR WIRELESS IMPLANTABLE MEDICAL DEVICES	 89
6.1 Introduction	89
6.2 System Model	92
6.3 Channel Models for WED and Adversary	94
6.4 Numerical Results	95
6.5 Conclusions	98
 CHAPTER 7: CONCLUSION AND OPEN ISSUES	 99
 REFERENCES	 100
 APPENDICES	 108
Appendix A: Copyright Permissions	109
Appendix B: List of Acronyms	117
 ABOUT THE AUTHOR	 End Page

## LIST OF TABLES

Table 6.1	Path loss model parameters [1].	94
-----------	---------------------------------	----



## LIST OF FIGURES

Figure 1.1	Block diagrams of popular multicarrier schemes (OFDM, FBMC, UFMC and GFDM) considered for 5G radio access.	6
Figure 1.2	Frequency responses of an OFDM subcarrier (sinc) and various filters.	7
Figure 1.3	PAPR comparison between single carrier signals with different modulation orders and OFDM with different number of subcarriers ( $N$ ).	9
Figure 1.4	Illustration of different numerologies.	10
Figure 2.1	Block diagram for the proposed system (AS aligns with the CP duration, the guard tones and the faded subcarriers at the receiver side).	19
Figure 2.2	Power distribution of plain OFDM and AS samples for CPA and JTFA in time for different channel decaying factors ( $\alpha = 0.25, \phi_{tr} = 0.2$ ).	22
Figure 2.3	PAPR performance for CPA, JTFA, and CCI for different $\lambda$ values ( $\alpha = 0.25, \tau = 0.2, \phi_{tr} = 0.2$ ).	23
Figure 2.4	OOBE performance for CPA, JTFA, and CCI for different $\lambda$ values ( $\alpha = 0.25, \tau = 0.2, \phi_{tr} = 0.2$ ).	24
Figure 2.5	BER performance for CPA, JTFA, and CCI for different MSEs ( $\sigma_e^2$ ) in channel estimation ( $\alpha = 0.25, \tau = 0.2, \phi_{tr} = 0.2$ ).	25
Figure 3.1	Block diagram for the proposed system.	28
Figure 3.2	Illustration for the covariance matrix of an alignment signal designed based on a uniform alignment filter.	35
Figure 3.3	Illustration for the covariance matrix of an alignment signal designed based on an exponentially decaying alignment filter.	36
Figure 3.4	BER curves for the plain OFDM, proposed static CP alignment (for intended users & eavesdroppers), original CP alignment [2] for different MSE values in channel estimation (Modulation type is 16-QAM).	38
Figure 3.5	OOB emission suppression performance of proposed method for different $\lambda$ values ( $\alpha = 0.25, K = N/4$ ).	40

Figure 3.6	PAPR performance for different $\lambda$ values ( $\alpha = 0.25, K = N/4$ ).	41
Figure 3.7	OOB leakage suppression and PAPR mitigation performance for uniform and exponentially decaying filters with different alignment filter lengths ( $\alpha = 0.25$ ).	42
Figure 4.1	Future wireless communication challenges aimed to be addressed by flexible RATs components.	46
Figure 4.2	The various parameters of OFDM and FBMC waveforms and the physical metrics they primarily affect (Further indirect relations could be considered, however, only the primary relations are embodied for the sake of clarity).	49
Figure 4.3	OFDM transceiver block diagram including windowing and filtering.	52
Figure 4.4	FBMC transceiver block diagram.	55
Figure 4.5	Ambiguity functions ( $10\log_{10}( \mathfrak{F}(\tau, \nu) ^2)$ ) generic root-raised cosine filters generated with various design parameters, used for adapting signal characteristics in time and frequency domains.	56
Figure 4.6	Two samples of flexible numerology design: Edge-windowed OFDM and edge-filtered FBMC numerologies.	59
Figure 4.7	Power leakage of OFDM subcarriers (sidelobes) windowing techniques and conventional approaches.	60
Figure 4.8	Power leakage of FBMC filters (tails) for edge filtering techniques and conventional approaches.	61
Figure 4.9	Examples of proposed single waveform numerology based frame design (Frame-1) and multiple waveform numerology based frame design (Frame-2) consisting of mixed OFDM and FBMC numerologies (Frame-1 can be considered as an improvement over currently discussed frame designs for achieving more flexibility while Frame-2 extends that flexibility to the usage of multiple waveforms based on the user needs, enabling the system to select the best waveform for each user).	62
Figure 4.10	AF of two OFDM subcarriers ( $\Delta F_1 = F/2, \Delta F_2 = F$ )	63
Figure 4.11	AF of an OFDM subcarrier ( $\Delta F = F/2$ ) and an FBMC subcarrier (RRC, $\alpha = 0$ )	64
Figure 4.12	AF of an OFDM subcarrier ( $\Delta F = F/2$ ) and an FBMC subcarrier (RRC, $\alpha = 1$ )	65
Figure 5.1	Calculation of synchronization metric by exploiting cyclic prefix.	70

Figure 5.2	Cyclic autocorrelation function (CAF) of a conventional CP-OFDM signal (same as conventional SC-FDE).	74
Figure 5.3	Illustration of cyclic feature concealing CP selection.	75
Figure 5.4	Illustration of the equalization part for an OFDM symbol designed with the proposed method.	75
Figure 5.5	Illustration of cyclic feature suppressing symbol time randomization and resulting randomized correlation peaks.	77
Figure 5.6	CAF for the CP selection and symbol time randomization methods.	81
Figure 5.7	BER performance of OFDM with regular CP (Reg-CP) and proposed CP (Sel-CP) selection for different number of channel taps ( $M = 64$ ).	82
Figure 5.8	BER performance of SC-FDE with regular CP (Reg-CP) and proposed CP (Sel-CP) selection for different number of channel taps ( $M = 64$ ).	83
Figure 5.9	BER performance of OFDM with regular symbol generation (Reg-Sym) and time-randomized symbol (Rand-Sym) for different number of channel taps ( $M = 64$ ).	85
Figure 5.10	BER performance of SC-FDE with regular symbol generation (Reg-Sym) and time-randomized symbol (Rand-Sym) for different number of channel taps ( $M = 64$ ).	86
Figure 5.11	CCDF of mitigated PAPR values obtained with symbol time randomization for different search ranges, varying the number of sub-carriers around 128.	87
Figure 5.12	Spectrum of sidelobe-suppressed OFDM signals with symbol time randomization for different search ranges, varying the number of sub-carriers around 128.	88
Figure 6.1	Wireless adversaries may perform various malicious attacks and compromise the safety of IMD using patients.	92
Figure 6.2	BER performance versus distance for different noise floors (NFs).	96
Figure 6.3	Adversary outage probabilities for different jammer signal powers.	97
Figure 6.4	Outage probabilities of WED's command with and without proposed technique represented by $P_{\text{outage1}}$ and $P_{\text{outage2}}$ , respectively.	98

## ABSTRACT

Support of many different services, approximately 1000x increase of current data rates, ultra-reliability, low latency and energy/cost efficiency are among the demands from upcoming 5G standard. In order to meet them, researchers investigate various potential technologies involving different network layers and discuss their trade-offs for possible 5G scenarios. Waveform design is a critical part of these efforts and various alternatives have been heavily discussed over the last few years. Besides that, wireless technology is expected to be deployed in many critical applications including the ones involving with daily life activities, health-care and vehicular traffic. Therefore, security of wireless systems is also crucial for a reliable and confidential deployment. In order to achieve these goals in future wireless systems, physical layer (PHY) algorithms play a vital role not only in waveform design but also for improving security.

In this dissertation, we draft the ongoing activities in PHY in terms of waveform design and security for providing spectrally efficient and reliable services considering various scenarios, and present our algorithms in this direction. Regarding the waveform design, orthogonal frequency division multiplexing (OFDM) is mostly considered as the base scheme since it is the dominant technology in many existing standards and is also considered for 5G new radio. We specifically propose two approaches for the improvement of OFDM in terms of out-of-band emission and peak to average power ratio. We also present how the requirements of different 5G RAN scenarios reflect on waveform parameters and explore the motivations behind designing advanced frames that include multiple waveforms with different parameters, referred to as numerologies by the 3GPP community, as well as the problems that arise with such coexistence. On the security aspect, we firstly consider broadband communication scenarios and propose practical security approaches that suppress the cyclic features of OFDM and single carrier-frequency domain equalization based waveforms and remove their vulnerability to the eavesdropping attacks. Additionally, an authentication mechanism

in PHY is presented for wireless implantable medical devices. Thus, we address the security issues for two critical wireless communication scenarios in PHY to contribute a confidential and reliable deployment of wireless technologies in the near future.

## CHAPTER 1

### INTRODUCTION<sup>1</sup>

#### 1.1 Introduction

Exponential growth in the variety and the number of data-hungry applications along with mobile devices leads to an explosion in the need for higher data rates, and this is definitely the main driving factor in 5G [5]. Therefore, a wide range of data rates up to gigabits per second are targeted in 5G technologies which are expected to be deployed around 2020. In order to achieve these goals, academia has been in a great collaboration with industry as obviously seen in European Union projects as 5GNOW [6], METIS [7], MiWaveS [8] and FANTASTIC-5G [9]. Along with those, standardization has been started in Third Generation Partnership Project (3GPP) to deliver the demanded services, timely.

One of the most challenging part of achieving targeted high data rates is physical scarcity of the spectrum and researchers have been putting an extensive effort to overcome that. One popular approach is to extend existing spectrum towards virgin higher frequencies up to 100 GHz [10]. Another approach is to increase spectral efficiency for a given spectral resource. millimeter wave (mmWave) communications and massive multiple-input-multiple-output (MIMO) are the representative concepts of these two approaches and very promising technologies for facilitating 5G goals, especially for enhanced-mobile broadband (eMBB) services which constitutes one of the main service groups considered for 5G radio-access network (RAN). In addition to improving broadband systems, massive machine type of communication and ultra-reliable and low latency services are in the main agenda of 5G and beyond. Deployment of wireless technology is expected to be

---

<sup>1</sup>This chapter was partially published in ZTE Communications Magazine [3] and in IEEE WAMICON 2016 [4]. Permission is included in Appendix A.

much more pervasive in our daily life with these services and therefore securing them against various attacks is a critical task for ensuring the confidentiality and reliability of these systems.

Even though not considered as the revolutionary part of 5G, one of the most fundamental components of any communication system in PHY is the waveform design. Therefore, intensive discussions have been done in academia and industry in order to select the proper waveform and physical layer algorithms enhancing the waveform characteristics. In this chapter, we draft various waveform techniques and selected PHY algorithms along with introducing a new paradigm to waveform parameterization, i.e., numerology. Then the security aspect of wireless technologies in PHY is summarized and dissertation outline is provided in the final section.

## **1.2 An Overview on Various Waveform Schemes Alternative to OFDM**

Among all the candidates, multicarrier techniques are prominent especially for broadband wireless communications due to several advantages such as immunity against frequency selectivity, multiuser diversity support and adaptive modulation/coding techniques. Orthogonal frequency division multiplexing (OFDM) has been the dominating technology so far and successfully deployed in many of the current standards such as Long Term Evolution (LTE) and WiFi. In the transition from existing technologies (4G) to the next generation, waveform selection ramifies to two paths for 5G RAN. The first one is re-considering OFDM based methods by improving its characteristics and handling its drawbacks with proper solutions. The second one, on the other hand, is to implement alternative multicarrier technologies and redesign everything based on a different rationale. Transceiver block diagrams for OFDM and other popular multicarrier schemes, filtered multi-tone mode of filter bank multicarrier (FBMC), universal filtered multicarrier (UFMC) and generalized frequency division multiplexing (GFDM) are given in Fig. 1.1. Let us firstly provide the merits and challenges of the multicarrier technologies considered as an alternative to OFDM in the context of 5G expectations.

### 1.2.1 FBMC

FBMC is one of the most well-known multi-carrier modulation format in wireless communications literature which is also discussed as a 5G waveform in [11]. It offers a great advantage of shaping each subcarrier and facilitate a flexible utilization of spectral resources along with meeting various system requirements, e.g., low latency, multiple access etc. This is also an advantage for making signal robust against channel effects, i.e., dispersion in time and frequency domains. For example, rectangular filters are preferable for time dispersive channels while raised cosine filter are more robust against frequency dispersion. Many other pulse shaping filters are also investigated in the literature to cope with various effects of the channel and provide a reliable system design based on different scenarios [12].

Despite all the advantages FBMC has, the significantly long filter lengths resulting in colossal symbol durations not only become a problem if low latency applications or short bursts of machine type communications are in focus [13], but also introduce a excessive computational complexity for MIMO detection as the channel coherence bandwidth would fall below

### 1.2.2 UFMC

UFMC is a generalized version of filtered multicarrier techniques where groups of subcarriers, i.e., sub-bands, are filtered rather than filtering each subcarrier individually [14]. By doing so, interference between neighboring sub-bands is decreased compared to conventional OFDM. Also, sub-band based filtering operation, when compared to the subcarrier filtering operation performed by FBMC, aims to increase the efficiency for short-burst type communications such as IoT scenarios or very low latency packets by reducing the filtered symbol duration and outperforms both cyclic prefix (CP)-OFDM and FBMC for such use cases [13]. A similar scheme is also presented as resource block (RB)-filtered OFDM in [15]. On the other hand, while UFMC aims to solve the problems of FBMC while maintaining its advantages, the increased fast Fourier transformation (FFT) length introduces complexity issues at the transmitter and receiver operations.



### 1.2.3 GFDM

GFDM is a block-based multicarrier filtered modulation scheme, designed to address the challenges in the vast usage scenarios of the fifth generation by providing a flexible waveform [13]. GFDM allows reuse of techniques that were originally developed for OFDM, as circular convolution is employed to filter the individual subcarriers, making the GFDM frame self-contained in a block structure. For tactile internet scenarios, GFDM can be distinguished from other multicarrier waveforms by how it achieves robustness over highly mobile channels. It is done via taking the advantage of the transmit diversity provided by the easy generation of impulse responses simply obtained with circularly shifting the single prototype filter in time and frequency. To improve the reliability and latency characteristics even further, the GFDM waveform can be combined with the Walsh-Hadamard transform for increased performance in single-shot transmission scenarios. When combined with offset quadrature amplitude modulation mapping, GFDM avoids self-generated interference if non-orthogonal filters are employed for next generation multiple accessing.

In a different point of view GFDM can be considered as a parameterization of waveform characteristics that are flexible across frames rather than a single waveform. It was shown in [13] that by adjusting the parameters accordingly, OFDM, single carrier (SC)-frequency domain equalization (FDE), FBMC and even Faster Than Nyquist schemes can be obtained. Although, these type of interesting flexibilities, being unable to use FFT/inverse fast Fourier transformation (IFFT) at the transmitter makes GFDM a computationally exhaustive scheme [16]. Furthermore, the circular convolution used in the filtering process, referred to as tail-biting in [17], introduces nonorthogonality across subcarriers as explained in [12]. Therefore, it requires a successive interference cancellation at the receiver side to remove inter-carrier interference (ICI) [18].

## 1.3 Improvements in Waveform Characteristics of OFDM

Unlike the aforementioned technologies, OFDM has been widely and successfully deployed in wireless communication standards such as LTE and Wi-Fi due to its numerous advantages, e.g. low-complexity implementation with FFT and the robustness against multipath channels with single-tap FDE. However, plain OFDM signals suffer from the distortions due to the non-linear characteristics

of power amplifier (PA). At the same time, the block nature of OFDM symbols may result in a high out-of-band (OOB) leakage and cause severe adjacent channel interference. Considering these issues, alternative schemes, GFDM, UFMC and FBMC definitely offer some advantages over OFDM. However, backward compatibility of OFDM with the existing technologies along with the other advantages makes enhancement of OFDM more appealing for the industry rather than going for a new waveform, as far as seen in the current standard discussions [19–21].

In a general sense, the key terms characterizing a basic OFDM waveform are multicarrier modulation and rectangular pulse shape<sup>2</sup>, and the majority of the advantages and disadvantages of OFDM are stemming from these features. In this section, we discuss how to improve characteristics of OFDM over well known approaches in the literature in order to make it a more convenient waveform for 5G RAN in terms of peak-to-average power ratio (PAPR) and OOB leakage.

### 1.3.1 OOB Leakage Suppression

High OOB leakage is a major issue in OFDM due to the inherent rectangular shape of OFDM symbols. In the frequency domain, subcarriers are shaped by sinc functions and addition of their sidelobes results in a considerable energy leakage on the neighboring channels as shown in Fig. 5.12. Although there are well-known filters emitting less energy on side bands, e.g., raised cosine and Gaussian filters, OFDM does not allow pulse shaping unlike FBMC and GFDM, and therefore, a severe interference might be inevitable for users operating on the neighboring frequencies, especially for asynchronous scenarios. Leaving sufficient guard bands between the users might be considered as a practical solution, but this would not be an efficient way of utilizing spectral resources. In 5G scenarios, as far as envisioned so far, a huge number of asynchronous and data-hungry users should co-exist within a limited spectrum. Therefore, OFDM signals should be more localized in the frequency domain by handling OOB leakage problem in a practical way to adapt OFDM to such scenarios.

For the aforementioned purpose, OOB leakage of OFDM signals have been extensively addressed with numerous techniques in the literature as reviewed and compared in [22]. For instance,

---

<sup>2</sup>CP deployment can also be considered among these terms, however, that will be discussed in later sections

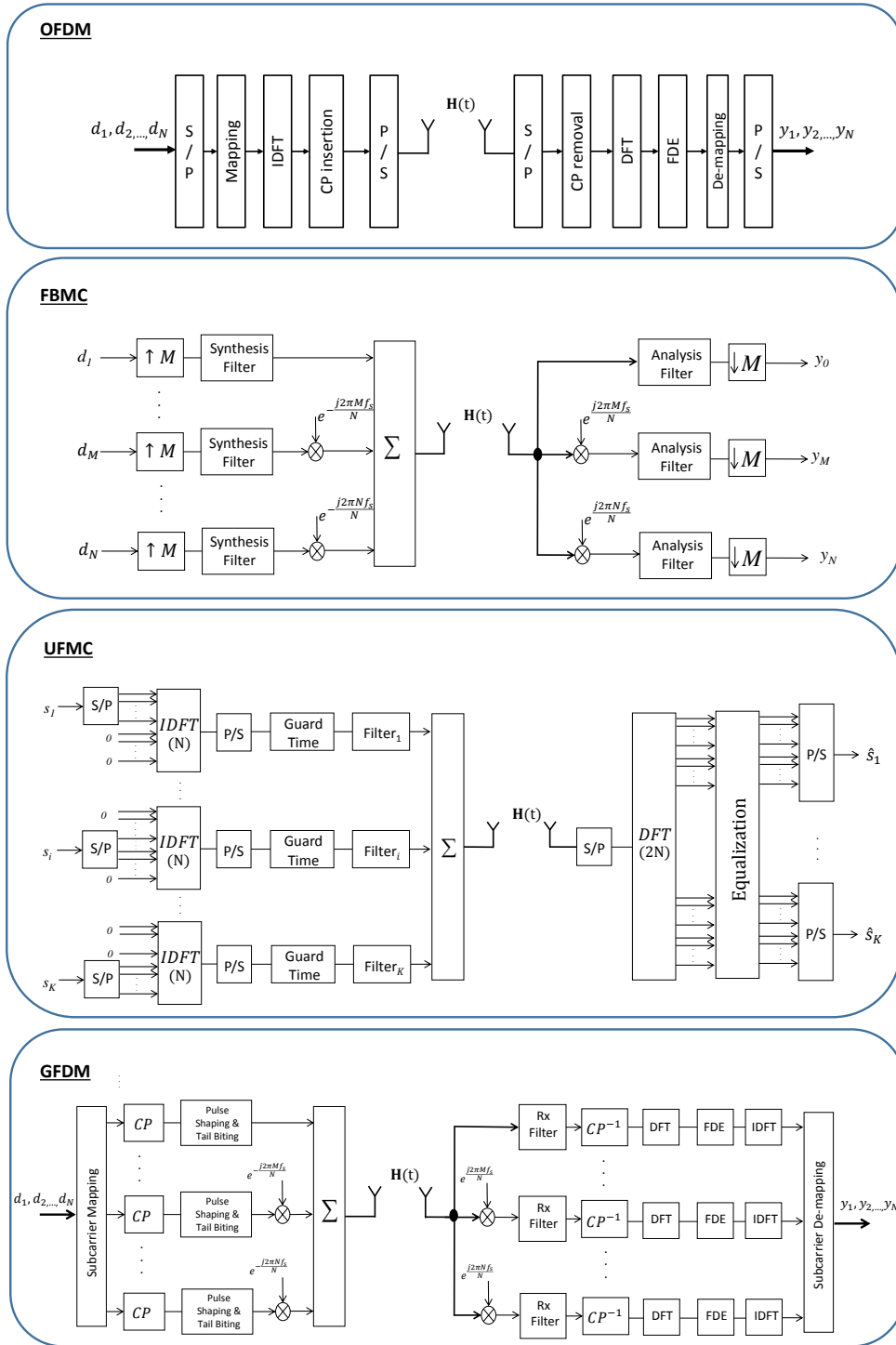


Figure 1.1 Block diagrams of popular multicarrier schemes (OFDM, FBMC, UFMC and GFDM) considered for 5G radio access.

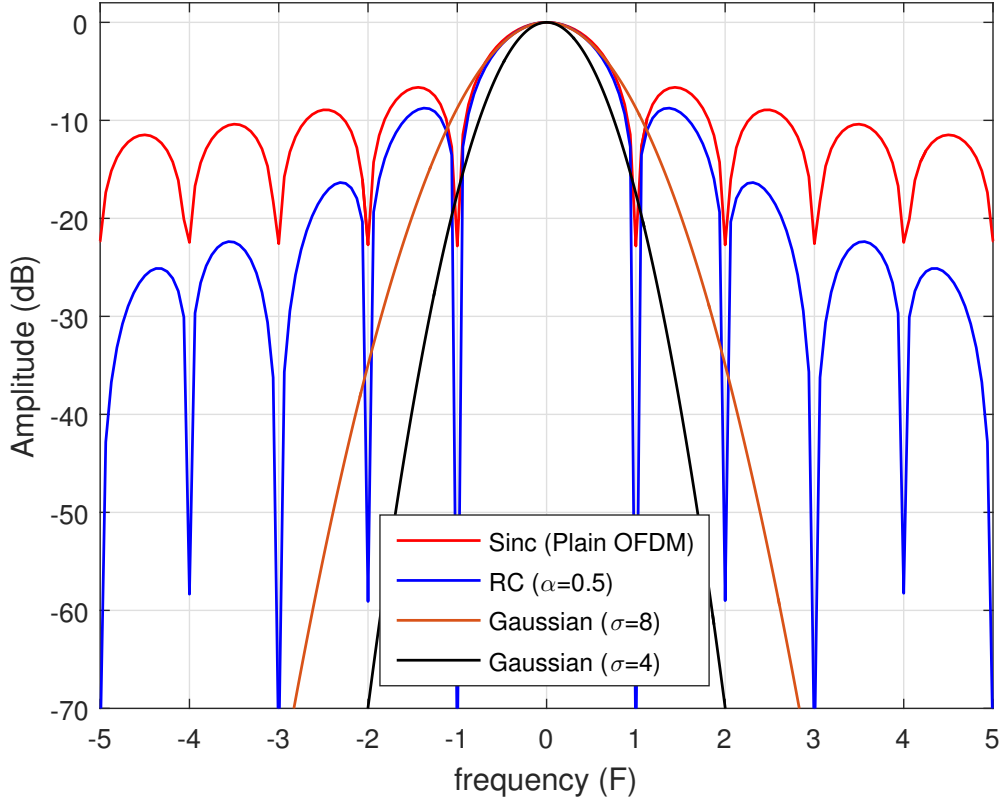


Figure 1.2 Frequency responses of an OFDM subcarrier (sinc) and various filters.

a time domain windowing approach is proposed in [23], in order to make the transitions between the OFDM symbols smoother and to avoid signal components at higher frequencies. Hence, the OOB leakage of OFDM symbols is significantly reduced. This approach became very popular due to its simplicity, effectiveness and requirement of no modification at the receiver side. However, the introduction of an extra redundancy as much as the windowing duration remained a problem. In [24], while the total duration for CP and windowing is kept constant for all subcarriers, windowing is mostly applied to the edge subcarriers since the leakage of edge subcarriers causes more interference on the adjacent frequencies. In a practical multiuser scenario where users need different CP sizes, this approach can decrease the windowing redundancy compared to the classical approach via a convenient user scheduling. Users with low time-dispersive channels are assigned to the edge subcarriers and users having highly time-dispersive channels are assigned to the inner

subcarriers. Thus, the total duration required for CP and windowing could be shorter without causing any problem. In [25–28], address the OOB leakage from frequency domain perspective. A set of subcarriers, named as cancellation carriers, are allocated for canceling the sidelobes in [25,26]. However, such approaches also introduce redundancy in the frequency domain and degrade spectral efficiency similar to classical windowing approach. In [27], sidelobe suppression is done by weighting subcarriers in such a way that sidelobes are combined on adjacent frequencies as destructively as possible. However, weighting leads to a pre-distortion of subcarriers and bit-error-rate (BER) performance naturally reduces. In order to limit this distortion, a frequency domain precoder is proposed in [28], which only maintains the spectrum of OFDM signals under the prescribed mask rather than forcing OOB leakage to zero. By doing so, interference on the adjacent frequencies are kept on a reasonable level at the expense of a smaller degradation BER performance.

### 1.3.2 PAPR Mitigation

As a consequence of multicarrier transmission, i.e., transmitting multiple signals in parallel, high PAPR is inevitable for OFDM signals due to the probable constructive combination of signals in time domain. In Fig. 5.11, a comparison between SC signals having various modulation orders up to 256-QAM, and OFDM signals having a different number of subcarriers ( $N$ ) is provided. Obviously, there is a huge difference in PAPR even when the number of subcarriers is as low as 32. It could be ignored for users requiring low power transmission. However, in many scenarios such as the mobile users on the cell edges, a reliable transmission requires high power and high PAPR of the signal for this scenario makes the signal vulnerable to non-linear effects of RF front-end components. These components typically have a limited linear range, and any part of the signal exceeding the linear range is non-linearly scaled. Non-linear scaling of a signal can also be referred as multiplying a part of signal components with various coefficients. This makes a time-varying channel effect on the signal, and the signal is distorted as if it is exposed to a Doppler spread effect at the transmitter. As a result, non-linearity of RF components may lead to severe interference not only in the user's band but also for the others operating on neighboring frequencies due to the spectral regrowth. At this point, one may notice that the OOB leakage is not only the function of the waveform itself but also

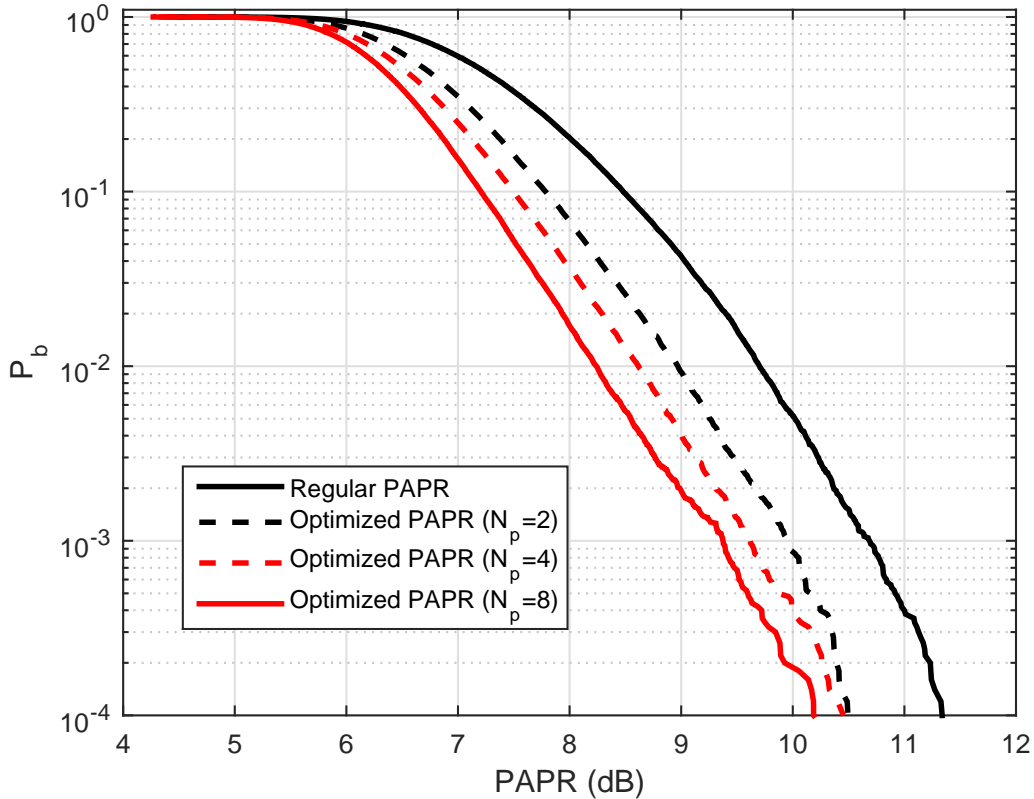


Figure 1.3 PAPR comparison between single carrier signals with different modulation orders and OFDM with different number of subcarriers ( $N$ ).

the spectral regrowth of the ideal waveform signals due to the high PAPR in practice. Then, even if the OOB suppression performance of the related studies in the literature are quite satisfactory, a good scheme needs to address PAPR and OOB leakage jointly for fixing these two shortcomings, practically.

PAPR suppression techniques are surveyed well in [29], however, many of them tackle with PAPR individually without considering OOB. On the other hand, some existing studies uses PAPR reduction concepts for also suppressing OOB. This is achieved by actively selecting some pre-designed sequences, i.e., selected mapping (SLM) sequences in [30]. Another well-known PAPR reduction method, partial transmit sequences are applied on OFDM signals partitioned into contiguous blocks in the frequency domain in [31]. Additionally, the optimized phase rotations are multiplied by each sub-block to provide a contiguous transition between the OFDM symbols to sup-

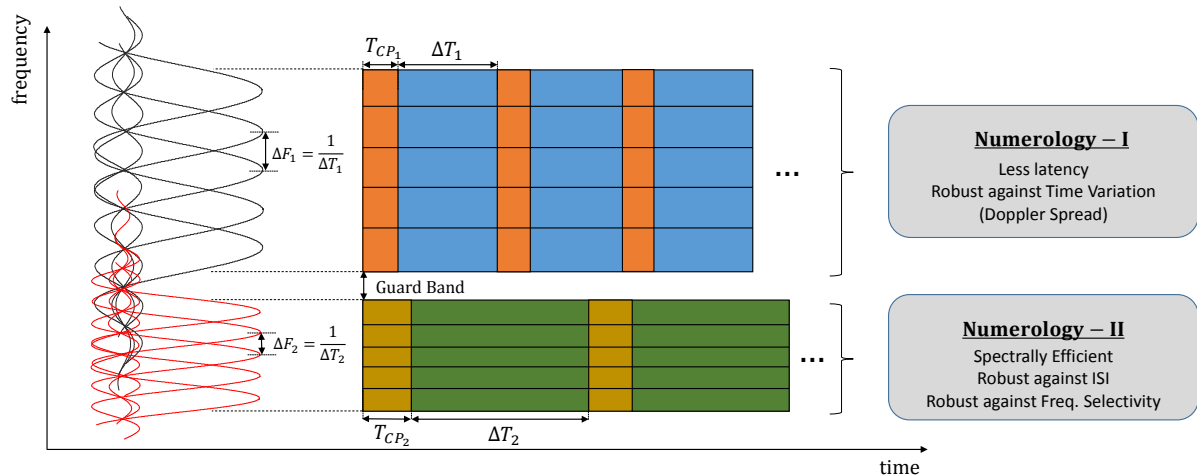


Figure 1.4 Illustration of different numerologies.

press OOB leakage along with PAPR. Another joint suppression method is presented in [32], where the constellation points are dynamically extended. For the similar purpose, a method called CP alignment is proposed in [33] similar to the interference alignment methods presented in [34,35]. The key idea in this method is to add a perturbation signal, called alignment signal (AS), to the plain OFDM symbols in order to reduce the PAPR and the OOB leakage such that the AS aligns with the CP duration of the OFDM symbols after passing through the channel. However, this method completely relies on the perfect channel estimation and any error might result in an interference on the data part. In order to fix this problem, a recent method called static CP alignment is proposed in [36] where the AS is designed based on a pre-determined filter independent of the channel.

Joint PAPR and OOB leakage suppression techniques are definitely offering a comprehensive solution in enhancing characteristics of OFDM signals. However, they require symbol based active optimization which introduce complexity issues at the transmitter side. Therefore, simpler solutions such as windowing are still needed in this field.

## 1.4 Numerology

Wireless users have different requirements in waveform based on the service that they get or channel conditions. Therefore, there is not any *one-size-fits-all solution* for waveform design. The

ongoing discussions on the usage of different numerologies also confirm this argument and consequently, one crucial expectation from future standards is the allowance to use multiple waveforms in one frame. This would definitely constitute a great relaxation in selecting the most proper waveform based on user needs. However, managing their coexistence is a critical issue. Especially, inter-user interference management for uplink/downlink, synchronous and asynchronous scenarios should be carefully investigated to utilize spectral resources efficiently.

In the context of 3GPP 5G standardization contributions, the term *numerology* refers to the configuration of waveform parameters, and different numerologies are considered as OFDM-based sub-frames having different parameters such as subcarrier spacing/symbol time, CP size etc. [37]. By designing such numerologies based on user requirements, industry targets to meet the aforementioned user-specific demands to some extent. A general illustration of such numerologies is provided in Fig. 1.4. Here, numerology-I would be properly assigned to highly mobile users having more time-variant channels and the ones with low latency requirement. On the other hand, numerology-II offers more robustness against frequency selectivity and includes less redundancy due to low CP rate.

Let us give more details on the role of the parameters and the importance of their selection for designing different numerologies:

- CP Length: The basic function of CP is to avoid inter-symbol interference and in-band interference. In order to achieve that, CP length should be specified as longer than the maximum excess delay of the channel impulse response. Therefore, users experiencing a wireless channel causing high dispersion in time (or more selectivity in frequency) should have longer CP lengths compared to the users with low dispersive channels. In addition, CP makes the signal robust against time synchronization errors. This might be very critical especially for asynchronous uplink (UL) scenarios and low latency demanding services.
- Subcarrier Spacing: It can also be referred to as subcarrier bandwidth and is directly related to the duration of an OFDM symbol. When the CP size is determined based on the channel conditions and the application requirements, decreasing subcarrier spacing



increases spectral efficiency as the CP rate decreases. However, for highly mobile users, channel response might vary within a symbol duration which leads to in-band interference. Therefore, symbol time should be kept smaller by increasing subcarrier spacing in order to make the transmission robust against time-varying, i.e., frequency dispersive channels. Additionally, proper choice of subcarrier spacing is very critical for immunity against phase noise which is specifically important for users operating on high frequencies such as mmWave frequencies.

In the light of aforementioned facts, obviously, the coexistence of different numerologies offers a great advantage in serving users with different requirements. However, such a design obviously removes the orthogonality between the numerologies, i.e., sinc shaped subcarriers with different spacings as illustrated in Fig. 1.4, and inter-numerology interference becomes inevitable. This is a major issue in numerology design and guard band determination between numerologies. Therefore, for the sake of communication performance and spectral efficiency, minimization of OOB leakage of each numerology or keeping their orthogonality with various methods should be investigated carefully.

## 1.5 Security

Throughout the last decade, wireless technologies have been deployed in many critical fields such as military and health-care, and it is envisioned that the usage of wireless devices will exponentially increase in the near future. For example, ongoing extensive research on internet-of-things (IoT) verifies that much more wireless devices will take place in our life and we will rely on these devices more in our daily activities. Also, the role of mobile terminals becomes more significant along with their continuously increasing capabilities and huge number of applications. However, the key requirement for providing a confident usage of these devices is to guarantee the security of their communication.

As a matter of fact, wireless signals remain vulnerable against malicious attacks because of the broadcast nature of the wireless medium. Adversaries that are likely located around legitimate users constitute a critical threat in terms of the security of the communications in different ways.

An adversary may passively wait to capture private information transferred between legitimate nodes (eavesdropping), may actively attempt to intervene the communication to deceive users (impersonation) or intercept the whole communication (blocking). Considering the existence of these adversaries and their attacks, developing solid countermeasures for different scenarios has gained a paramount importance to ensure the security of communication systems.

In order to design a secure communication system, cryptography has been widely used for wireless systems. Basically, legitimate nodes are encrypting their information based on a shared secret key and adversaries are prevented from carrying out eavesdropping or impersonation attacks. Recently, security in physical layer (PHY) has been proposed as an additional and complementary countermeasure against wireless attacks and has become very popular in the literature. Unlike cryptography, PHY security achieves the avoidance of malicious attacks in signal level, e.g., eavesdroppers are prevented from receiving the signal properly rather than hiding the actual content of the information carried by the signal. Thus, adversaries are precluded by another means of security. Considering the widespread usage of wireless technologies, PHY security algorithms provide a great opportunity to ensure a safe and reliable utilization of broadband and narrow band systems.

## **1.6 Dissertation Outline**

In this dissertation, we present PHY algorithms for improving the spectral efficiency and reliability of wireless communication systems. In Chapter 1, we drafted the various aspects of these algorithms which also represent the content of the dissertation. In Chapter 2, an algorithm jointly suppressing the OOB emission and PAPR of OFDM based waveforms by utilizing the time domain and frequency domain resources is presented. In Chapter 3, we present a novel approach that removes the practically challenging assumptions of the algorithm provided in Chapter 2 at the expense of some performance degradation. In Chapter 4, we discuss the radio access technologies beyond 5G and introduce new concepts in waveform parameterization and frame design via including multiple waveform techniques. In Chapter 5, two methods removing the cyclic features of OFDM signal are proposed in order to design broadband signals robust against eavesdropping attacks. In Chapter 6, the security of wireless implantable medical device applications is considered and an

authentication mechanism ensuring the security of these devices against impersonation attacks is presented. Chapter 7 concludes the dissertation along with a final summary and open issues in proposed algorithms.

## CHAPTER 2

# JOINT TIME/FREQUENCY ALIGNMENT FOR SUPPRESSING OOBE AND PAPR OF OFDM-BASED WAVEFORMS<sup>1</sup>

### 2.1 Introduction

OFDM has been the prominent waveform in the literature due to its flexibility in spectrum, robustness against frequency selective channels, and simplicity in equalization. Therefore, it has been adopted in many wireless communication standards such as 5th generation (5G) New Radio, Wi-Fi, and Long Term Evolution. However, high out-of-band emission (OOBE) degrades the spectral compactness of OFDM and may cause severe interference on adjacent channels in certain scenarios. Additionally, its high PAPR makes the OFDM signal vulnerable against non-linear distortion due to PAs, and decreases the coverage range in cellular scenarios. Therefore, maintaining OOBE and PAPR low for OFDM signals is critically important for an efficient deployment of OFDM in future standards including 5G.

Although OOBE and PAPR of OFDM signals are well discussed separately in the literature, only few approaches investigate their joint suppression. In [32], a joint OOBE and PAPR suppression technique is proposed for cognitive radio scenarios. In [31], partial-transmit sequences (PTS) are deployed for the same goal, however, it requires sharing PTS information for each OFDM symbol. Recently, CP alignment (CPA) concept is proposed in [2]. In this method, an additive signal, called AS, is designed for joint OOBE and PAPR suppression and transmitted along with the OFDM symbol. After passing through the wireless channel, the AS aligns with the CP portion, similar to the alignment concept presented in [34,35], and offers a promising solution to high PAPR and OOBE without introducing any problem at the receiver side. However, the suppression performance of this

---

<sup>1</sup>This chapter was patented [38] and published in IEEE Communications Letters [39]. Permission is included in Appendix A.

method heavily depends on the degrees-of-freedom (DoF) provided by the CP size, which may be small in certain scenarios. In addition, due to the constraint of alignment with CP duration, which is a local portion of OFDM symbol in time domain, the AS mostly concentrates around CP and does not effectively reduce the amplitude variation of OFDM symbol. Therefore, CPA is limited especially in PAPR suppression. In [40], channel independent CPA where the alignment is achieved by receive filter is also investigated. However, no solution is provided for the aforementioned problems.

In this chapter, we introduce a novel joint time-frequency alignment (JTFA) concept to overcome the shortcomings of original CPA. We allow AS to align with both time and frequency domain resources that are not effectively used at the receiver, i.e. CP, guard tones, and subcarriers that are severely faded by the channel. Thus, not only is the available DoF for AS generation substantially increased as compared to the CPA, but also the power of AS is optimally distributed across time and frequency domains in the sense that it leads to further PAPR and OOB suppression, jointly.

The remainder of the chapter is organized as follows. Section II explains system model and Section III presents the proposed method. Numerical results are provided in Section VI and Section V concludes the chapter.

In our notation,  $\mathbf{I}_N$  represents  $N \times N$  identity matrix and  $\mathbf{0}_{N \times M}$  is  $N \times M$  zero matrix.  $(\cdot)^T$ ,  $(\cdot)^H$  and  $\ker(\cdot)$  denote transpose, conjugate transpose and kernel of a matrix.  $\mathcal{CN}(0, \mathbf{C})$  represents a zero mean complex Gaussian distribution with the covariance matrix  $\mathbf{C}$ .  $\mathbb{R}$  and  $\mathbb{C}$  denote the real and complex number fields, respectively.

## 2.2 System Model

We consider a single link OFDM-based communication system with  $N$  subcarriers. The  $i$ th OFDM symbol,  $\mathbf{x}^{(i)} \in \mathbb{C}^{(N+K) \times 1}$ , is expressed in time domain as

$$\mathbf{x}^{(i)} = \mathbf{A}\mathbf{F}^H\mathbf{M}\mathbf{d}_i, \quad (2.1)$$

where  $\mathbf{d}_i \in \mathbb{C}^{N_s \times 1}$  is the vector of data symbols,  $\mathbf{M} \in \mathbb{R}^{N \times N_s}$  is the mapping matrix assigning the data symbols to the selected subcarriers,  $\mathbf{F}$  is the  $N$ -point DFT matrix,  $\mathbf{A} \in \mathbb{R}^{(N+K) \times N}$  represents

the CP insertion matrix explicitly given by

$$\mathbf{A} = \begin{bmatrix} \mathbf{0}_{K \times N-K} & \mathbf{I}_K \\ & \mathbf{I}_N \end{bmatrix}, \quad (2.2)$$

$K$  is the number of samples in CP, and  $N_s$  is the number of data symbols. In [2], PAPR and OOB characteristics of OFDM signals are improved by adding an AS,  $\mathbf{c}_i \in \mathbb{C}^{(N+K) \times 1}$ , and the transmitted signal is formed as

$$\mathbf{t}_i = \mathbf{x}^{(i)} + \mathbf{c}_i. \quad (2.3)$$

The AS vector  $\mathbf{c}_i$  can be calculated as

$$\mathbf{c}_i = \mathbf{P}\mathbf{s}_i. \quad (2.4)$$

In (3.4),  $\mathbf{P} \in \mathbb{C}^{(N+K) \times \hat{K}}$  is an orthonormal precoder matrix<sup>2</sup> that generates the AS vector  $\mathbf{c}_i$  from any  $\mathbf{s}_i \in \mathbb{C}^{\hat{K} \times 1}$  where  $\hat{K}$  represents the DoF for designing  $\mathbf{c}_i$ <sup>1</sup>. In CPA,  $\hat{K}$  corresponds to CP size to avoid interference on the information symbols.

We assume that  $\mathbf{t}_i$  passes through an independently and identically distributed multipath channel with  $R$  taps whose vector representation is given by  $\mathbf{h}(t) = [h_0, h_1, \dots, h_R]^T \sim \mathcal{CN}(0, \mathbf{I}_{R+1}/(R+1))$ . Power Delay Profile (PDP) of  $\mathbf{h}(t)$  is considered as an exponential decaying channel. We then calculate the  $i$ th received signal vector as

$$\mathbf{r}_i = \begin{bmatrix} \mathbf{H}_p & \mathbf{H} \end{bmatrix} \begin{bmatrix} \mathbf{t}_{i-1} \\ \mathbf{t}_i \end{bmatrix} + \mathbf{n}, \quad (2.5)$$

where  $\mathbf{n} \in \mathbb{C}^{(N+K) \times 1} \sim \mathcal{CN}(0, \sigma^2 \mathbf{I}_{N+K})$  is an additive white Gaussian noise vector,  $\mathbf{H}_p \in \mathbb{C}^{(N+K) \times (N+K)}$  characterizes the leakage of the previous signal  $\mathbf{t}_{i-1}$  on the current signal  $\mathbf{t}_i$ , and  $\mathbf{H} \in \mathbb{C}^{(N+K) \times (N+K)}$  is the channel convolution matrix.

<sup>2</sup>Since  $\mathbf{P}$  is an orthonormal matrix,  $\mathbf{c}_i^T \mathbf{c}_i = \mathbf{s}_i^T \mathbf{P}^T \mathbf{P} \mathbf{s}_i = \mathbf{s}_i^T \mathbf{s}_i$ .

After discarding the CP, the signal can be expressed as

$$\begin{aligned} \mathbf{y}_i = \mathbf{B}\mathbf{r}_i &= \mathbf{B}\mathbf{H}\mathbf{A}\mathbf{F}^H\mathbf{M}\mathbf{d}_i + \mathbf{B}\mathbf{H}\mathbf{c}_i \\ &+ \mathbf{B}\mathbf{H}_p\mathbf{A}\mathbf{F}^H\mathbf{M}\mathbf{d}_{i-1} + \mathbf{B}\mathbf{H}_p\mathbf{c}_{i-1} + \mathbf{n}, \end{aligned} \quad (2.6)$$

where  $\mathbf{B} \in \mathbb{R}^{N \times (N+K)}$  is the CP removal matrix as

$$\mathbf{B} = \begin{bmatrix} \mathbf{0}_{N \times K} & \mathbf{I}_N \end{bmatrix}. \quad (2.7)$$

Discarding the CP nullifies the third and fourth terms of (3.8) as the leakage from the  $(i-1)$ th OFDM symbol falls into  $i$ th symbol's CP duration. Then, after the DFT and de-mapping operations, the received signal in frequency domain can be calculated as

$$\tilde{\mathbf{y}}_i = \mathbf{M}^H\mathbf{F}\mathbf{B}\mathbf{H}\mathbf{A}\mathbf{F}^H\mathbf{M}\mathbf{d}_i + \mathbf{M}^H\mathbf{F}\mathbf{B}\mathbf{H}\mathbf{P}\mathbf{s}_i + \hat{\mathbf{n}}. \quad (2.8)$$

The second term in (3.10) corresponds to the interference because of the AS and  $\hat{\mathbf{n}}$  is the noise. Hence,  $\mathbf{M}^H\mathbf{F}\mathbf{B}\mathbf{H}\mathbf{P}\mathbf{s}_i$  should be zero for carrying out an interference free transmission. In [2], this is ensured by setting the columns of  $\mathbf{P}$  in a way that they span the null space of  $\mathbf{B}\mathbf{H}$ , i.e.  $\ker(\mathbf{B}\mathbf{H})$ . Thus,  $\mathbf{P}\mathbf{s}_i$  can be optimized for PAPR and OOB suppression while  $\mathbf{s}_i$  is mapped into the null space of  $\mathbf{B}\mathbf{H}$ , which corresponds to the CP part of the OFDM symbols.

### 2.3 Joint Time-Frequency Alignment for Joint OOB and PAPR Suppression

In the proposed method, to enable joint utilization of time and frequency domain resources, we design the mapping matrix  $\mathbf{M}$  such that it discards the guard tones and the subcarriers experiencing a deep channel fading for data transmission. This is done by selecting the active data subcarriers and forming  $\mathbf{M}$  with  $N_s$  corresponding columns of  $\mathbf{I}_N$ . The columns of  $\mathbf{P}$  span the null space of  $\mathbf{\Gamma}$ , i.e.  $\ker(\mathbf{\Gamma})$ , where  $\mathbf{\Gamma} = \mathbf{M}^H\mathbf{F}\mathbf{B}\mathbf{H} \in \mathbb{C}^{N_s \times (N+K)}$ . Thus, by generating  $\mathbf{c}_i$  as  $\mathbf{P}\mathbf{s}_i$ , we can allow the AS to align with the CP duration in time domain, the guard tones and the subcarriers faded by the channel in frequency domain. As we also include the frequency domain resources in

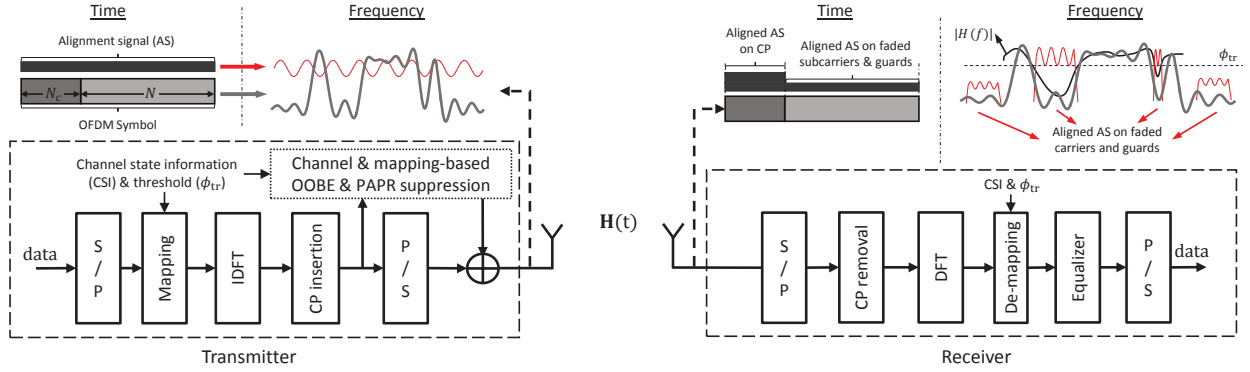


Figure 2.1 Block diagram for the proposed system (AS aligns with the CP duration, the guard tones and the faded subcarriers at the receiver side).

null space calculation,  $\hat{K}$  increases to the sum of the CP size, the number of allocated subcarriers experiencing a deep fading and the guard tones. Then, a more effective  $\mathbf{s}_i$  can be designed for joint PAPR and OOB suppression, as compared to CPA.

It is worth noting that we introduce a small loss in capacity due to the faded subcarriers allocated for the alignment purpose. These subcarriers are selected based on a threshold in channel gain,  $\phi_{tr}$ . In other words, the subcarriers experiencing a channel gain below the selected threshold are exploited for alignment purpose and ignored at the receiver side. For instance, the receiver can decide  $\phi_{tr}$  based on a tolerable loss in capacity and feedback that information to the transmitter along with the channel state information (CSI). Then, the transmitter determines the active subcarriers, design AS based on the CSI and  $\phi_{tr}$ , and transmit the OFDM signal combined with AS. Finally, the active subcarriers are selected at the receiver side and data detection is performed. The block diagram of the transceiver with JTFA and illustrations of transmitted and received signals are provided in Fig. 3.1.

Using singular value decomposition,  $\mathbf{\Gamma}$  can be decomposed as  $\mathbf{\Gamma} = \mathbf{U}\mathbf{\Sigma}\mathbf{V}^H$ , where  $\mathbf{U} \in \mathbb{C}^{N_s \times N_s}$  and  $\mathbf{V} \in \mathbb{C}^{(N+K) \times (N+K)}$  are unitary matrices that contain the singular vectors of  $\mathbf{\Gamma}$ , and  $\mathbf{\Sigma} \in \mathbb{R}^{N_s \times (N+K)}$  is a diagonal matrix including the singular values of  $\mathbf{\Gamma}$ , arranged in descending order. As the null space of  $\mathbf{\Gamma}$  is spanned by the last  $\hat{K}$  columns of  $\mathbf{V} = [\mathbf{v}_0, \mathbf{v}_1, \dots, \mathbf{v}_{N+K-1}]$ ,  $\mathbf{P} \in \mathbb{C}^{(N+K) \times \hat{K}}$  can be created as  $\mathbf{P} = [\mathbf{v}_{N+K-\hat{K}}, \mathbf{v}_{N+K-\hat{K}+1}, \dots, \mathbf{v}_{N+K-1}]$ .



After guaranteeing the avoidance of AS's interference with the precoding matrix  $\mathbf{P}$ ,  $\mathbf{s}_i$  can be optimized for suppressing OOBE and PAPR of the digital signal  $\mathbf{x}^{(i)}$  as

$$\begin{aligned} \mathbf{s}_i &= \arg \min_{\hat{\mathbf{s}}_i} (1 - \lambda) \|\mathcal{F}_O(\mathbf{x}^{(i)} + \mathbf{P}\hat{\mathbf{s}}_i)\|_2 + \lambda \|\mathbf{x}^{(i)} + \mathbf{P}\hat{\mathbf{s}}_i\|_\infty \\ \text{over } \hat{\mathbf{s}}_i &\in \mathbb{C}^{K \times 1} \\ \text{subject to } &\|\hat{\mathbf{s}}_i\|_2 \leq \sqrt{\alpha} \|\mathbf{x}^{(i)}\|_2, \end{aligned} \tag{2.9}$$

where  $\mathcal{F}_O$  is the matrix that contains the rows of an oversampled DFT matrix, corresponding to the signal elements in the out-of-band region,  $\alpha$  is a power limiting parameter for  $\mathbf{c}_i$ , and  $\lambda \in [0, 1]$  is the weighting factor in the joint OOBE and PAPR optimization. While larger  $\lambda$  yields a lower PAPR, smaller  $\lambda$  leads to a better OOBE suppression. Also,  $\|\cdot\|_2$  and  $\|\cdot\|_\infty$  represent the 2-norm and infinity norm operators, respectively.

The objective function and the constraint are both convex in (3.18). Therefore, the problem can be solved by a convex optimization solver. In this study, YALMIP is utilized [41].

## 2.4 Numerical Results

In this section, we demonstrate BER, OOBE, and PAPR suppression performance of the JTFA through simulations. We consider OFDM symbols with 128 subcarriers and 16 samples for CP, where the 64 subcarriers of each OFDM symbol are utilized for 16-QAM symbols. PDP of the channel is assumed to be a 17-tap exponential decaying function, expressed as  $h(\tau) = ae^{-\tau n}$ , where  $a$  is the normalization factor,  $n$  indicates the tap index,  $\tau$  is the decaying factor, and the amplitude of each tap follows Rayleigh distribution. In the simulations, we set  $\tau$  to 0.2 unless otherwise stated. The threshold  $\phi_{\text{tr}}$  is set to 0.2. We also compare JTFA with CPA [2] and cancellation carrier insertion (CCI) [42]. For the sake of a fair comparison, we use the same set of subcarriers for both CCI and JTFA, and keep the total signal power the same for all the approaches.

In Figure 2.2, we show the energy distribution of the AS in time domain for CPA and JTFA for  $\lambda = 0.99$ . When AS is designed based solely on CP duration, as done in CPA method, most of the energy concentrates around the CP duration and dramatically decreases on the middle samples

even for large  $\lambda$  values. As shown in Figure 2.2, the energy of the samples located in the data duration of OFDM symbol is approximately 13 dB weaker than the samples of OFDM symbol for CPA, even when the channel decaying rate,  $\tau$ , is zero which corresponds to a uniform PDP. As  $\tau$  increases, which is likely in practical scenarios, AS concentrates further on the edges. Since any sample may have a high amplitude in an OFDM symbol, the AS in CPA is ineffective to cancel the peak sample, which yields a limited PAPR suppression. In JTFA, since time and frequency domain resources are jointly utilized, the energy of the samples of AS are distributed more uniformly across the useful OFDM symbol duration as shown in Figure 2.2. Hence, JTFA is more effective than CPA to reduce PAPR.

In Fig. 2.3, the PAPR performances are provided for JTFA, CPA, and CCI when  $\alpha = 0.25$  and  $\lambda = \{0.5, 0.9, 0.98\}$ . The simulation results show that JTFA method achieves 4 dB suppression while CPA can only suppress less than 1 dB for  $\lambda = 0.98$ , as compared to plain OFDM symbols. As discussed earlier, this is because of the fact that JTFA is more effective than CPA to cancel the peak sample of OFDM symbols since it exploits the frequency domain resources along with the CP duration. It is also worth noting that CCI remains around 3 dB reduction in PAPR as only frequency domain resources are employed in this scheme. As a result, JTFA is superior to CPA and CCI in terms of PAPR suppression. This is achieved at the expense of approximately 6% capacity loss when  $\gamma = 10$  dB, which is calculated based on Shannon's channel capacity.

In Fig. 2.4, we compare OOB reduction performance of aforementioned schemes. JTFA method reduces the OOB up to 24 dB when  $\lambda = 0.5$ , while CPA and CCI provide approximately 13 dB and 10 dB suppressions, respectively. Our simulation results show that JTFA is better than CPA and CCI in both OOB and PAPR reduction for the investigated  $\lambda$  values.

In Fig. 2.5, BER results are provided for JTFA, CPA and CCI for different mean-square errors (MSEs) in channel estimation. We quantify MSE as the expected value of the normalized difference between the channel response  $h$  and the channel estimated by the receiver  $\tilde{h}$ , and defined as  $\sigma_e^2 = \frac{E[|\tilde{h}-h|^2]}{E[|h|^2]}$  where  $E[\cdot]$  denotes the expected value. When there is no channel estimation error, i.e.  $\sigma_e^2 = 0$ , CPA, JTFA and CCI methods are slightly worse than the plain OFDM generated with the same active subcarriers since a part of the power (20% for  $\alpha = 0.25$ ) is used for either AS or

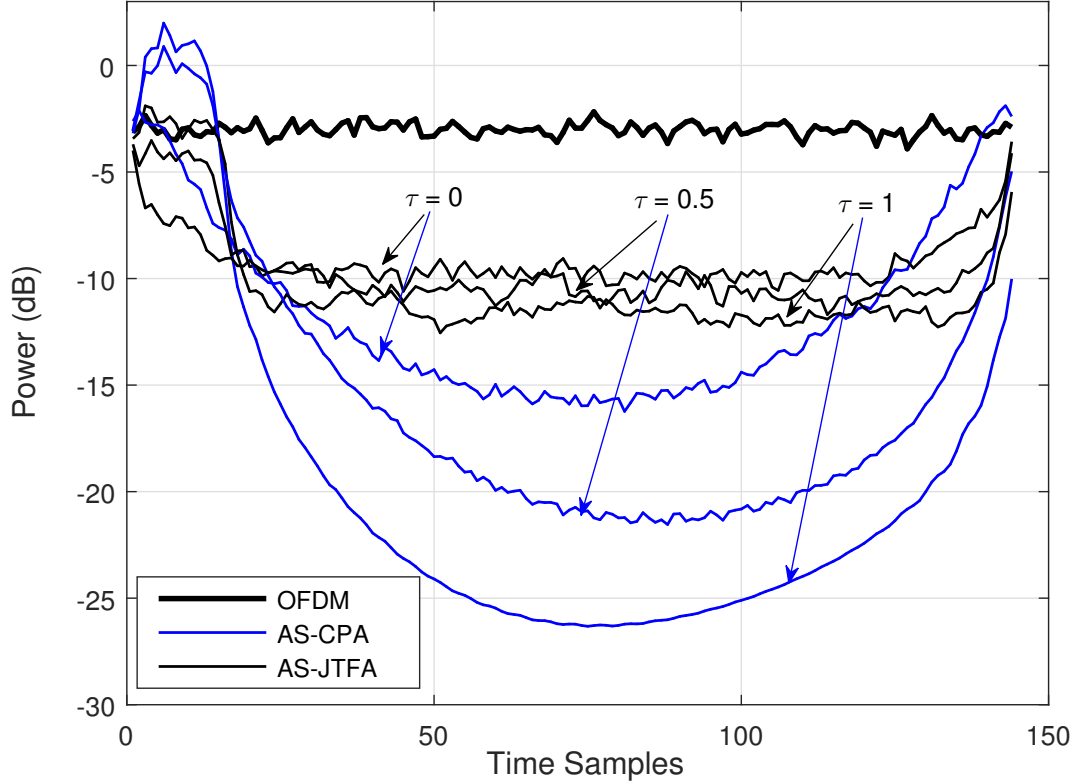


Figure 2.2 Power distribution of plain OFDM and AS samples for CPA and JTFA in time for different channel decaying factors ( $\alpha = 0.25, \phi_{\text{tr}} = 0.2$ ).

inserted carriers. However, the impact of equalization with an erroneous channel estimation mostly dominates the effect of power discrepancy and BER performances of JTFA and CPA become similar to that of CCI and regular OFDM transmission, respectively, for  $\sigma_e^2 > 0$ .

## 2.5 Conclusion

In this study, we present a joint PAPR and OOBRE reduction technique for OFDM systems. We significantly increase the DoF in designing AS by jointly exploiting specific subchannels, i.e. guard tones and subcarriers faded by the channel, and CP in the optimization. Thus, a substantial suppression is obtained in PAPR and OOBRE at the cost of a small loss in capacity.

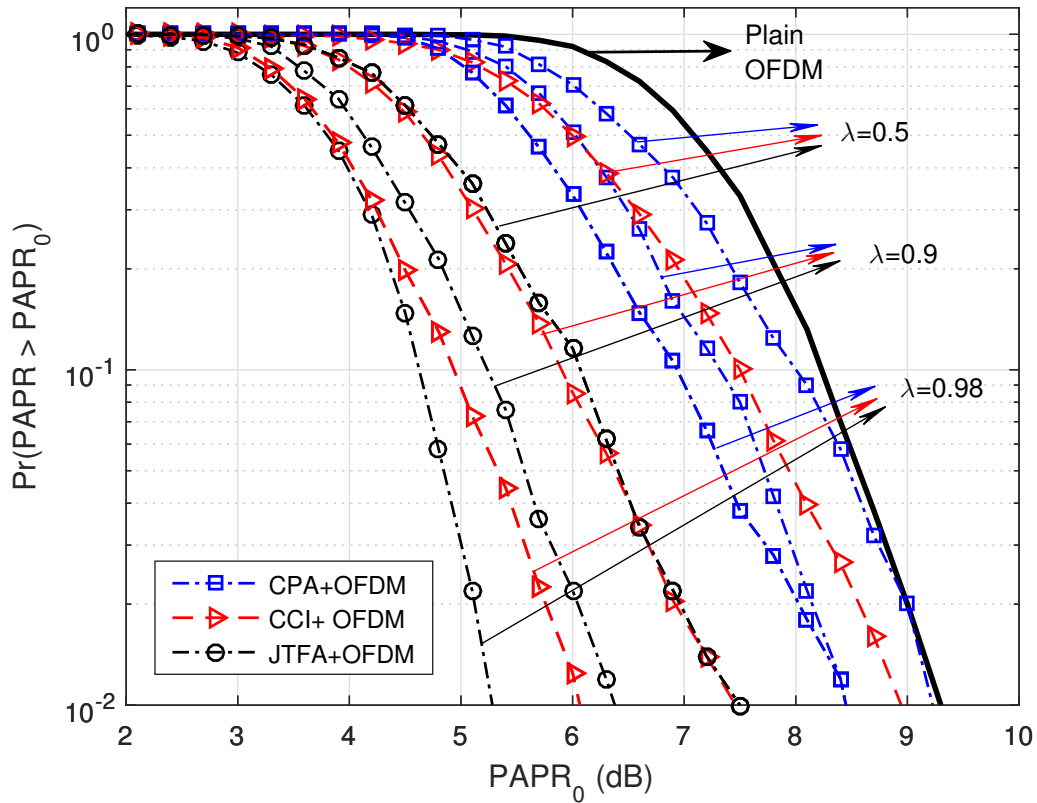


Figure 2.3 PAPR performance for CPA, JTFA, and CCI for different  $\lambda$  values ( $\alpha = 0.25, \tau = 0.2, \phi_{tr} = 0.2$ ).

## 2.6 Acknowledgment

The authors would like to thank Rui Yang and Erdem Bala for their technical support and discussions.

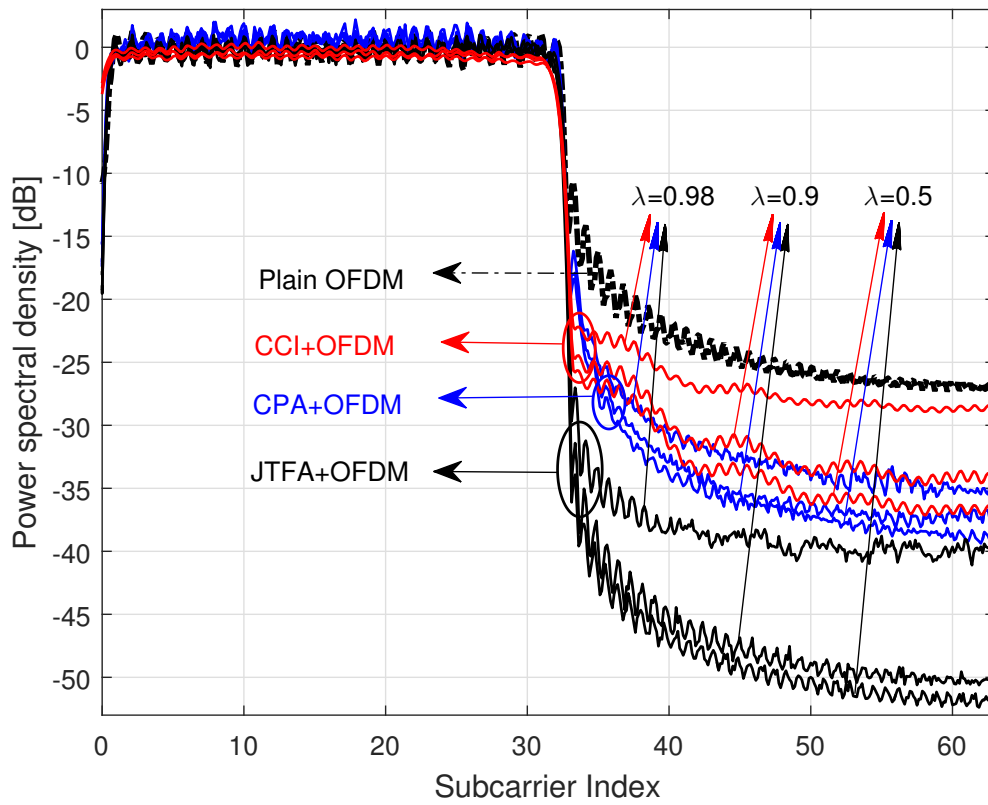


Figure 2.4 OOB performance for CPA, JTFA, and CCI for different  $\lambda$  values ( $\alpha = 0.25, \tau = 0.2, \phi_{tr} = 0.2$ ).

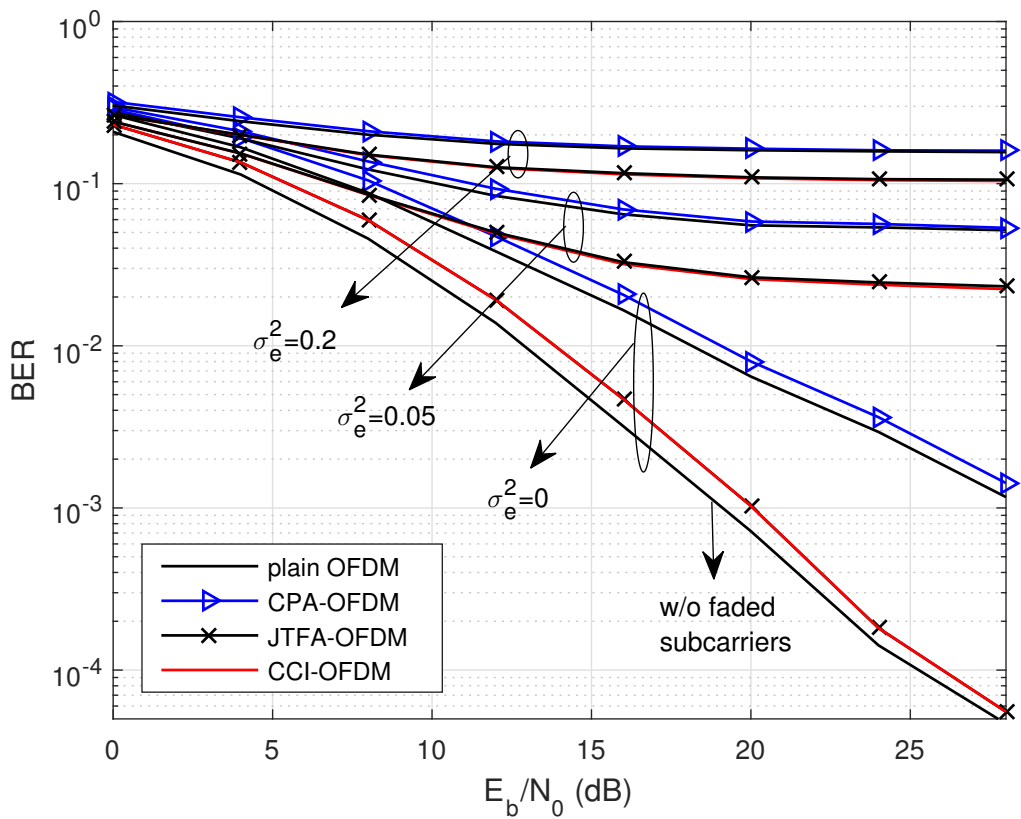


Figure 2.5 BER performance for CPA, JTFA, and CCI for different MSEs ( $\sigma_e^2$ ) in channel estimation ( $\alpha = 0.25, \tau = 0.2, \phi_{tr} = 0.2$ ).

## CHAPTER 3

### STATIC CP ALIGNMENT<sup>1</sup>

#### 3.1 Introduction

OFDM has been widely used in wireless digital communication systems such as LTE and Wi-Fi due to its numerous advantages such as low-complexity implementation with FFT and the robustness against multipath channels with single-tap frequency domain equalization (FDE). However, plain OFDM signals suffer from the distortions due to the non-linear characteristics of PA. At the same time, the block nature of plain OFDM symbols may cause severe adjacent channel interference.

In the literature, PAPR and OOB leakage of OFDM signals have been extensively studied and addressed with numerous techniques. In reference [23], a time domain windowing is applied to the OFDM symbols in order to smooth the transitions between the OFDM symbols. Hence, the OOB leakage of OFDM symbols is significantly reduced. In reference [24], the time-domain windowing approach is particularly applied to the edge subcarriers as the edge subcarriers cause more interference to the adjacent channels than the inner subcarriers. In references [25–28], the OOB leakage is addressed in frequency domain. While a set of subcarriers in the band, known as cancellation carriers, are allocated in order to cancel the sidelobes in reference [25], a set of carriers located at the adjacent channels and the redundancy of CP duration are utilized for the same purpose in reference [26]. In reference [27], a sidelobe suppression method based on the multiplication of the used subcarriers with some weights is proposed. Similarly, a frequency domain precoding which maintains the spectrum of OFDM signals under the prescribed mask is introduced in reference [28].

---

<sup>1</sup>This chapter was published in IEEE Global Communication Conference, 2016 [40]. Permission is included in Appendix A.

Albeit their remarkable OOB performance of the aforementioned approaches, in practice, the OOB leakage is not only the function of the waveform itself but also the PAPR characteristics of the waveform. This is due to the fact that the PA distorts ideal waveform signals and also causes spectral regrowth. Therefore, a good scheme needs to address PAPR and OOB leakage jointly. In reference [30], the joint reduction is achieved by actively selecting some predesigned sequences, i.e., selected mapping (SLM) sequences. In reference [31], OFDM signal is partitioned into contiguous blocks in frequency and partial transmit sequences (PTS) are applied to reduce the PAPR. In addition, the optimized phase rotations are applied to each sub-block to maintain the contiguity between the OFDM symbols. In reference [32], joint PAPR reduction and sidelobe suppression are achieved by dynamically extending the constellation points. For the similar purpose, recently, a method called CP alignment is introduced in reference [43] and [2], similar to the interference alignment methods presented in [34, 35]. The key idea in this method is to add a perturbation signal, called AS, to the plain OFDM symbols in order to reduce the PAPR and the OOB leakage such that the AS aligns with the CP duration of the OFDM symbols after passing through the channel. Therefore, the AS improves the signal characteristics at the transmitter side while it does not cause any interference on the data symbols at the receiver side. On the other hand, the AS does not align with the CP duration, i.e., remains spread on the OFDM symbols after passing through a channel different than the channel of the intended user. Thus, the AS also provides PHY security by distorting the data symbols of any users except the intended user.

There are two major challenges with original CP alignment method. First, the original approach requires the exact CSI in order to maintain the alignment with the CP duration. However, due to the mobility and the channel estimation error in low signal-to-noise ratio (SNR) conditions, the exact CSI and the CSI used in the design of AS may not match in practice (see e.g., [44, 45], and the references listed therein). Second, the original approach requires strong frequency selective multipath channel for enhancing the waveform characteristics [2, 43]. This is due to the fact that the AS spreads in time domain at the transmitter side when the channel is frequency selective. For example, the peak value may occur in any sample of an OFDM symbol. Then, in order to suppress the peaks, AS should be able to reach any sample of the OFDM symbol effectively. However, the



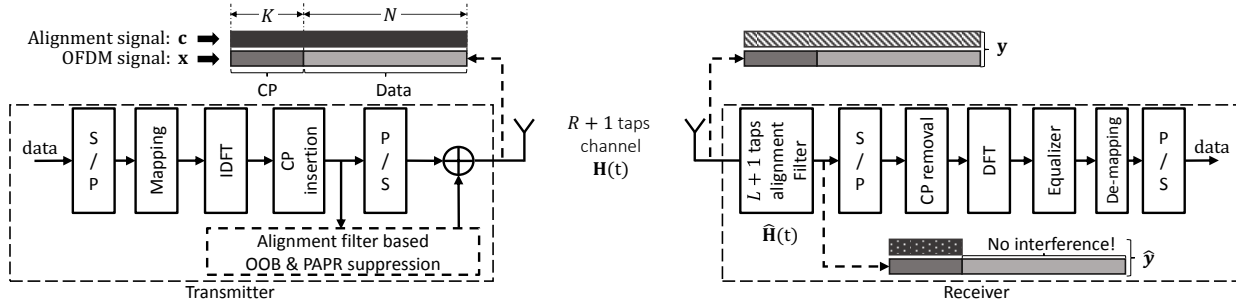


Figure 3.1 Block diagram for the proposed system.

AS remains localized in the CP duration when the channel is not frequency selective. In this case, the original approach cannot reduce the PAPR efficiently. In order to overcome these challenges, i.e., misalignment due to the outdated CSI and channel estimation errors, and the need of strong frequency selectivity, we propose a CP alignment method referred to as *static CP alignment*, which generates the AS based on a predetermined receiver filter, rather than the instantaneous CSI. Our contributions with this scheme can be given as follows:

- In order to achieve perfect alignment, the need of having the exact CSI at transmitter is eliminated. Hence, the proposed scheme provides seamless alignment in mobile scenarios where the CSI is time-varying.
- The need of strong frequency selective multipath channel of the original method is removed. Hence, the proposed method provides enhancements in waveform characteristics even in frequency flat channels.
- The proposed scheme reduces PAPR and OOB leakage, jointly. At the same time, it does not cause any interference to the data symbols.

The rest of the chapter is organized as follows: In Section II, the system model is provided. The concept of static CP alignment is described in Section III. The numerical results are given in Section IV. Finally, the concluding remarks are provided in Section V.

In our notation,  $\mathbf{I}_N$  is the  $N \times N$  identity matrix,  $\mathbf{0}_{N \times M}$  is the  $N \times M$  zero matrix. Hermitian operation and the transpose operation are denoted by  $(\cdot)^H$  and  $(\cdot)^T$ , respectively. The 2-norm and

infinity norm are denoted by  $\|\cdot\|_2$  and  $\|\cdot\|_\infty$ , respectively.  $E[\cdot]$  represents the expectation operator while  $\ker(\cdot)$  denotes the kernel of the matrix. Zero mean complex Gaussian distribution with the covariance matrix  $\mathbf{C}$  is denoted by  $\mathcal{CN}(0, \mathbf{C})$ . The field of real and field of complex numbers are represented by  $\mathbb{R}$  and  $\mathbb{C}$ , respectively.

### 3.2 System Model

We consider an OFDM-based single link communication system as shown in Fig. 3.1. The  $i$ th OFDM signal can be analytically expressed as

$$\mathbf{x}^{(i)} = \mathbf{A}\mathbf{F}^H\mathbf{M}\mathbf{d}_i, \quad (3.1)$$

where  $\mathbf{x}^{(i)} \in \mathbb{C}^{(N+K) \times 1}$  is the OFDM symbol vector in time,  $\mathbf{d}_i \in \mathbb{C}^{N_d \times 1}$  is the data vector,  $\mathbf{M} \in \mathbb{R}^{N \times N_d}$  is the subcarrier mapping matrix that maps the data symbols to the active data subcarriers,  $\mathbf{A} \in \mathbb{R}^{(N+K) \times N}$  is the CP insertion matrix given by

$$\mathbf{A} = \begin{bmatrix} \mathbf{0}_{K \times N-K} & \mathbf{I}_K \\ & \mathbf{I}_N \end{bmatrix}, \quad (3.2)$$

$\mathbf{F}$  is the  $N$ -point DFT matrix,  $K$  is the number samples for CP duration, and  $N_d$  is the number of data symbols.

As shown in [2], the PAPR and OOB leakage performance of OFDM can be improved by addition of an alignment signal vector  $\mathbf{c}_i = [c_{i,1}, c_{i,2}, \dots, c_{i,N+K}]^T$ . The transmitted signal vector can be expressed as

$$\mathbf{t}_i = \mathbf{x}^{(i)} + \mathbf{c}_i, \quad (3.3)$$

where

$$\mathbf{c}_i = \mathbf{P}\mathbf{s}_i. \quad (3.4)$$

Here,  $\mathbf{P} \in \mathbb{C}^{(N+K) \times \hat{K}}$  forms  $\mathbf{c}_i$  as the alignment signal vector that aligns on the first  $\hat{K}$  samples of the CP after passing through the channel, and  $\mathbf{s}_i \in \mathbb{C}^{\hat{K} \times 1}$  is a data-dependent vector which is optimized to minimize the PAPR and the OOB leakage of the plain OFDM symbols, jointly. In order not to cause interference due to the vector  $\mathbf{c}_i$ ,  $\mathbf{P}$  is designed based on the CSI.

In this study, the channel between the transmitter and the receiver is characterized as an i.i.d. Rayleigh fading channel with the vector of  $\mathbf{h}(t) = [h_0(t), h_1(t), \dots, h_R(t)]^T \sim \mathcal{CN}(0, \mathbf{I}_{R+1}/(R+1))$ . After the signal passes through the channel, the received signal vector can then be calculated as

$$\mathbf{r}_i = \begin{bmatrix} \mathbf{H}_p & \mathbf{H} \end{bmatrix} \begin{bmatrix} \mathbf{t}_{i-1} \\ \mathbf{t}_i \end{bmatrix} + \mathbf{n}, \quad (3.5)$$

where  $\mathbf{n} \in \mathbb{C}^{(N+K) \times 1} \sim \mathcal{CN}(0, \sigma^2 \mathbf{I}_{N+K})$  is an additive white Gaussian noise vector,  $\mathbf{H}_p \in \mathbb{C}^{(N+K) \times (N+K)}$  and  $\mathbf{H} \in \mathbb{C}^{(N+K) \times (N+K)}$  are the convolution matrices, explicitly given by

$$\mathbf{H}_p = \begin{bmatrix} 0 & \dots & \dots & h_R(t) & \dots & h_0(t) \\ \vdots & \ddots & \ddots & \ddots & \ddots & \vdots \\ \vdots & \ddots & \ddots & \ddots & \ddots & h_R(t) \\ \vdots & \ddots & \ddots & \ddots & \ddots & 0 \\ \vdots & \ddots & \ddots & \ddots & \ddots & \vdots \\ 0 & \dots & \dots & \dots & \dots & 0 \end{bmatrix}, \quad (3.6)$$

and

$$\mathbf{H} = \begin{bmatrix} h_0(t) & 0 & \dots & \dots & \dots & \dots & 0 \\ \vdots & \ddots & \ddots & \ddots & \ddots & \ddots & \vdots \\ \vdots & \ddots & \ddots & \ddots & \ddots & \ddots & \vdots \\ h_R(t) & \dots & \dots & h_0(t) & 0 & \dots & 0 \\ 0 & \ddots & \ddots & \ddots & \ddots & \ddots & \vdots \\ 0 & \ddots & 0 & h_R(t) & \dots & \dots & h_0(t) \end{bmatrix}. \quad (3.7)$$

At the receiver side, the resulting signal after CP removal operation can be expressed as

$$\begin{aligned} \mathbf{y}_i &= \mathbf{B}\mathbf{r}_i \\ &= \mathbf{B}\mathbf{H}\mathbf{A}\mathbf{F}^H\mathbf{M}\mathbf{d}_i + \mathbf{B}\mathbf{H}\mathbf{c}_i \\ &\quad + \mathbf{B}\mathbf{H}_p\mathbf{A}\mathbf{F}^H\mathbf{M}\mathbf{d}_{i-1} + \mathbf{B}\mathbf{H}_p\mathbf{c}_{i-1} + \mathbf{n}, \end{aligned} \quad (3.8)$$

where  $\mathbf{B} \in \mathbb{R}^{N \times (N+K)}$  is the CP removal matrix given by

$$\mathbf{B} = \begin{bmatrix} \mathbf{0}_{N \times K} & \mathbf{I}_N \end{bmatrix}. \quad (3.9)$$

Since the contribution of the  $(i-1)$ th symbol falls into the CP duration of  $i$ th symbol, the CP removal operation makes the third and fourth terms of (3.8) zero and after the DFT operation, the received signal in frequency domain is obtained as

$$\tilde{\mathbf{y}}_i = \mathbf{F}\mathbf{B}\mathbf{H}\mathbf{A}\mathbf{F}^H\mathbf{M}\mathbf{d}_i + \mathbf{F}\mathbf{B}\mathbf{H}\mathbf{P}\mathbf{s}_i + \hat{\mathbf{n}}. \quad (3.10)$$

In (3.10), the second term represents the interference due to the AS and  $\hat{\mathbf{n}}$  is the noise in frequency domain. In order to avoid interference on the data symbols, the second term should be zero, which can be achieved by forming the columns of  $\mathbf{P}$  as spanning the null space of  $\mathbf{B}\mathbf{H}$ , i.e.,  $\ker(\mathbf{B}\mathbf{H})$ . In the original scheme [2], the vector  $\mathbf{P}\mathbf{s}_i$  is optimized to minimize the PAPR and OOB leakage while

the precoder  $\mathbf{P}$  maps  $\mathbf{s}_i$  into the null space of the matrix  $\mathbf{B}\mathbf{H}$ , i.e., the CP duration of the OFDM symbols. As a result, the interference on the data symbols is avoided at the receiver side. Detailed discussions regarding the practical issues such as synchronization are provided in [2].

Note that the transmitter should be able to calculate the matrix  $\mathbf{P}$  based on the CSI. However, in practice, the CSI may be aged due to the mobility and it may erroneous due to imperfect channel estimation. Therefore, the alignment may not be achieved perfectly and the data symbols are interfered by the alignment signal.

### 3.3 Static CP Alignment

In this section, we describe the static CP alignment method which introduces an extra filtering operation with an alignment filter at the receiver. Let  $\hat{\mathbf{h}}(t)$  be  $[\hat{h}_0, \hat{h}_1, \dots, \hat{h}_L] \in \mathbb{C}^{1 \times (L+1)}$ . At the receiver side, the received signal is filtered with the alignment filter  $\hat{\mathbf{h}}(t)$  before the CP removal operation. Then, the conventional OFDM receiver structure is applied as

$$\hat{\mathbf{y}}_i = \mathbf{F}\mathbf{B}\hat{\mathbf{H}}\mathbf{H}\mathbf{A}\mathbf{F}^H\mathbf{M}\mathbf{d}_i + \mathbf{F}\mathbf{B}\hat{\mathbf{H}}\mathbf{H}\mathbf{P}\mathbf{s}_i + \hat{\mathbf{n}}, \quad (3.11)$$

where the convolution matrix of  $\hat{\mathbf{h}}(t)$ ,  $\hat{\mathbf{H}} \in \mathbb{C}^{(N+K) \times (N+K)}$  is given as

$$\hat{\mathbf{H}} = \begin{bmatrix} \hat{h}_0 & 0 & \dots & \dots & \dots & \dots & 0 \\ \vdots & \ddots & \ddots & \ddots & \ddots & \ddots & \vdots \\ \vdots & \ddots & \ddots & \ddots & \ddots & \ddots & \vdots \\ \hat{h}_L & \dots & \dots & \hat{h}_0 & 0 & \dots & 0 \\ 0 & \ddots & \ddots & \ddots & \ddots & \ddots & \vdots \\ 0 & \ddots & 0 & \hat{h}_L & \dots & \dots & \hat{h}_0 \end{bmatrix}. \quad (3.12)$$

As shown in (3.11), the new interference term with the alignment filter becomes  $\mathbf{B}\hat{\mathbf{H}}\mathbf{H}\mathbf{P}\mathbf{s}_i$ . Therefore, the precoder matrix should be designed such that  $\mathbf{P}\mathbf{s}_i$  is in the null space of  $\mathbf{B}\hat{\mathbf{H}}\mathbf{H}$ . At this point, it is important to emphasize that our goal is to achieve a channel-independent precoder, rather than

increasing the channel selectivity. In the following part of this section, we will show that a subspace of the  $\ker(\mathbf{B}\hat{\mathbf{H}}\mathbf{H})$  is static due to the pre-determined alignment filter.

Note that we partially use the CP for the alignment purposes in the proposed approach and set  $\hat{K} = L$ . In order to maintain the circularity and avoid inter-symbol interference, CP size is determined based on the number of taps for multipath channel and alignment filter, i.e.,  $K \geq L + R$ .

Let  $\hat{\mathbf{B}} \in \mathbb{R}^{(N+R) \times (N+K)}$  be an auxiliary matrix given by

$$\hat{\mathbf{B}} = \begin{bmatrix} \mathbf{0}_{(N+R) \times L} & \mathbf{I}_{N+R} \end{bmatrix}. \quad (3.13)$$

Using singular value decomposition,  $\hat{\mathbf{B}}\hat{\mathbf{H}}$  can be decomposed as

$$\hat{\mathbf{B}}\hat{\mathbf{H}} = \mathbf{U}\mathbf{\Sigma}\mathbf{V}^H, \quad (3.14)$$

where  $\mathbf{U} \in \mathbb{C}^{(N+R) \times (N+R)}$  and  $\mathbf{V} \in \mathbb{C}^{(N+K) \times (N+K)}$  are unitary matrices containing the singular vectors of  $\hat{\mathbf{B}}\hat{\mathbf{H}}$ , and  $\mathbf{\Sigma} \in \mathbb{C}^{(N+R) \times (N+K)}$  is a diagonal matrix consisting of the singular values of  $\hat{\mathbf{B}}\hat{\mathbf{H}}$ . Since the last  $L$  columns of the matrix  $\mathbf{V} = [\mathbf{v}_0, \mathbf{v}_1, \dots, \mathbf{v}_{N+L-1}]$  spans the null space of  $\hat{\mathbf{B}}\hat{\mathbf{H}}$ ,  $\mathbf{P} \in \mathbb{C}^{(N+K) \times L}$  is formed as  $\mathbf{P} = [\mathbf{v}_N, \mathbf{v}_{N+1}, \dots, \mathbf{v}_{N+L-1}]$ .

Since the cascaded filtering operation has commutative property,  $\mathbf{H}$  and  $\hat{\mathbf{H}}$  in the interference term given in (3.11) can be replaced as

$$\mathbf{F}\hat{\mathbf{B}}\hat{\mathbf{H}}\mathbf{H}\mathbf{P}\mathbf{s}_i = \mathbf{F}\mathbf{B}\mathbf{H}\hat{\mathbf{H}}\mathbf{P}\mathbf{s}_i. \quad (3.15)$$

Then, let  $\hat{\hat{\mathbf{H}}}$  be

$$\hat{\hat{\mathbf{H}}} \equiv \begin{bmatrix} \mathbf{W} \\ \hat{\mathbf{B}}\hat{\mathbf{H}} \end{bmatrix}, \quad (3.16)$$

where  $\mathbf{W} \in \mathbb{C}^{L \times (N+K)}$  consists of the first  $L$  rows of  $\hat{\mathbf{H}}$ . As  $\hat{\mathbf{H}}$  is multiplied with the matrix  $\mathbf{P}$  in (3.15), the resulting matrix can be obtained as

$$\hat{\mathbf{H}}\mathbf{P} \equiv \begin{bmatrix} \mathbf{WP} \\ \hat{\mathbf{B}}\hat{\mathbf{H}}\mathbf{P} \end{bmatrix} \stackrel{(a)}{=} \begin{bmatrix} \hat{\mathbf{W}}_{L \times L} \\ \mathbf{0}_{(N+R) \times L} \end{bmatrix}. \quad (3.17)$$

In (3.17), (a) holds true as the vector  $\mathbf{s}_i \in \mathbb{C}^{L \times 1}$  is designed such that  $\mathbf{P}\mathbf{s}_i$  lies in  $\ker(\hat{\mathbf{B}}\hat{\mathbf{H}})$ . As a result, the interference term  $\mathbf{F}\hat{\mathbf{B}}\hat{\mathbf{H}}\mathbf{P}\mathbf{s}_i$  becomes zero regardless of the channel condition.

Based on the optimization problem proposed in [2], we can then generate  $\mathbf{c}_i$  for reducing OOB emission and PAPR as

$$\mathbf{c}_i = \arg \min_{\hat{\mathbf{c}}_i} (1 - \lambda) \|\mathcal{F}_O(\mathbf{x}^{(i)} + \hat{\mathbf{c}}_i)\|_2 + \lambda \|\mathbf{x}^{(i)} + \hat{\mathbf{c}}_i\|_\infty \quad (3.18)$$

$$\text{over } \hat{\mathbf{c}}_i \in \mathbb{C}^{(N+K) \times 1}$$

$$\text{subject to } \hat{\mathbf{B}}\hat{\mathbf{H}}\hat{\mathbf{c}}_i = 0,$$

$$\|\hat{\mathbf{c}}_i\|_2 \leq \sqrt{\alpha} \|\mathbf{x}^{(i)}\|_2,$$

where  $\mathcal{F}_O$  is the matrix that extracts the signal components in the OOB region,  $\alpha$  is a parameter that limits the power of  $\mathbf{c}_i$ , and  $\lambda \in [0, 1]$  is the weighting factor for the joint optimization of OOB and PAPR. Note that while increasing  $\lambda$  yields a scheme with a lower PAPR, small  $\lambda$  achieves a better OOB leakage performance [2].

In (18), since the constraint and the objective function are convex, the problem becomes a convex optimization problem and its numerical solution could be done by a convex optimization solver. In this study, we use YALMIP as the underlying solver [41].

### 3.4 Practical Issues

#### 3.4.1 Design of Alignment Filter

The characteristics of the alignment filter determines the improvement on the PAPR and OOB leakage performance. There are two fundamental approaches for design of the alignment filter.

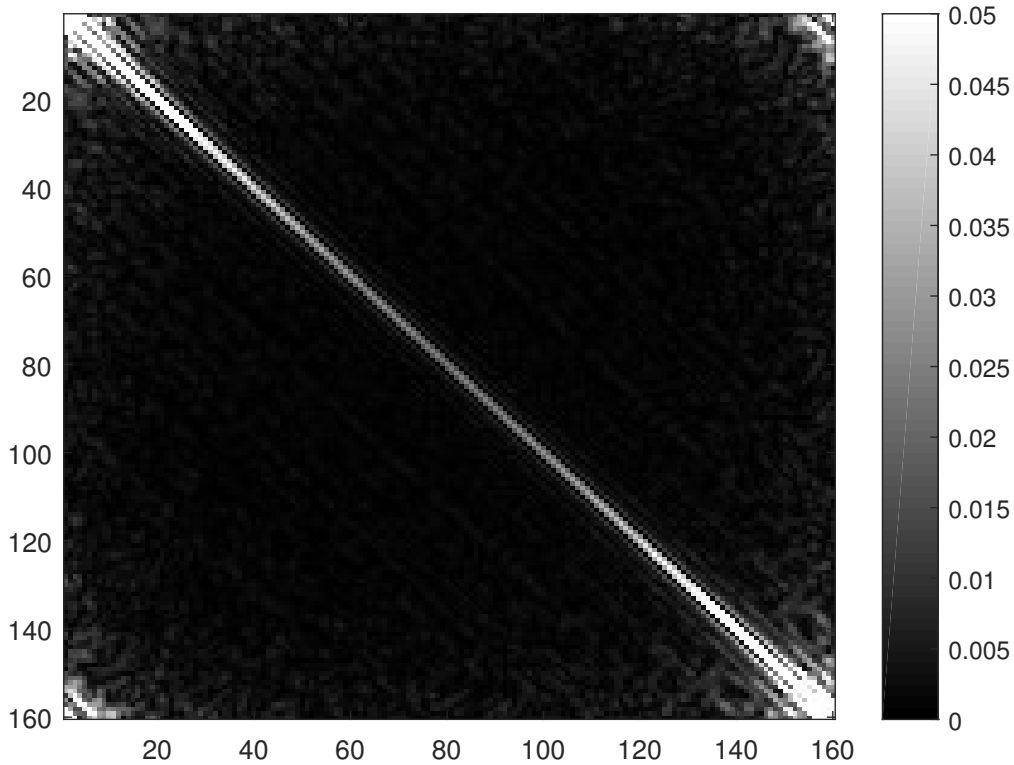


Figure 3.2 Illustration for the covariance matrix of an alignment signal designed based on a uniform alignment filter.

In the first case, the alignment filter is generated based on a properly shared CSI. Although this approach may not yield an optimum filter design, the scheme allows enhancement on the physical layer security for TDD-based systems. This is due to the fact that the same channel cannot be estimated by an adversary and the AS remains as an interference signal on non-intended users.

In the second case, the transmitter and the receiver share the information of alignment filter. Therefore, it is possible to design an alignment filter which achieves better OOB leakage performance and PAPR reduction. In order to achieve that, the alignment signal's energy should be spread on the OFDM symbol as uniform as possible. This is because the peak power may occur in any sample of the OFDM symbol. Thus, maximum control on the PAPR and OOB leakage can be obtained by having the flexibility of modifying any sample of the OFDM symbol. Filters having a uniform power profile are prominent for designing such an AS. In order to verify that, covariance matrices



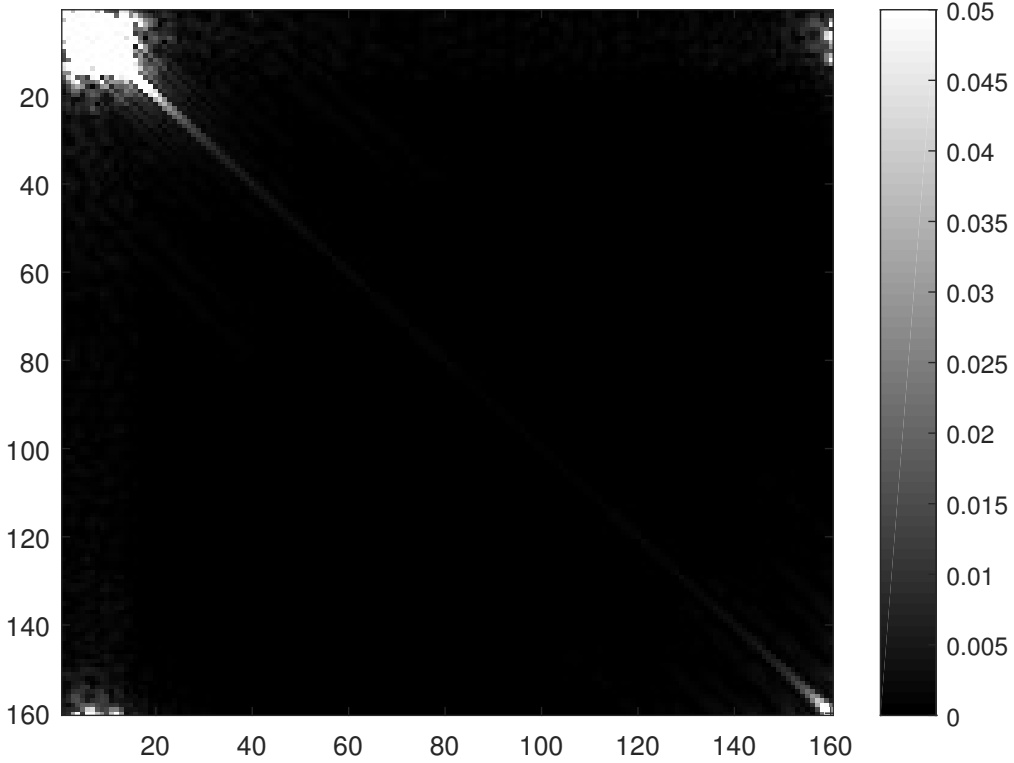


Figure 3.3 Illustration for the covariance matrix of an alignment signal designed based on an exponentially decaying alignment filter.

of ASs designed with filters having a uniform ( $\hat{h}(\tau) = 1$ ) and exponential decaying ( $\hat{h}(\tau) = e^{-\tau}$ ) power profiles are illustrated in Fig. 3.4.1 and 3.4.1 where  $N = 128$ , the CP rate is  $1/4$ ,  $\lambda = 0.99$  and  $\alpha = 0.25$ . Here, half of the CP is utilized for alignment purposes, i.e.,  $\hat{K} = N/8$ . As shown on the diagonal of each diagram whose elements correspond to the expected power of AS on each sample, the uniform filter spreads the energy of AS while the exponentially decaying filter cannot disperse the AS effectively, i.e., the energy of AS spread mostly over the first 20 samples. Therefore, the uniform filter yields a better OOB leakage and PAPR reduction performance.

### 3.4.2 Complexity

In the original CP alignment [2], the feasible solutions for the alignment signal lie on the null space of  $\mathbf{BH}$ . Therefore, the precoder  $\mathbf{P}$  in which its columns span the null of  $\mathbf{BH}$  needs to

be calculated for a given CSI. However, the complexity of calculating the precoder matrix  $\mathbf{P}$  is  $\mathcal{O}(N(N + K)^2)$  with singular value decomposition. The proposed method eliminates the need of this operation as the feasible solutions are in the null space of  $\hat{\mathbf{B}}\hat{\mathbf{H}}$ , which is not a function of the multipath channel. Therefore, the subspace for the feasible solutions can be calculated offline.

The optimization problem in (18) reduces to a least squares with quadratic inequality constraint (LSQI) if  $\lambda = 0$ . In this case, LSQI problem can be solved over Lagrangian function with bisection method. It is worth noting that the roots of the Lagrangian function can also be obtained with a closed-form expression for a given Lagrangian multiplier [2]. Thus, by rewriting the optimization problem with Lagrangian function, it is possible to obtain a closed-form linear precoder, which leads to the complexity of  $\mathcal{O}(2(N + G)L)$ . If  $\lambda > 0$ , there is no closed-form solution available for the optimization problem in (18) and the optimizer should follow an iterative strategy. Nevertheless, (18) is a convex optimization problem and it can still be solved efficiently.

### 3.5 Numerical Results

In this section, the proposed scheme is evaluated through simulations. We consider an OFDM system where the IDFT size is 128 and the number of active subcarriers is 64. Throughout the simulations, we consider 16-QAM and the CP rate is set to 1/4. A seventeen tap Rayleigh fading multipath channel is generated for each realization, and the power delay profile (PDP) is assumed to be exponentially decaying as  $h(\tau) = e^{-\tau}$  where  $\tau = 1$ . For the alignment filter, we consider a filter which has the same number of taps with the channel and has a uniform power profile in the light of our discussions in Section IV.

In Fig. 6.2, BER results are provided for plain OFDM, OFDM with original CP alignment [2], and OFDM with the proposed method. For the simulations, we consider a scenario where the CSI at the transmitter is stale (or outdated) due to the high-mobility. This is quantified by MSE of the estimated channel,  $\tilde{h}$ , defined as  $\sigma_e^2 = \frac{\mathbb{E}[|\tilde{h} - h|^2]}{\mathbb{E}[|h|^2]}$ . Under these circumstances, the original method fails to maintain the alignment on the CP duration due to the stale CSI and the AS interferes with the actual data which results in significant degradation on the BER performance. In addition, as illustrated in Fig. 6.2, the interference due to the AS increases with the MSE

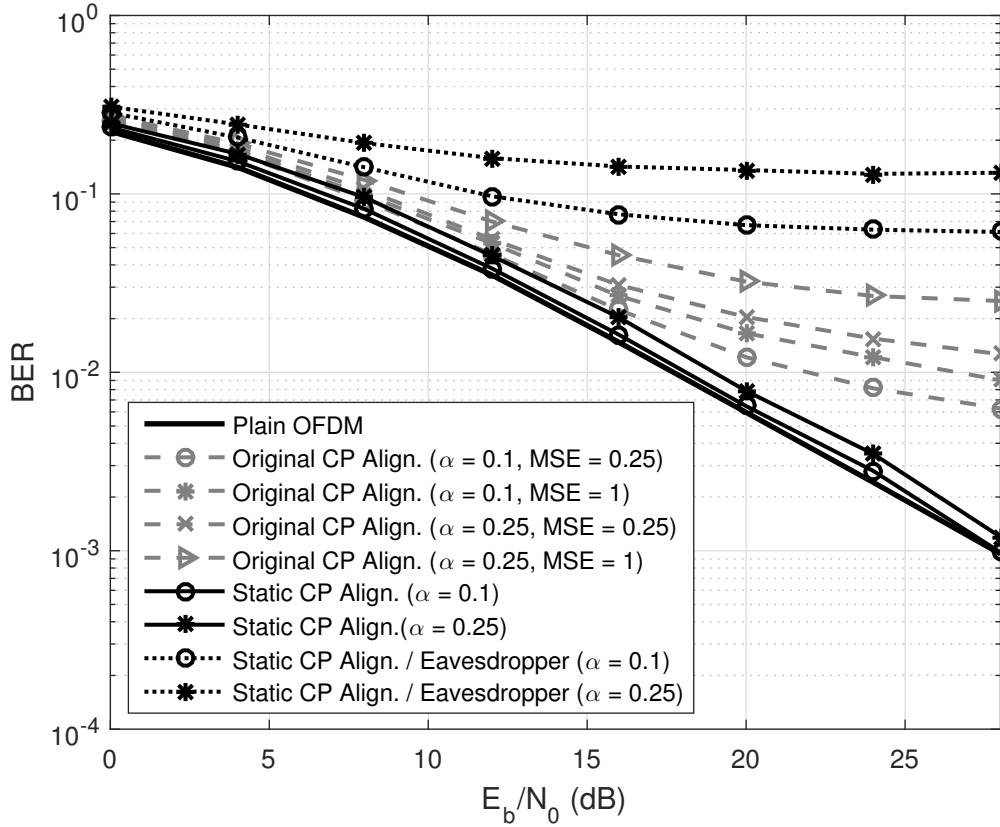


Figure 3.4 BER curves for the plain OFDM, proposed static CP alignment (for intended users & eavesdroppers), original CP alignment [2] for different MSE values in channel estimation (Modulation type is 16-QAM).

of the channel estimation and  $\alpha$  parameter which controls the energy of AS. On the other hand, the proposed method relies on the alignment filter at the receiver side without the CSI at the transmitter. Therefore, we achieve perfect alignment and eliminate the limitation of the original method as shown in Fig. 6.2. In this analysis, we assume that the total signal power is shared by the AS and the plain OFDM signal. Therefore, the proposed method causes a shift in the BER performance, i.e., less than 0.5 dB when  $\alpha = 0.1$  and less than 1.5 dB when  $\alpha = 0.25$ . Nevertheless, the proposed method does not introduce any error floor.

It is worth noting that the addition of AS causes severe interference on the data symbols if the alignment filter is not employed at the receiver side. This is exactly the case for an illegitimate user who does not have the alignment filter information. Therefore, if the alignment filter is

securely shared between the legitimate nodes, the illegitimate users such as eavesdroppers receive distorted data symbols due to the AS. In order to illustrate that, we also provide BER curves for an eavesdropper in Fig. 6.2. As clearly seen, a significant error floor is introduced and therefore, the proposed technique also enhances the security of the signal in PHY.

In order to show the OOB leakage suppression performance, the simulations are performed for different values of  $\lambda$  which weights the optimization toward PAPR or OOB leakage suppression. As shown in Fig. 5.12, the OOB leakage of the plain OFDM is suppressed around 8 dB and 14 dB for  $\lambda = 0.99$ , and  $\lambda = 0.9$ , respectively. On the other hand, the original method presented in [2] achieves 5 dB suppression at most, even though the CP is fully utilized for the alignment purpose. This is because of the fact that the AS of the original method is designed based on the CSI where the PDP is modeled as exponentially decaying. On the other hand, the proposed method provides the flexibility of using a more proper filter, i.e., a uniform filter, as discussed in Section 3.4.1. Because of this flexibility, the proposed method achieves a better suppression even with less CP usage for the alignment.

In Fig. 5.11, the PAPR reduction performance of the proposed approach is investigated. We observe that the proposed method yields more than 1 dB improvement when  $\lambda = 0.9$  which is better than the performance of [2]. The suppression performance increases close to 2 dB for  $\lambda = 0.99$  while it is around 1 dB for the original method. Note that the power of the AS provides an additional degree of freedom for a better OOB leakage and PAPR reduction, i.e., the suppression performance can be enhanced further by increasing  $\alpha$ . However, we do not set it more than 0.25 in our simulations to maintain the power efficiency.

In Fig. 3.7, we investigate the effect of the alignment filter length on the PAPR reduction and OOB leakage suppression. The suppression of the OOB leakage over the subcarrier indexes from 60 to 64 and the reduction of the PAPR are provided for different  $\lambda$  values. It is observed that the filter length has significant effect on the suppression performance. Also, the analysis are performed for an exponentially decaying and uniform alignment filters to show the importance of alignment filter choice. As discussed in Section 3.4.1, the AS cannot be spread when it is designed based on

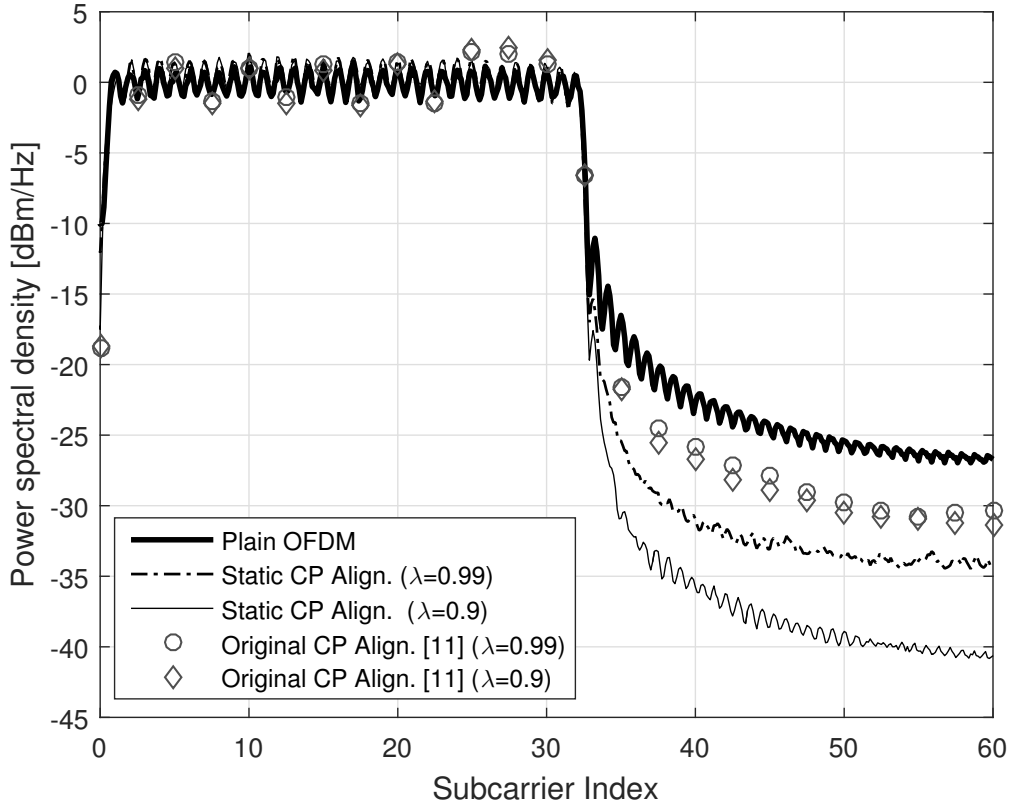


Figure 3.5 OOB emission suppression performance of proposed method for different  $\lambda$  values ( $\alpha = 0.25, K = N/4$ ).

an exponentially decaying filter. On the other hand, uniform filters allow transmitter to design a well spread AS. Therefore, a better suppression performance is achieved with uniform filters.

### 3.6 Conclusion

In this study, we propose a practical solution to the outdated CSI problem of the original CP alignment method. Unlike the original approach where the AS is generated based on CSI at transmitter, the proposed method generates the AS by utilizing a fixed receive filter which maintains the alignment on a portion of the CP duration. As a result, the waveform characteristics are enhanced regardless of the frequency selectivity of the channel while the original approach requires a strong frequency selective channel. Static CP alignment also offers less complexity than that of

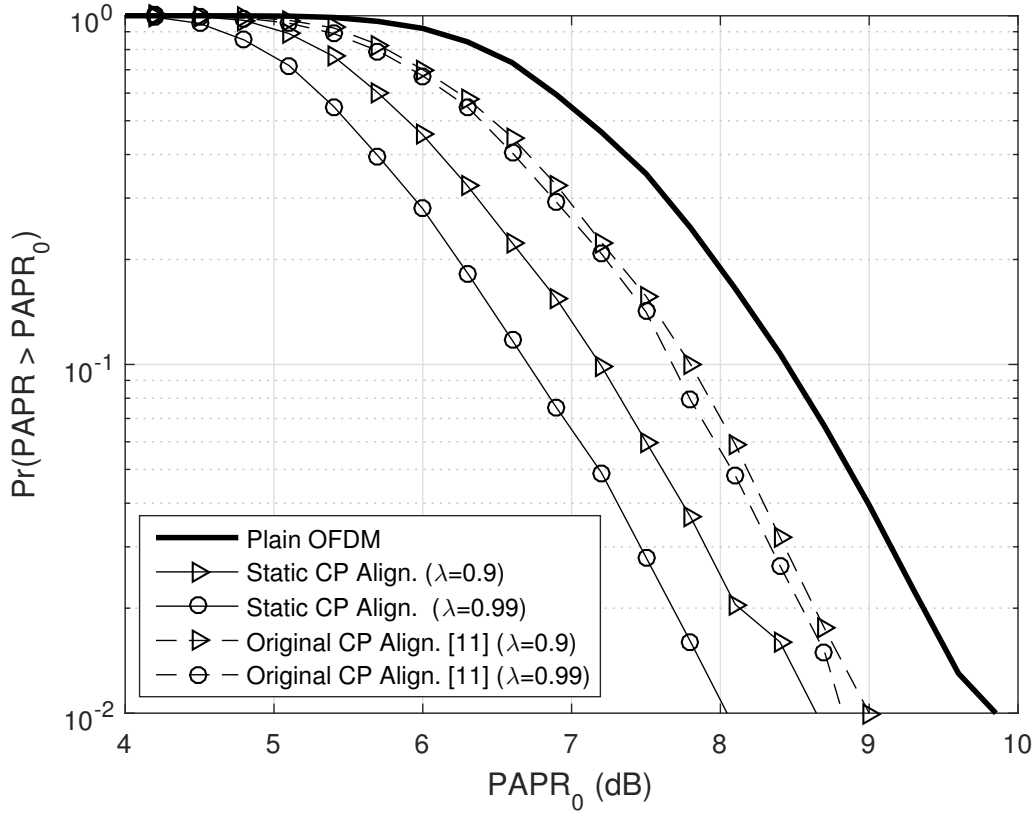


Figure 3.6 PAPR performance for different  $\lambda$  values ( $\alpha = 0.25, K = N/4$ ).

the original CP alignment method since the exact CSI does not involve in the calculation of AS. As compared to conventional joint OOB leakage and PAPR mitigation methods for OFDM, the proposed scheme achieves the same goal without introducing any distortion on the received data symbols and yields a BER performance without error floor. Additionally, since the alignment filter can be generated based on the outdated channel, the proposed scheme may also provide improvement in PHY security.

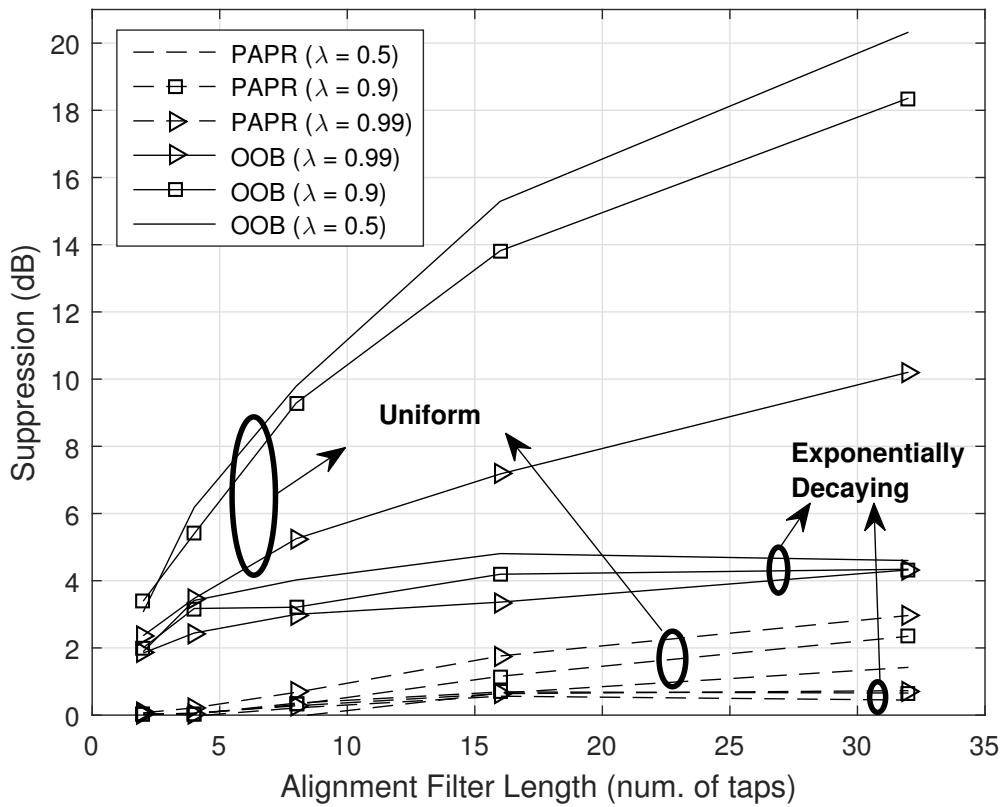


Figure 3.7 OOB leakage suppression and PAPR mitigation performance for uniform and exponentially decaying filters with different alignment filter lengths ( $\alpha = 0.25$ ).

## CHAPTER 4

### FLEXIBLE RADIO ACCESS BEYOND 5G: A FUTURE PROJECTION ON WAVEFORM, NUMEROLOGY AND FRAME DESIGN PRINCIPLES <sup>1</sup>

#### 4.1 Introduction

Exponential growth in variety and quantity of mobile devices along with the mobile applications lead to an explosion in the need for higher data rates, reliability, power efficiency, low latency and vast number of diverse connectivity [5, 47]. Such needs are the main driving factors in 5G and many projects have been launched to deliver them on time, as done in European Union projects e.g., 5GNOW [6], METIS [7], MiWaveS [8] and FANTASTIC-5G [9]. Mainly, three services in 5G agenda can be given as; eMBB, ultra reliable and low latency communications (URLLC) and massive machine type communications (mMTC). The standardization has already started by 3GPP and the first products are expected to be available by 2020.

Although there is not an expectation of a major shift in base waveform selection for 5G new radio (NR) <sup>2</sup>, the need for flexibility is strongly highlighted for embracing diverse applications, channel conditions and system scenarios [48]. For example, large subcarrier spacing is preferable for URLLC applications due to the smaller symbol time. It is also better for highly mobile users because of the robustness against Doppler spread. On the other hand, small subcarrier spacing is more convenient for supporting massive connectivity which is required for mMTC scenarios and for reducing the effect of delay spread. Considering numerous cases as these examples, academia and industry agreed on the need of more flexible radio access technologies (RATs). Thus, usage of resource blocks with different parameters can be enabled and various user requirements can be met

---

<sup>1</sup>This chapter was published in IEEE Access, 2017 [46]. Permission is included in Appendix A.

<sup>2</sup>OFDM will remain as the base technology for 5G NR.



properly. For that purpose, co-existence of different numerologies, i.e., different parameterization of different subframes, have been intensively discussed in ongoing 5G standardization activities [49].

As a matter of fact, the number of users and the diversity in user requirements, e.g., demanded services, channel conditions, used applications, types of mobile devices etc., are going to keep increasing with the lapse of time. For example, in a forecast provided by [50], the number of smartphone users will be 264.3 million in the United States by 2021, while it was 189 million in 2015. As a result of a global projection of that increase, monthly mobile data traffic will reach up to 30.6 exabytes which is eightfold of the one in 2015 [51]. Such a growth in traffic will likely lead to some enhancements on current concepts such as operation in much higher frequencies beyond the currently discussed mmWave bands ( $<100$  GHz), deployment of more antennas than the presented massive-MIMO systems. In this case, current problems faced in these concepts will definitely be more severe. On the other hand, researchers should get ready for brand new problems as well, with the development of the novel future concepts which are hard to predict for the time being. Considering these facts, potential future scenarios will lead to an increase in aforementioned radio access flexibility requirement for the standards beyond 5G. However, the majority of the current discussions on flexibility for the RATs in NR design are conducted in a limited range by only focusing on adopting OFDM-based waveform parameters. Reviewing the user requirements along with the trend from 2G to potential 5G technologies, we believe that the definition of radio access flexibility should gain a much broader meaning for meeting the future service needs optimally. Therefore, in this chapter, we discussed some potential directions and provide our proposals on RATs that enable much more flexibility for standards beyond 5G. In order to avoid any confusion in terminology, let us define the fundamental terms of RATs in the context of our discussions and wireless communications literature.

- **Waveform:** Signal shape in the physical medium formed by a specific method. We consider waveform as the most basic component of RATs.

- Numerology: Waveform parameterization to form resource blocks based on user requirements and channel conditions. It could be applied to all the users uniformly, or specifically to user subgroups having similar requirements.
- Frame: The data unit encapsulating the resource blocks generated for the users in the system. It can be formed using single or multiple numerologies.

The core discussions of this chapter are conducted on the flexibilization of these three elements representing the RATs. These elements and the challenges to be addressed in order to achieve the future expectations beyond 5G are visualized in Fig. 4.1. Our contributions in this direction can be given herein as follows:

- Selected waveform technologies and their flexibility aspects considering the basic waveform expectations are analyzed.
- Promising concepts are proposed for more advanced parameterization schemes in numerology design.
- Novel frame design principles are proposed and a framework is provided for developing more flexible radio accessing schemes.
- Potential solutions for the issues of future heterogeneous cellular systems are discussed utilizing flexible RATs.
- Future research directions to develop more efficient multiple accessing schemes using flexible RATs are provided.

In the rest of the chapter, we provide a historical overview on flexible signaling and radio accessing schemes from 2G to 5G in Section II. Then, discussions evaluating the selected waveform technologies are provided in Section III. In Section IV, potential improvements upon the numerology design principles are proposed in order to serve various users more properly with the existing waveform technologies. In Section V, we introduce new frame design concepts based on the proposed numerology principles and two different numerology containment strategies. The first strategy is

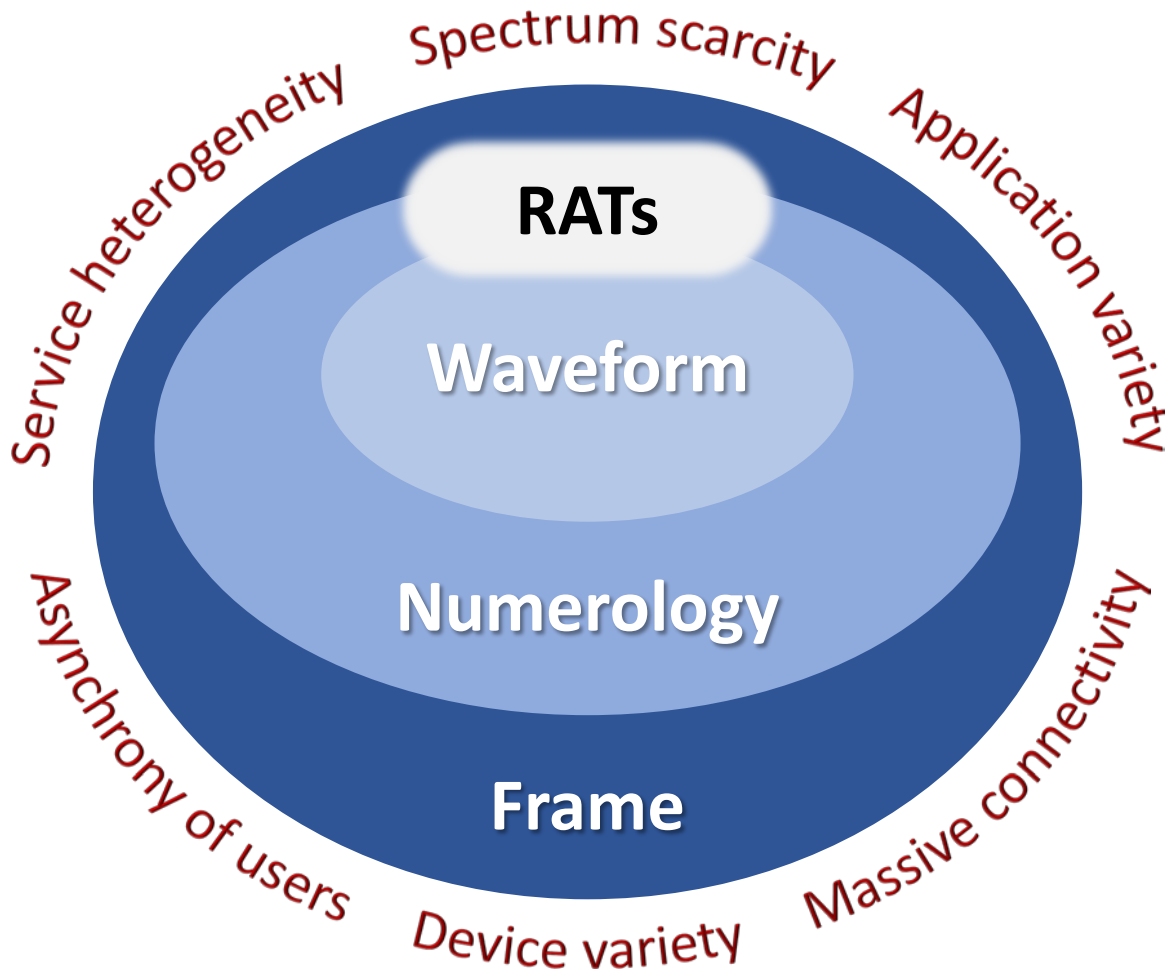


Figure 4.1 Future wireless communication challenges aimed to be addressed by flexible RATs components.

based on forming the frame with numerologies set by *one-waveform and multiple-parameter*, while the second strategy expands that to a hybrid frame consisting of *multiple-waveform and multiple-parameter* numerologies. Then, the role that will potentially be played by the flexible RATs for handling the problems of future cellular systems is discussed in Section VI. Finally, how different multiple accessing schemes can be enhanced using flexible RATs is discussed in Section VII, and Section VIII concludes the chapter.

## 4.2 A Historical Overview on Flexible Signaling and Radio Access Schemes

Flexible signaling was introduced to cellular communications as early as 2G standardization via link adaptation techniques, e.g., power control, adaptive modulation and coding (AMC) [52–55]. Such methods improved the user experience by satisfying user needs in various ways [56]. For example, with AMC, users with low SNR could still receive the data by maintaining the error performance with lower coding rates or low order (less sensitive) modulations, while users with higher SNR are able to experience higher data rates [57]. Also, via power control techniques, SNR of a user can be controlled and a balance between the error performance and power efficiency is provided.

Link adaptation techniques operate based on the observed SNR without considering the elements forming the noise<sup>3</sup> effect on the signal. If the increase in the error rate occurs due to the insufficient received power compared to the thermal noise floor, aforementioned link adaptation techniques are quite useful for sustaining the communication quality. However, degradation in SNR might also be caused by interference effects (self-interference, other user interference) and hardware impairments, and link adaptation techniques are usually ineffective in such cases [58]. At this point, waveform design emerges as another degree-of-freedom to cope against various signal distortions and interference types. By adapting the waveform parameters properly, wireless signals can easily gain more robustness against interference [59] and maintain the communication performance [14]. For example, if the time dispersiveness of the medium increases for any reason, extending the CP rate as much as the increase in time dispersion avoids inter-symbol interference (ISI) for OFDM-based signals at the expense of some degradation in spectral efficiency. In addition, different waveform technologies exhibit different inherent advantages under specific scenarios and circumstances [60]. Therefore, flexibility in waveform selection and parameter adaptation based on varying medium and user conditions are very critical to optimize the communication performance for all the users.

The early indications of the paradigm shift from the constant waveform design is seen in 4G standardization for all the links. In Evolved Universal Mobile Telecommunications Service (UMTS) Terrestrial Radio Access (E-UTRA), usage of different waveforms was proposed for the first time

---

<sup>3</sup>Noise represents all the distortion sources in the given SNR expression, here.

to address the different requirements in the UL and downlink (DL) [61]. As a matter of fact, DL prioritizes spectral efficiency to satisfy the data hungry users whereas power efficiency is more critical in the UL to minimize the power consumption of the size limited and battery operated mobile terminals. Therefore, OFDM is used for the DL while the single carrier-frequency division multiple accessing (SC-FDMA) is deployed for the UL [62]. Also, in LTE-Advanced (LTE-A), the first flexible parameter utilization is offered for OFDM based waveforms. Depending on the cell size, OFDM symbols are designed with either normal CP or extended CP at the base station in order to maintain interference-free communications [63]. These steps could be considered as the initial phase of the transition from the fixed waveform to the flexible waveform paradigm. However, provided flexibility still remains very limited since all the users in a cell are still forced to operate with a predefined waveform even if they have different requirements.

In order to address the diversified user requirements more conveniently, the trend in 5G standardization is to extend waveform flexibility to additional parameters such as subcarrier spacing [64]. For carrying that out, the concept of multiple numerology usage, i.e., assigning specific numerologies to the subgroups formed by users with similar requirements/channel conditions, is proposed and mostly accepted in 3GPP discussions [65,66]. This concept constitutes a critical milestone in the development of flexible RATs, however, peaceful coexistence of different numerologies should be investigated carefully.

### 4.3 Flexibility in Waveform Design

Many waveform schemes addressing various issues have been proposed in the literature so far and each of them provides different advantages on different use cases and medium conditions. In 3GPP standardization discussions, OFDM-based technologies have become prominent especially for broadband systems because of their tempting advantages experienced in the previous generation and backward compatibility with the existing technologies [67]. However, OFDM is not the optimum waveform for meeting all the user requirements and has serious shortcomings in some specific scenarios. Based on the applications, channel conditions and user requirements, alternative waveforms have obvious advantages and flexibilities not present in OFDM. For example, inherent

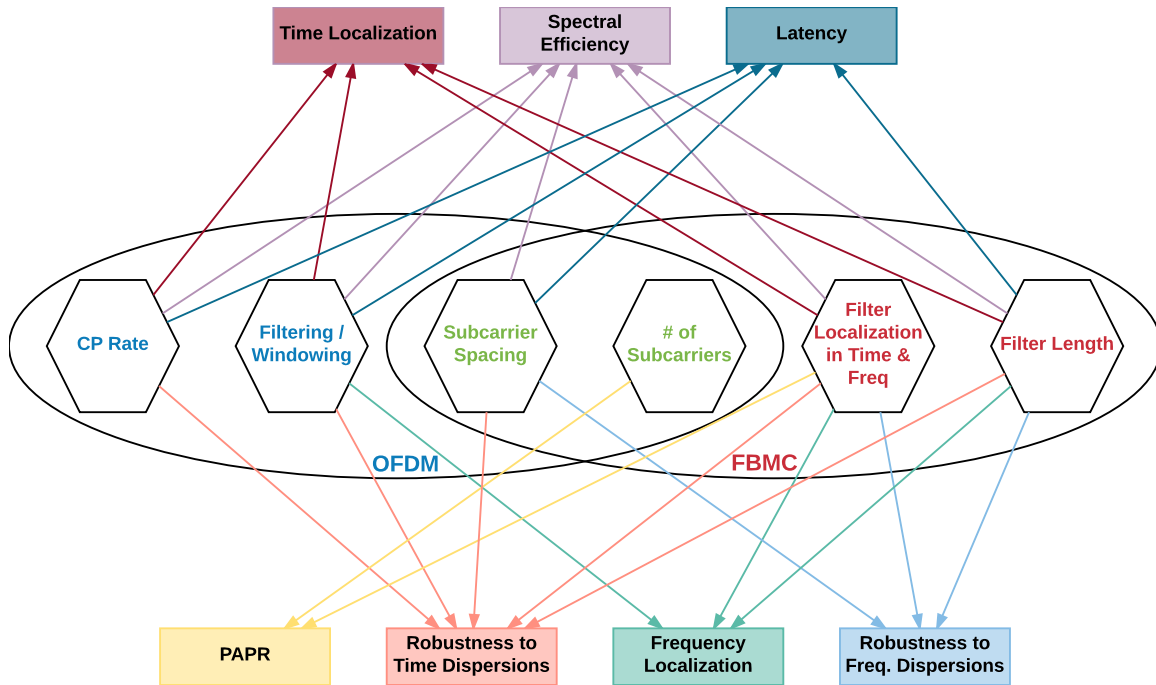


Figure 4.2 The various parameters of OFDM and FBMC waveforms and the physical metrics they primarily affect (Further indirect relations could be considered, however, only the primary relations are embodied for the sake of clarity).

rectangular pulse shaping of OFDM symbols forms the OFDM subcarriers with a sinc function. Therefore, a significant interference on the neighboring frequencies occurs due to the combination of many subcarrier sidelobes. Also, sinc shaped OFDM subcarriers are very sensitive to channel frequency dispersions and not preferable for highly mobile scenarios. On the other hand, FBMC allows subcarrier based filtering with various pulse shaping functions, and forms the time-frequency characteristics of the signal flexibly. Therefore, aforementioned OFDM problems can easily be solved by FBMC with a frequency localized pulse shaping function such as root-raised cosine (RRC).

As a matter of fact, each waveform technology is formed by their own specific parameters. Since these parameters constitute the flexibility aspect of waveform design, their investigation is critically important for future RATs. However, our goal is to introduce a framework for designing flexible RATs beyond 5G, rather than a detailed investigation of existing technologies. Therefore, our arguments and concept proposals will be provided for two fundamental waveforms, OFDM and

FBMC, for the sake of a clear presentation. However, proposed concepts can be generalized over other popular waveforms such as UFMC and GFDM as well.

Various waveform parameters representing the flexibility aspects of OFDM and FBMC are summarized and matched with the main waveform requirements in Fig. 4.2. Note, more parameters and further relations between these parameters and metrics could be established. However, our goal is to draft the general picture containing various metrics that could be primarily controlled by widely known given parameters. These parameters will also be re-visited for the later sections in which we discuss the potential concepts for developing a fully flexible radio accessing scheme including the proposals on numerology and frame design principles.

### 4.3.1 OFDM

OFDM is firstly proposed in the 1960s by Chang [68] and Saltzberg [69], and became very popular following the development of FFT algorithm. A basic block diagram of its transceiver is given in Fig. 4.3. It has already been widely deployed in previous wireless digital communication standards such as LTE and Wi-Fi because of its tempting advantages, e.g., low-complexity implementation and the robustness against multipath channels with single-tap FDE [70]. However, plain OFDM signals have high PAPR as a result of parallel signal transmission, and therefore, suffer from the distortions due to the non-linear characteristics of the PAs [12]. In addition, sinc shaped subcarriers make OFDM vulnerable against Doppler spread and result in a high OOB radiation which degrades the efficiency of overall spectrum utilization. Considering these advantages and shortcomings, the main parameters representing the flexibility aspect of OFDM can be given as follows.

- CP Rate: One of the most critical and characteristic parameters of OFDM is CP which enables converting the linear convolution of the wireless channel and signal to a circular convolution, and facilitates the single-tap FDE. When CP length is determined as large as the delay spread, an ISI-free transmission is guaranteed. Therefore, CP rate directly provides robustness against the time dispersion effect of the wireless medium. Also, CP enables compensation of timing errors unless the error is smaller than the CP duration [71].

In addition to these advantages, CP could be exploited for many useful receiver operations such as signal parameter estimation [72], synchronization [73] and channel estimation [74] without pilot signals, i.e., blindly. However, increasing CP rate results in a degradation in spectral efficiency along with more latency and the introduced cyclic features might degrade the signal security [75].

- Windowing/Filtering<sup>4</sup>: In order to suppress OOB leakage, transmitter windowing and filtering operations are well-accepted methods in the literature because of their low complex implementation and compatibility with the conventional receivers. Also, windowing at the receiver reduces the interference received from adjacent channels [76]. However, they require an extension in CP size for maintaining ISI-free transmission which decreases the spectral efficiency and increases the latency.
- Subcarrier Spacing: Multicarrier systems inherently provide robustness to time dispersions by dividing the wide transmission band into smaller subcarriers whose bandwidth is less than the coherence bandwidth. However, that cause a serious extension in symbol time and in highly mobile/time-varying medium, OFDM signals may seriously suffer from Doppler spread if the channel response significantly changes within a symbol duration. Therefore, subcarrier spacing should also be large enough to keep the symbol time shorter than the effective channel coherence time [77]. This is also critical for users demanding low latency requiring services [78] and mmWave systems that experience high phase noise with increasing carrier frequency. Yet, reducing symbol time corresponds to a proportional increase in CP rate for a given CP length and therefore, degrades the spectral efficiency.
- Num. of Subcarriers: Data transmission speed is directly related to the bandwidth and the only way of increasing it for a given subcarrier spacing is to increase the number of subcarriers. However, this corresponds to parallel transmission of more signals which leads to a proportional growth in PAPR problem [79].

---

<sup>4</sup>Windowing and filtering based OFDM signals are also considered as different waveforms in the literature, i.e., filtered-OFDM and WOLA-OFDM. However, we prefer to include them in OFDM parameters for providing a better understanding of OFDM flexibility.



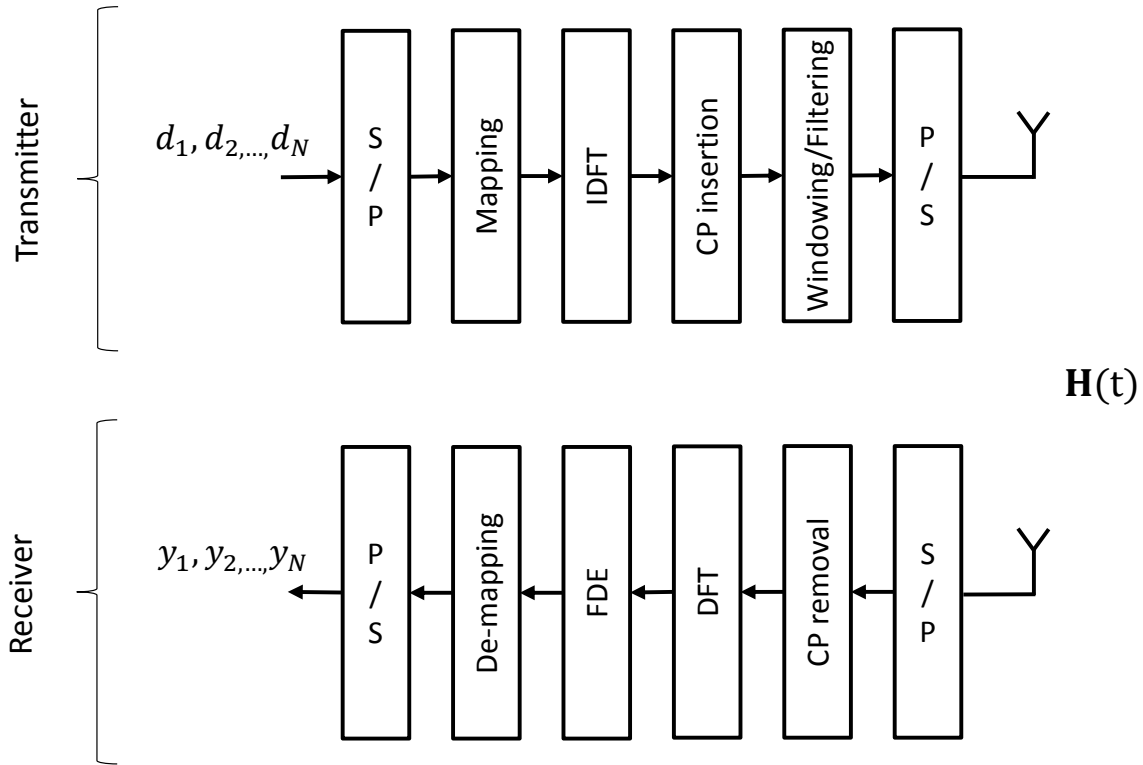


Figure 4.3 OFDM transceiver block diagram including windowing and filtering.

Backward compatibility with the existing technologies along with the aforementioned advantages makes OFDM an appealing technology. Therefore, the primary waveform preference will be in favor of OFDM rather than going for a new waveform, as can be seen in the current standard discussions [19–21] conducted for 5G. However, alternative schemes, e.g., GFDM, UFMC and FBMC, offer critical advantages over OFDM in various scenarios and should still be considered for future standards.

### 4.3.2 FBMC

FBMC is one of the most well known multicarrier modulation methods in wireless communications literature whose basic transceiver block diagram is given in Fig. 4.4. It is also discussed as a waveform candidate for 5G and beyond in [11]. Its main advantages stem from the shaping ability of each subcarrier individually and the availability of many pulse shaping filters in the literature as

drafted in [12]. There are filters fully orthogonal in both domains while being very sensitive against impairments in one domain, e.g., rectangular, raised cosine, Mirabbasi-Martin etc. On the other hand, non-orthogonal pulse shaping functions such as Gaussian and Prolate introduce some interference between neighboring symbols but confines the pulse energy well in both domains. Freedom in selecting any of these filters facilitate a great flexibility in the utilization of spectral resources along with meeting various user requirements such as robustness against channel dispersions. For example, a rectangular filter is preferable for time dispersive channels while raised cosine filter is more robust against frequency dispersion. Many other pulse shaping filters are investigated in the literature to cope against channel dispersions and to provide a reliable system design based on different scenarios [12].

Besides the filter selection flexibility of FBMC, filter specific parameters could be used to enable more sensitive adjustments in filter characteristics and enhance the flexibility further. Additionally, unlike OFDM, there is no CP or guard time requirement in FBMC. Therefore, spectral efficiency is not degraded by such redundancies. Some of the important parameters providing flexibility in FBMC waveforms can be given as follows.

- **Filter Length:** Especially for ideally infinite filters, this is an important parameter. Keeping the filter length shorter reduces the effect of one symbol on other successive symbols. Also, latency could be decreased by truncating filter tails for small size frames. However, truncation corrupts the ideal structure of these filters and cause orthogonality loss in the time domain and spectral growth in the frequency domain.
- **Filter Localization in Time/Frequency:** For a given filter length, time and frequency domain localization of various filters could be adjusted in a trade off fashion by filter specific parameters, e.g., the roll-off factor ( $\alpha$ ) of RRC and standard deviation ( $\sigma$ ) for Gaussian filters. This is a significant advantage for adapting the signal against varying channel effects, i.e., dispersion in time and frequency domains. For example, making filters more frequency localized increases the robustness of signal against Doppler spread. On the

other hand, time localized filters are better for time dispersive channels and also prevent the filter tails from being added on top of consecutive symbols which lowers the PAPR.

*"Subcarrier spacing"* and *"number of subcarriers"* have similar effects as explained for OFDM. Therefore, they are not given for FBMC, separately.

Despite all the advantages offered by FBMC, implementation and equalization are not as simple as OFDM for many scenarios and this constitutes its primary drawback [13]. Also, usage of long filters introduces an excessive computational complexity for MIMO detection as the channel coherence bandwidth would fall below the subcarrier bandwidth [80], which would cause a problem in one of the most popular services in 5G. However, aforementioned advantages still keep its potential for many of the future applications and scenarios.

#### 4.4 Flexibility in Numerology Design

Providing the aforementioned flexibility requirements by utilizing the parameters of a single waveform is not possible as each technology has its own advantages and drawbacks. If a novel waveform technology addressing all the user requirements and channel conditions could be developed and widely accepted by the academia and industry, a system design with a single waveform would be possible. However, the existing technologies can only provide a different trade-off for a given set of parameters. Therefore, the only option for a sufficiently flexible radio access is to enable the coexistence of multiple numerologies as proposed in the 5G standardization. However, currently proposed numerologies provide a limited flexibility due to the fix parameterization strategy. In this section, we discuss how to apply more advanced waveform parameterization methods to achieve further flexibility in numerology design.

Since OFDM is the dominant candidate as the base waveform of 5G technologies, current numerology discussions are mostly done on OFDM parameters, e.g., CP rate, subcarrier spacing etc. To the best of our knowledge, one of the first schemes proposing the usage of multiple numerologies is presented in [81] for OFDM blocks divided in the time domain. Based on the user needs, these blocks are generated with different CP sizes and subcarrier spacings, and successively aligned (i.e., consecutively transmitted) in the time domain. Since OFDM is a well-localized waveform in time

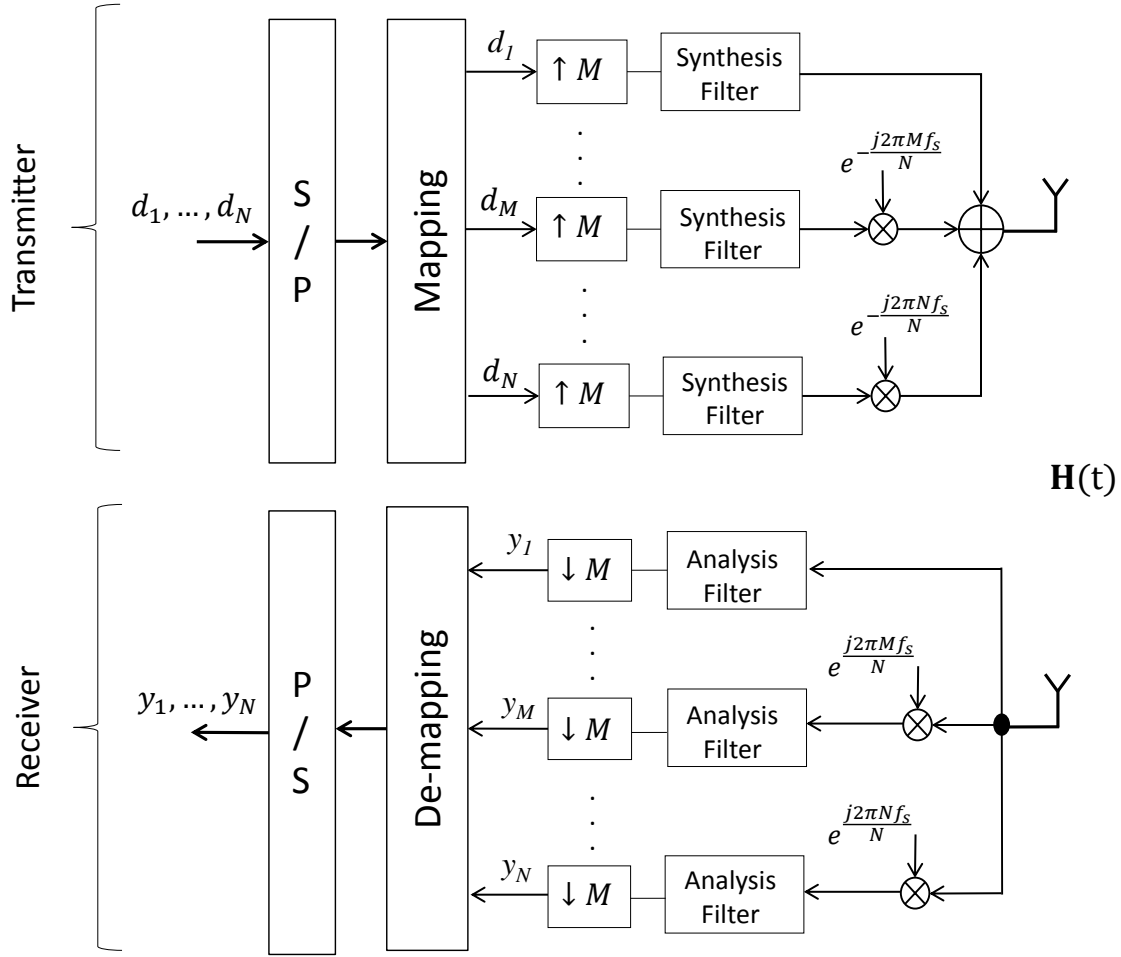


Figure 4.4 FBMC transceiver block diagram.

domain, orthogonality between the consecutive blocks (subframes) is perfectly maintained as well. However, limiting the placement of numerologies only to time domain prevents a fully flexible utilization of time/frequency plane especially for the users requiring different numerologies at the same time. Therefore, aligning different numerologies in the frequency domain is also included in 3GPP discussions even though there will be a non-orthogonality issue between the subframes.

A similar numerology design can also be considered for FBMC schemes in terms of FBMC parameters. Prototype filters, filter specific parameters and subcarrier spacing values could be selected based on the user groups to provide a proper service. In order to show how such a parameterization affects the time-frequency characteristics of FBMC numerologies, an illustration of

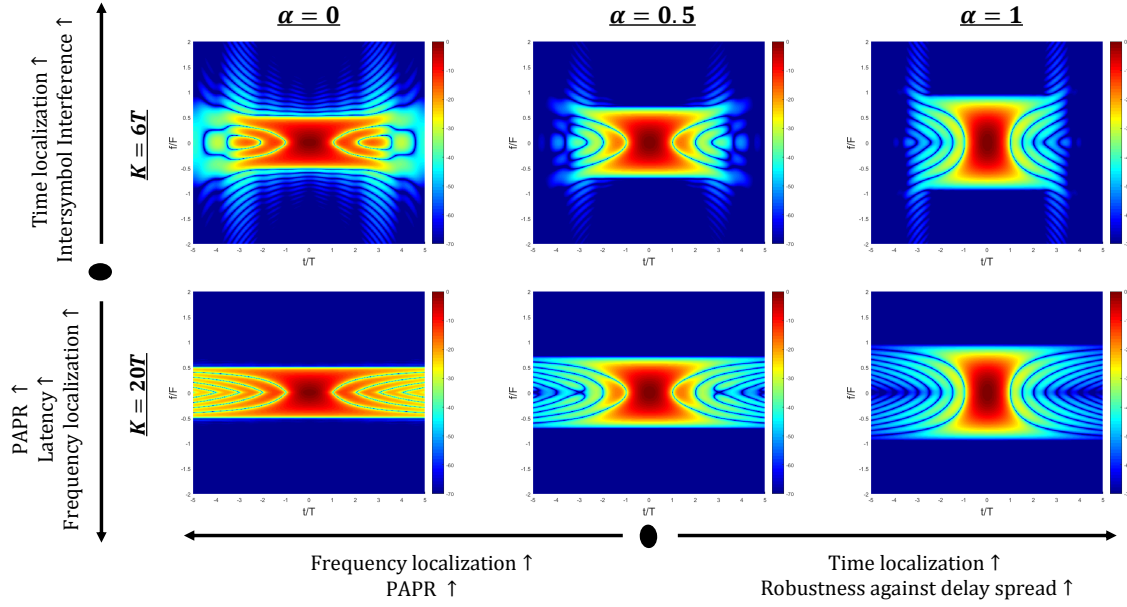


Figure 4.5 Ambiguity functions ( $10\log_{10}(|\mathfrak{S}(\tau, \nu)|^2)$ ) generic root-raised cosine filters generated with various design parameters, used for adapting signal characteristics in time and frequency domains.

RRC filters with different roll-off factors ( $\alpha$ s) and filter lengths ( $K$ s) is provided in Fig. 4.5 via ambiguity functions (AFs). which is a two-dimensional correlation function in the time-frequency plane, whose analytical expression is given as

$$\mathfrak{S}(\tau, \nu) = \int_{-\infty}^{\infty} p_{\text{tx}}(t + \frac{\tau}{2}) p_{\text{rx}}^*(t - \frac{\tau}{2}) e^{-j2\pi\nu t} dt, \quad (4.1)$$

where  $p_{\text{tx}}(t)$  represents the transmitter filter and  $p_{\text{rx}}^*(t)$  is the complex conjugate of receiver filter. By taking the projection of the receiver filter on the transmitter filter, AFs not only show the distribution of pulse energy in time and frequency domains but also visualize the required time/frequency offset values for keeping the filters orthogonal. In another aspect, AFs illustrates the filter robustness against ICI/ISI due to different effects, such as the dispersion of the wireless channel.

As seen in Fig. 4.5,  $\alpha$  and  $K$  are very critical parameters for RRC shaped signals and should be selected carefully considering the user requirements and channel conditions. Although the examples are given over RRC pulses, aforementioned statements are also valid for different pulse shaping functions. Considering their inherent advantages, alternative filters along with their design

parameters should also be considered in FBMC numerology design for meeting the user requirements more properly [82].

FBMC numerologies would be very convenient for different users sharing the frequency resources at the same time. Since FBMC blocks can be designed as well localized in frequency domain, orthogonality between the different numerologies will not be lost when they align in frequency domain unlike the case with OFDM numerologies. From that perspective, OFDM and FBMC numerologies are perfectly complementing each other.

Aforementioned numerology design, based on user specific determination of the parameters such as CP and subcarrier spacing in OFDM and prototype filters in FBMC, definitely provides important flexibility features for an efficient sharing of the spectral resources. However, in order to enable further flexibility and increase the overall efficiency, different parameters and more advanced parameterization methods should be jointly considered. For example, in OFDM signals, there are other critically important parameters such as windowing which can be utilized to develop much-advanced OFDM numerologies. A good example of this claim is presented in [24] where the size of windowing functions are gradually applied within a subframe. By keeping the total guard interval the same, edge subcarriers are designed with more windowing while the inner subcarriers have lower windowing. Since the OOB leakage mostly occurs due to the edge carriers, interference emission of the OFDM block is well suppressed while the inner subcarriers conserve their robustness against larger delay spreads. By performing an OFDM numerology design with this concept along with a proper scheduling, a subgroup of the users could be served in the same numerology much more properly. The users experiencing higher delay spreads could be assigned to the inner subcarriers while the ones with low delay spread can utilize the edge subcarriers [83]. By doing so, no need remains for a separate numerology design for the users with different CP requirements, which is a great advantage compared to the classical numerology design strategies. An illustration of this advanced parameterization is exemplified in Fig. 4.6 which is referred to as edge-windowed OFDM numerology. As seen in this example, usage of such parameters and parameterization methods can enable much flexible numerology designs. Also, there is an obvious research gap in this direction considering other various windowing and filtering techniques as presented in [84].

A similar parameterization strategy is proposed in [85] for filtered multitone (FMT) mode of FBMC schemes. Rather than using a prototype filter for all the users, user-specific filters are dynamically utilized to control the effect of time and frequency dispersions, i.e., ISI and ICI. RRC filters are deployed for this study and filter adaptation is done with  $\alpha$ . This strategy is presented for a specific scenario, however, it could be generalized for forming more flexible numerologies. For example, if the interference between successive blocks in time is the main issue, edge symbols in time can be shaped with sharper filters in time domain (designed with larger  $\alpha$ s) as illustrated in Fig. 4.6 which is referred to as edge-filtered FBMC numerology. For the same purpose, shorter filter lengths can also be applied to the edges. One may note that such methods might introduce some ICI for the edge symbols due to the expansion in frequency caused by either filter truncation or larger  $\alpha$  usage. However, by assigning those symbols to the users that are more computationally capable and be able to perform interference cancellation, error performance can be maintained and energy leakage from the FBMC block can easily be controlled in time domain.

In order to understand the effect of such techniques and compare with the classical approaches, power emission of OFDM subcarriers in frequency domain and FBMC filter tails in time domain are given in Fig. 4.4 and Fig. 4.4. For OFDM, 64 edge subcarriers on the right side are windowed with a raised cosine function where  $\alpha = 0.1$  and no windowing is applied for the 64 subcarriers on the left side (having negative indices). Then it is compared with no windowing and regular windowing approaches. Similarly, 64 FBMC symbols on the right edge are shaped with an RRC filter whose  $\alpha$  is 0.1 while the symbols on the left side are shaped with an RRC having  $\alpha = 0$ . Then it is compared with regular prototype filtering for  $\alpha = 0$  and  $\alpha = 0.1$ . As obviously seen, edge operations are significantly suppressing the sidelobe/tail energies on a target region while providing more flexible numerology structures.

It should be noted that these examples are only given to express how such concepts can enable a flexible numerology design for a given waveform and to fix specific problems such as the interference emitted by numerologies. Considering different problems, user needs, system requirements and waveform parameters many research opportunities can be created in flexible numerology design context.

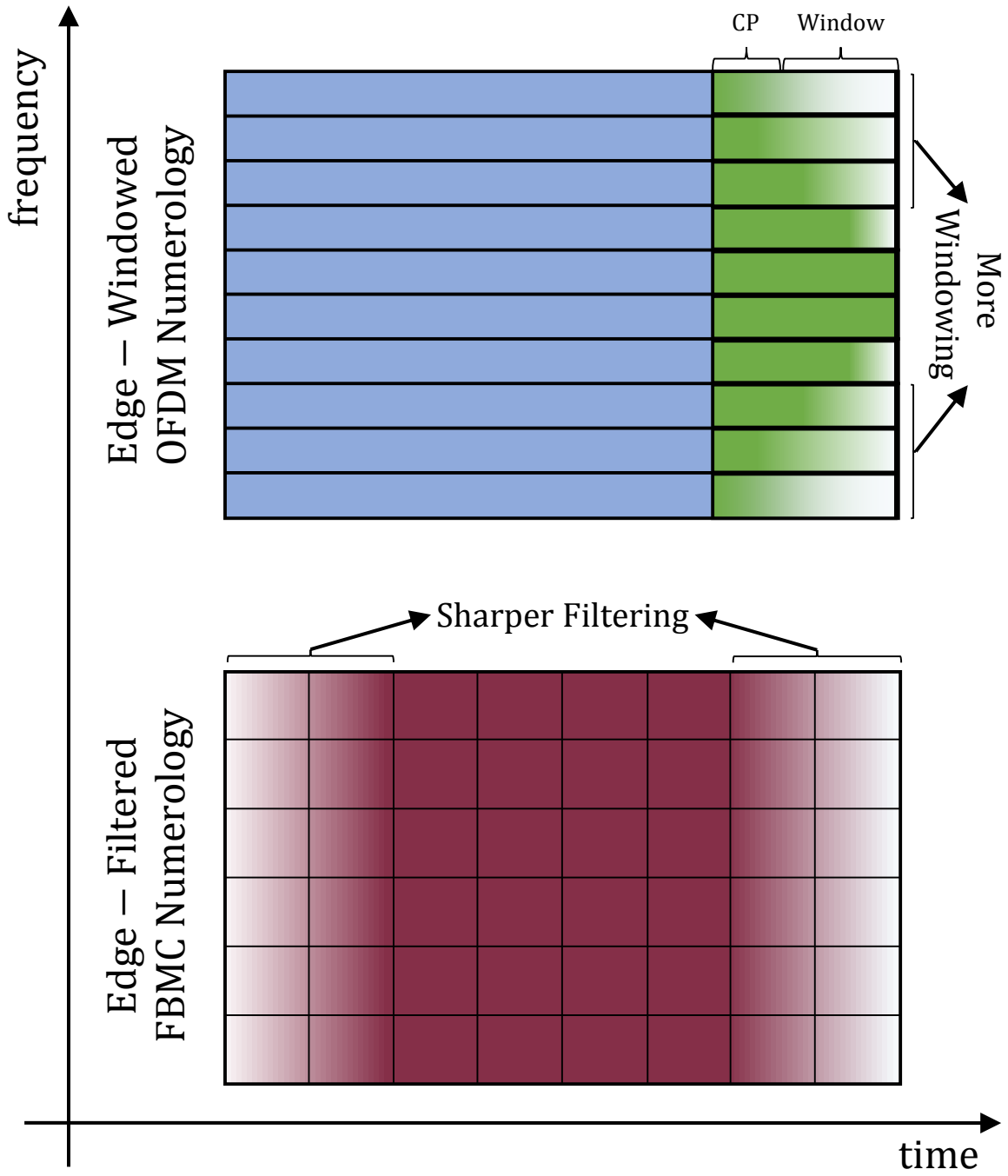


Figure 4.6 Two samples of flexible numerology design: Edge-windowed OFDM and edge-filtered FBMC numerologies.



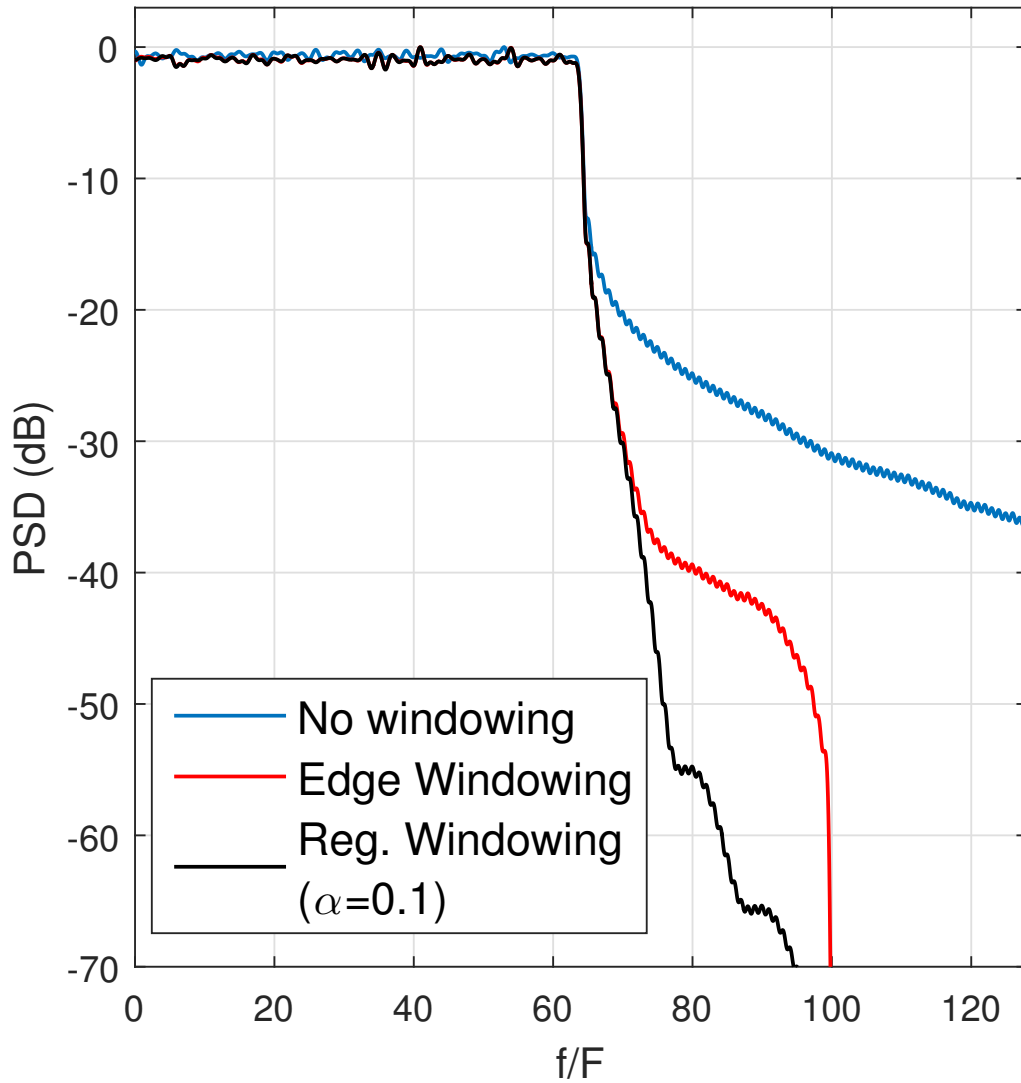


Figure 4.7 Power leakage of OFDM subcarriers (sidelobes) windowing techniques and conventional approaches.

#### 4.5 Flexibility in Frame Design

In order to provide a complete picture of our future vision, in this section, we raise the question of how to form flexible frames in the light of our earlier discussions and proposals. We firstly discuss how to improve the existing frame design paradigm where multiple numerologies based on a single waveform coexist in one frame. Secondly, in order to provide further flexibility

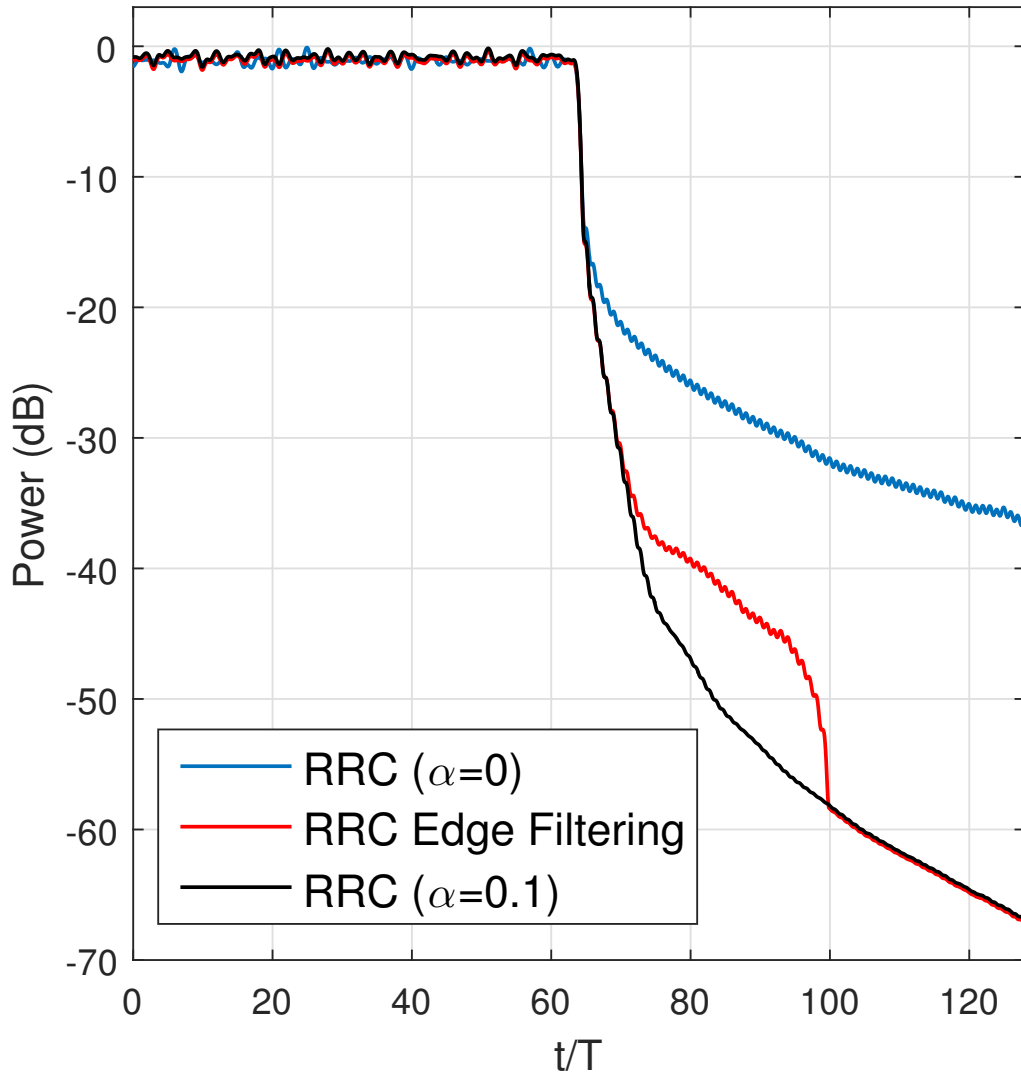


Figure 4.8 Power leakage of FBMC filters (tails) for edge filtering techniques and conventional approaches.

and spectral efficiency for future radio access schemes, we propose and investigate the concept of hybrid frames including multiple numerologies based on multiple waveform technologies.

#### 4.5.1 Single Waveform Numerology-based Frame Design

In single waveform numerology based frame design procedure, frames are formed with multiple numerologies which differ in parameterization while the base waveform technology is the same.

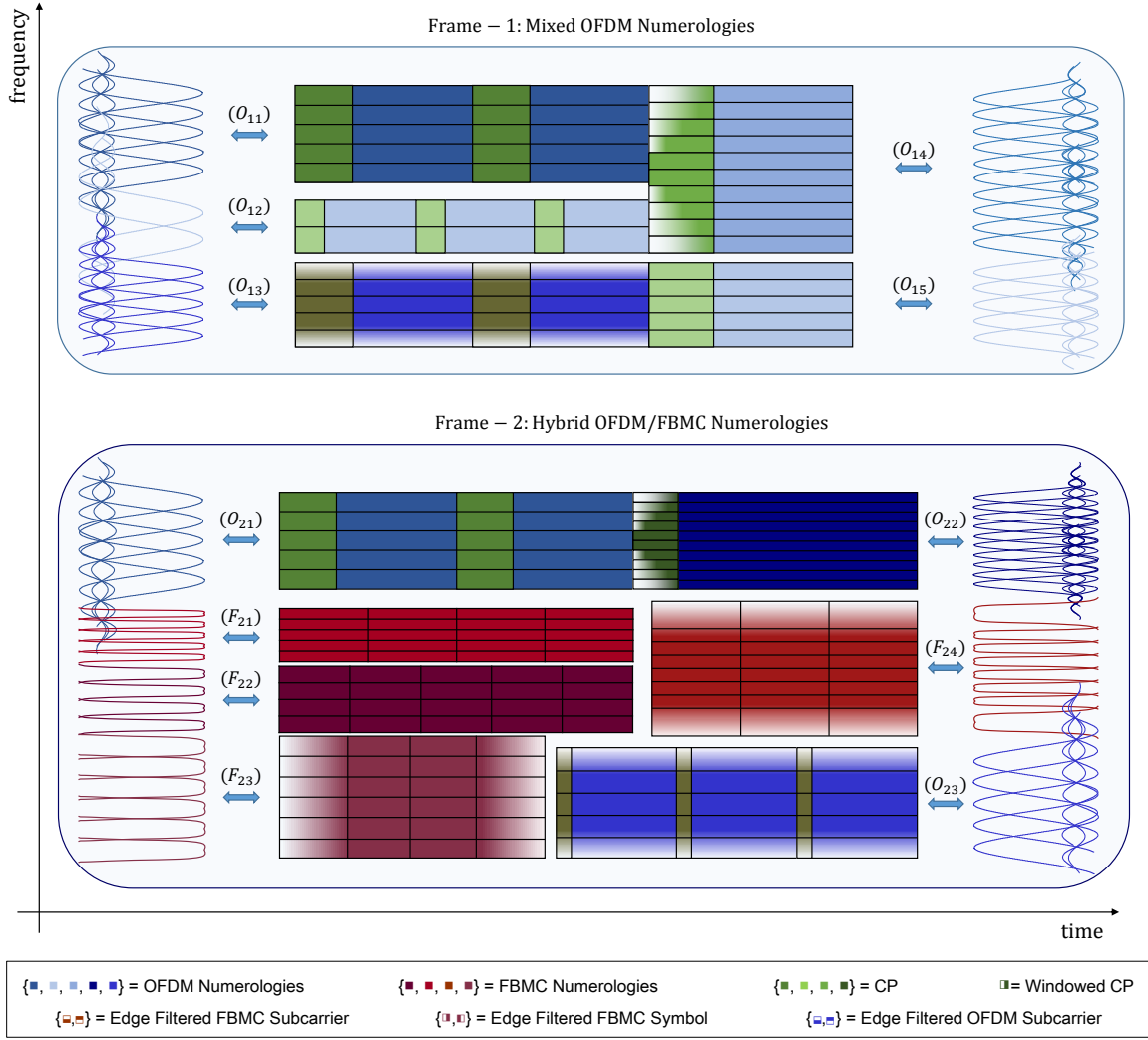


Figure 4.9 Examples of proposed single waveform numerology based frame design (Frame-1) and multiple waveform numerology based frame design (Frame-2) consisting of mixed OFDM and FBMC numerologies (Frame-1 can be considered as an improvement over currently discussed frame designs for achieving more flexibility while Frame-2 extends that flexibility to the usage of multiple waveforms based on the user needs, enabling the system to select the best waveform for each user).

The 5G frame design discussions can be considered in this category since the numerology discussions are mostly conducted on the OFDM waveforms and parameters.

The main issue discussed for multiple numerology based frame design is inter-numerology interference (INI). OFDM based numerologies are fully orthogonal in time domain, however, mismatch in some parameters such as different subcarrier spacings leads to INI in frequency domain.

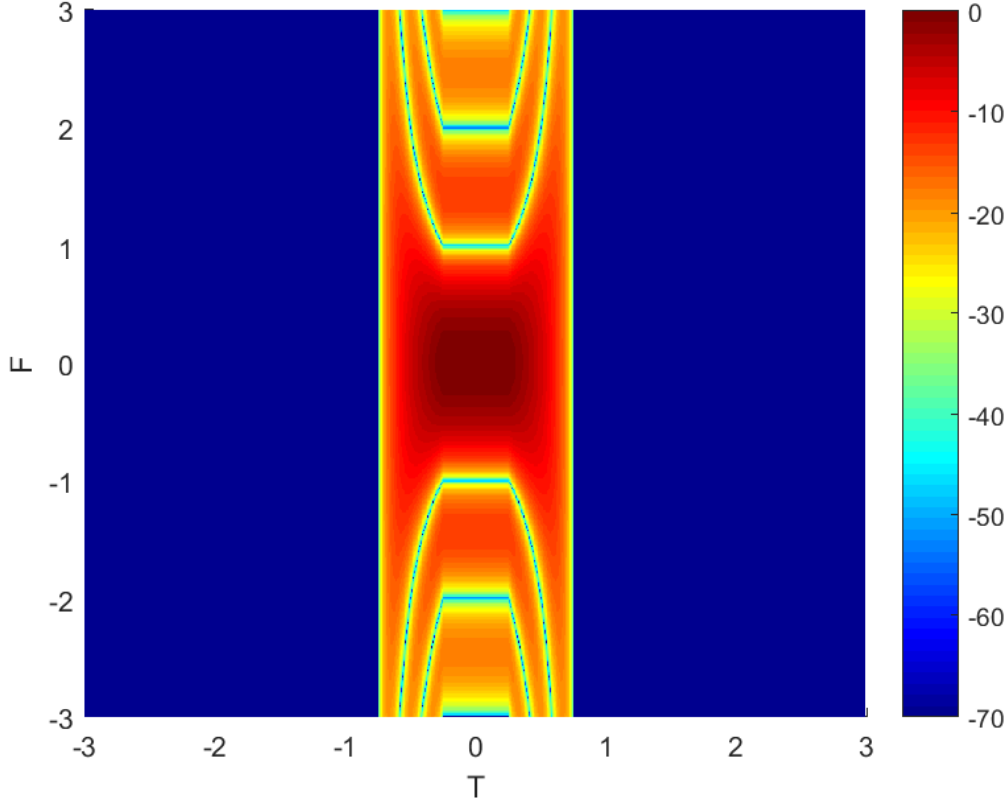


Figure 4.10 AF of two OFDM subcarriers ( $\Delta F_1 = F/2, \Delta F_2 = F$ )

Therefore, coexistence of OFDM numerologies is addressed via OOB leakage suppression of each numerology which is mostly done by applying classical windowing and filtering techniques. Thus, the required guard bands between numerologies could be significantly reduced. However, classical windowing and filtering techniques either require an extension in CP size or introduce ISI as mentioned earlier. Therefore, spectral degradation or signal distortion still remains as an issue to solve. In order to overcome this problem, we propose to deploy aforementioned flexible numerology designs such as the ones generated with edge-windowing. In Fig. 4.9, such a frame structure is exemplified in Frame-1 and an edge-windowed numerology is illustrated ( $O_{14}$ ). When this structure is combined with the proper user scheduling, spectral efficiency and the flexibility can jointly be provided for satisfying a wide variety of user requirements [83]. Note that, edge windowing represents a con-

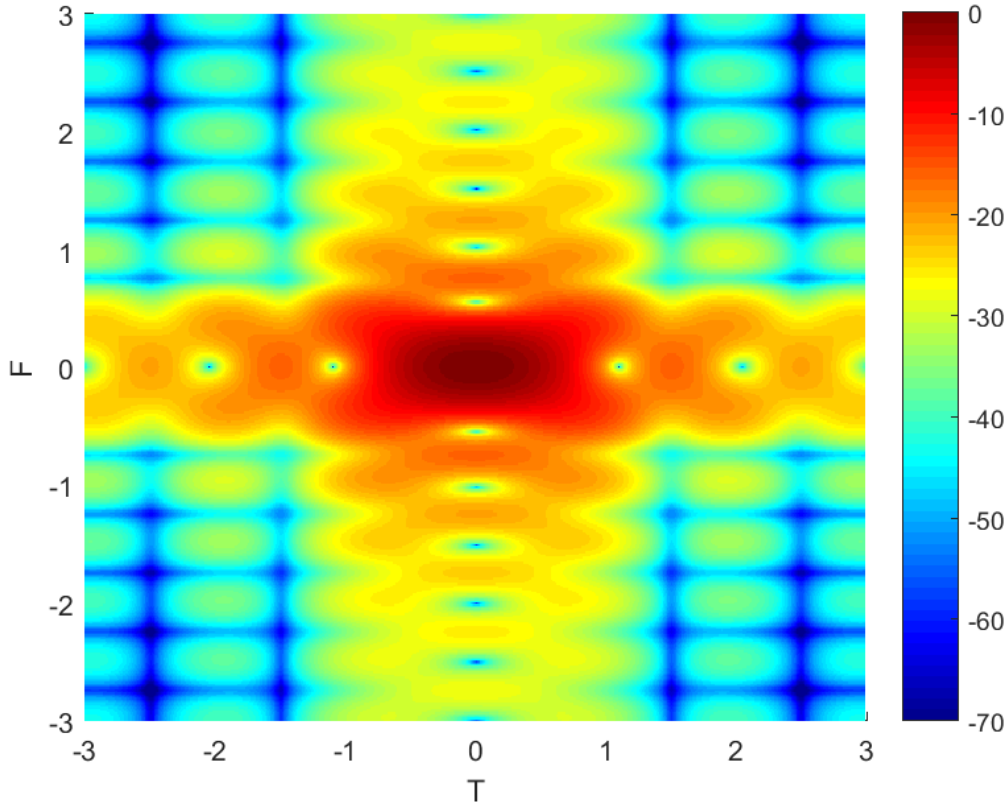


Figure 4.11 AF of an OFDM subcarrier ( $\Delta F = F/2$ ) and an FBMC subcarrier (RRC,  $\alpha = 0$ )

cept here and can be generalized to different techniques with different parameters such as sharper filtering (in frequency domain) of edge carriers as shown in Fig. 4.9 ( $O_{13}$ ).

FBMC numerology based frames should also be evaluated in this context for future standards. Due to the good frequency localization and subcarrier based filtering ability of FBMC numerologies, inherent and complementary advantages can be provided for many scenarios over OFDM based frames. For example, multiplexing different numerologies in frequency domain might be highly preferred for designing a frame with the purpose of serving the users who need multiple services simultaneously. Furthermore, FBMC can easily handle the high mobility scenarios that are problematic for OFDM. All in all, FBMC based frames could close the gaps of OFDM-only based frame deployments. In case of a time domain multiplexing scenario, which is the dual problem of

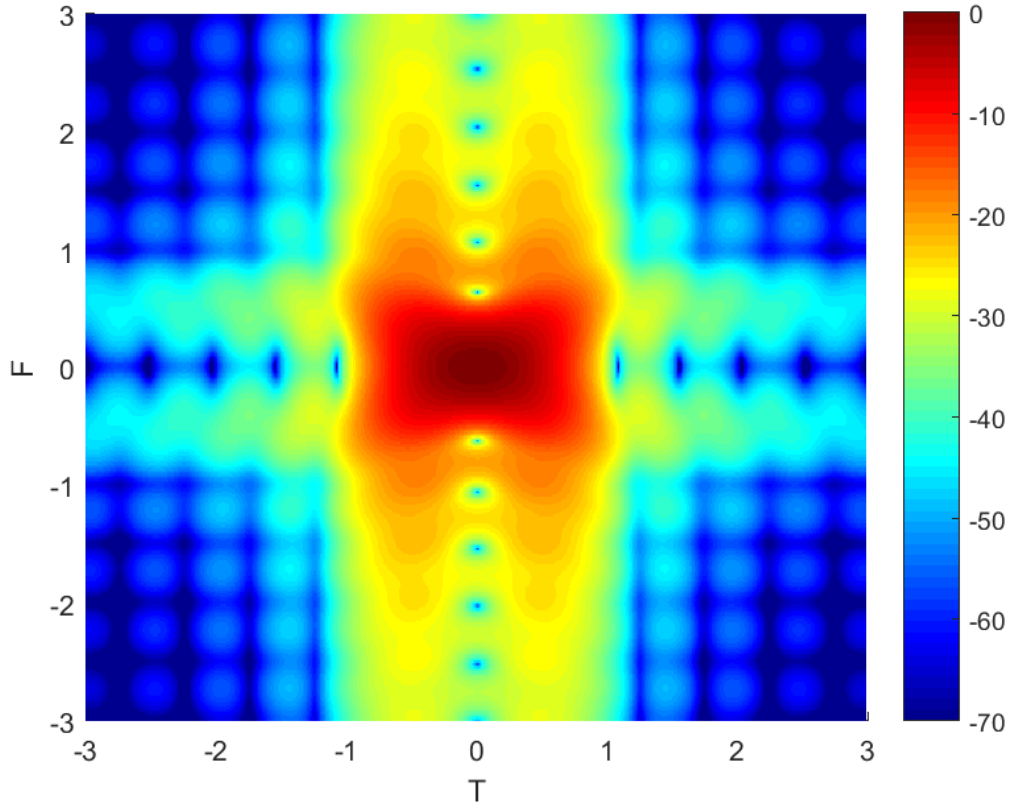


Figure 4.12 AF of an OFDM subcarrier ( $\Delta F = F/2$ ) and an FBMC subcarrier (RRC,  $\alpha = 1$ )

FBMC analogous to the frequency domain multiplexing issue of OFDM numerologies, edge filtering type of concepts can lower the required guard times and facilitate a spectrally efficient frame design.

#### 4.5.2 Hybrid Waveform Numerology-based Frame Design

The agreement on usage of multiple numerologies in the same frame represents a critical milestone and we provided our proposals to enhance this structure via using more advanced numerologies. However, defining multiple numerologies in terms of the same base waveform technology is still a limitation for the flexibility. Therefore, we propose a novel concept of hybrid frame design via the inclusion of multiple waveform based numerologies as illustrated in Fig. 4.9 (Frame-2).

As mentioned in the previous subsection, the main concern in coexistence of multiple numerologies is the INI, which might occur even if they are generated with the same waveform technology. For example, in Fig. 4.5, AF of two OFDM subcarriers with different bandwidths (subcarrier

spacing) is given where  $\Delta F_1 = F/2, \Delta F_2 = F$ . As obviously seen, they are only orthogonal when the narrower subcarrier is aligned with the null of broader subcarrier. That means, half of the subcarriers are interfered for the numerology with smaller subcarrier spacing while all the subcarriers are interfered on the side of numerology with larger spacing. At this point, we raise our question: *Does this issue get worse when different waveforms are used in a hybrid fashion?*

Let us consider two user groups where the group-1 suffers from high delay spread while the group-2 is highly mobile. In the context of 5G discussions, both numerologies would be OFDM based and subcarrier spacing for the group-2 would be determined as larger to increase robustness against Doppler spread. On the other side, smaller subcarrier spacing is more preferable for the group-1 in order to keep CP redundancy lower and to make subcarriers more robust against frequency selectivity. At this point, let us extend this structure to a hybrid frame and allow the group-2 to use an FBMC based numerology whose subcarriers are shaped with RRC filters. From the group specific perspective, FBMC numerology is definitely a better option for the group-2's scenario as the subcarriers could be well-localized and robust against Doppler spread. The critical question here is how an OFDM numerology and FBMC numerology can coexist. Intuitively, an FBMC numerology causes lower interference to an OFDM based numerology on a neighboring frequency compared to another OFDM based numerology with different subcarrier spacing. In Fig. 4.5, this is illustrated via the AF of one OFDM ( $\Delta F = F/2$ ) and one RRC shaped FBMC subcarriers ( $\Delta F = F/2, \alpha = 0$ ). Obviously, periodic nulls exist on time and frequency axes for this example which means coexistence of OFDM and FBMC pulses does not create more severe problems compared to the coexistence of two differently parameterized OFDM subframes. One may point out the interference pattern in time axis of Fig. 4.5, however, proper adjustments on filter parameters would provide a solution as shown in Fig. 4.5 where the RRC filter is generated for  $\alpha = 1$ . For instance, in Fig. 4.9, the guard time requirement between  $(F_{23})$  and  $(O_{23})$  can be decreased via using sharp filters (in time domain) for edge symbols of  $(F_{23})$ . Additionally, adjusting OFDM and FBMC numerologies jointly with aforementioned windowing/filtering methods could also enable a more peaceful coexistence. For example, required guard band between the OFDM numerology,  $(O_{22})$ , and FBMC numerology,  $(F_{24})$ , can be reduced via jointly applying edge windowing and edge filtering techniques.

Considering such examples from a wider perspective including alternative waveform and numerology design strategies, we strongly believe that extending the flexibility in frame design with hybrid waveform numerologies would not only provide a more satisfactory experience to the users with a wide variety of requirements, but also can lead to a more efficient usage of spectral resources.

#### **4.6 Conclusion**

In this chapter, considering the future growth in the quantity of wireless devices, applications and heterogeneity of user requirements, we presented a framework for developing flexible RATs aimed at standards beyond 5G. This framework is supported via proposing novel concepts for forming advanced and flexible RAT elements. Pointing out the inefficiency of the fixed waveform parameterization of 5G numerologies, advanced numerology design principles are explained over flexible parameterization methods for a more efficient exploitation of existing waveform technologies. Then, in order to achieve further flexibility, we proposed novel frame design strategies based on the advanced numerologies. Thus, a comprehensive picture of our vision on future flexible RATs is provided to facilitate supporting a wide variety of services and meeting highly diversified user requirements.

#### **4.7 Acknowledgement**

This study is supported in part by the US National Science Foundation (NSF) under Grant ECCS-1609581.



## CHAPTER 5

### CYCLIC FEATURE SUPPRESSION FOR PHYSICAL LAYER SECURITY<sup>1</sup>

Cyclic prefix (CP) is a very useful signal component in broadband wireless communication techniques such as single-carrier frequency domain equalization (SC-FDE) and orthogonal frequency division multiplexing (OFDM). In time dispersive channels, its usage offers a considerable advantage in equalization complexity. For instance, when an OFDM symbol in time domain is cyclically extended longer than the maximum excess delay of the multipath channel, linear convolution of the transmitted signal and the channel impulse response (CIR) can be considered as a circular convolution at the receiver. Therefore, transmitted symbol bins mixed up with the previous ones due to the time dispersion effect of multipath channel can be recovered with a single-tap frequency domain equalizer and equalization complexity decreases significantly. In addition to these advantages, CP introduces cyclic features to the signal and they can be utilized for many useful receiver operations such as signal parameter estimation [72, 86–88], synchronization [73, 89] and channel estimation [74, 90] without needing extra training signals.

Considering the aforementioned advantages, CP might be assumed as a very beneficial component of the signal rather than a redundant extension. On the other hand, unauthorized users may also attempt to exploit the cyclic features introduced by CP in order to extract the signal parameters, achieve synchronization and decode the data for malicious purposes. In such a scenario, even well-known secure communication techniques such as frequency hopping (FH) and direct sequence spread spectrum (DSSS) may remain vulnerable, since the cyclic features exist anyways when the CP is conventionally deployed [91]. Conventional encryption based techniques providing bit-level security have already been deployed at the application layer to secure the data against eavesdroppers.

---

<sup>1</sup>This chapter was published in Elsevier Physical Communication [75] as an extension of [97]. Permissions are included in Appendix A.

However, further secrecy precautions might still be essential for many applications especially for the critical domains such as health care, public safety and military. Physical layer (PHY) security offers a promising solution to meet this requirement by providing the security in the transmission level. In this context, cyclic feature suppression is also very critical and should be achieved for a covert signaling.

In the literature, various techniques are presented to achieve cyclic feature suppression especially for OFDM systems. One of the first studies in this direction is done in [92] where cyclic features introduced by the preambles are highlighted. In order to facilitate time and frequency synchronization pseudo-random sequences are used instead of conventional preambles and then, a random frequency offset is added to each preamble to mask the spectral lines further. In [93], embedding OFDM symbols into a notched ultra wide band (UWB) noise signal is proposed. The goal here is to build a secure network among radars via making the system spectrally undetectable. However, sharp filters are used for designing such a system, and bit error rate (BER) performance is degraded due to the noise addition. Another technique for achieving a covert communication is UWB-OFDM where the signal spreads over a very large band in frequency domain and the power level of the signal becomes smaller than the noise level. However, UWB suffers from in-band interference and has practical difficulties in hardware design. OFDM signals are generated with a random frequency jitter in [91] to conceal cyclic signatures. Time jitter can also be used in FH-OFDM signals for suppressing spectral lines at symbol and hopping periods. In [94], CP and pilot tones are completely removed to suppress OFDM features, and inter-symbol interference (ISI) is handled using a decision feedback equalizer (DFE). However, such an approach obviously increases the receiver complexity and eliminates the advantage of OFDM in handling multipath by using CP. As a practical solution, random data sequences with various sizes are inserted between OFDM symbols in [95] to remove the periodicity of CP. Additionally, CP length is adaptively adjusted based on the maximum excess delay of the channel as an extra precaution. An alternative approach for slowly fading channels is proposed in [96] where CP length is pseudo-randomly changed. However, both techniques lead to waste of spectral resources by either using the CP longer than required or inserting irrelevant signals between the data symbols. If the CP size is determined shorter than

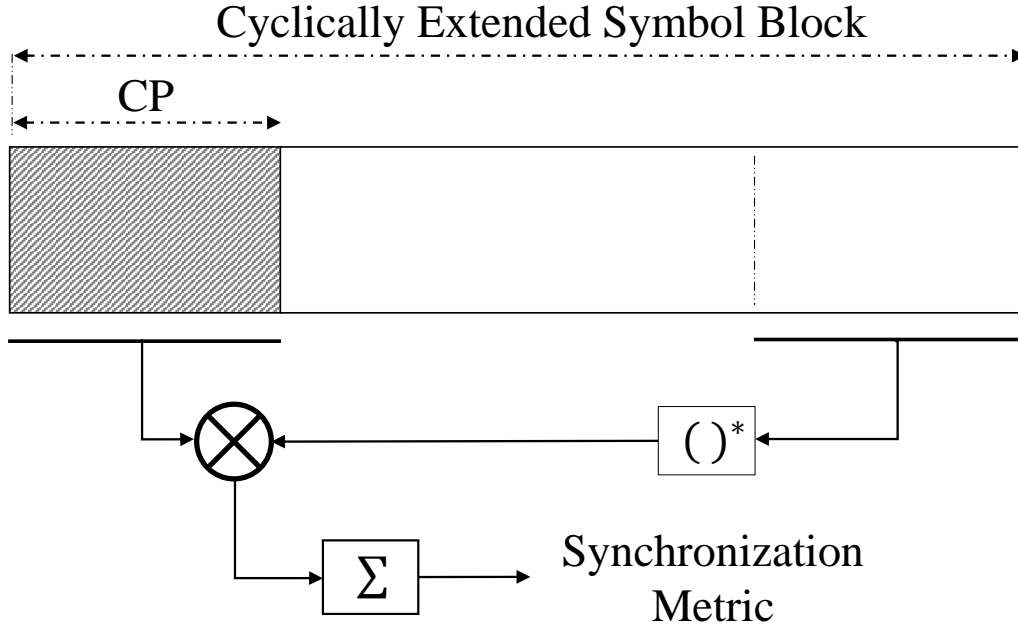


Figure 5.1 Calculation of synchronization metric by exploiting cyclic prefix.

maximum excess delay of the channel for some of the symbols, not to degrade spectral efficiency, then ISI would emerge as another issue. In [97], cyclic feature suppression is achieved without introducing aforementioned spectral redundancies via a novel CP selection mechanism. Basically, shifting the CP selection region towards the next OFDM symbol by a positive random variable is proposed without changing CP size. By doing so, cyclic features will be suppressed without adding any redundancy to the signal as the CPs will not be correlated with the last samples of the actual data periodically. However, this technique requires a modified equalization with more complexity and leads to a bit of degradation for the bit-error-rate (BER) performance of OFDM signals.

In this chapter, along with our technique presented in [97], we propose a novel cyclic feature suppression technique by randomizing actual data transmission time for each OFDM symbol. Unlike the conventional procedure, symbol time is varied in a random manner by changing the number of quadrature amplitude modulation (QAM) symbols carried by an OFDM signal while CP duration is kept the same. In this way, periodicity of CPs will be removed and cyclic features will be suppressed without introducing any extra resource usage. Note that, this operation corresponds to changing IFFT/FFT size in generation of OFDM symbols and this change is directly related to the symbol

duration. Then, bandwidth of each subcarrier will change inversely, i.e., if the symbol duration is increased for an OFDM symbol, more subcarriers will be fit into the total given bandwidth. Therefore, more time duration means more data transmission for one OFDM symbol, and vice versa. By doing so, the spectral efficiency is kept constant for each symbol. In addition, the number of QAM symbols is determined considering PAPR mitigation and out-of-band leakage, i.e., sidelobe, suppression. Thus, a further improvement is obtained at the expense of an extra signaling and complexity in signal generation.

In both techniques a random variable should be shared by the legitimate users. In order to carry that out securely without any extra signaling, we exploit the channel state information (CSI), which is always required for equalization, to generate a seed number. Then random variables for each symbol are identically generated in a pseudo-random manner by both users, and seed can be updated based on the variations in CSI. However, CSI based random number cannot be used for PAPR or sidelobe suppression purposes due to the dependency on data for each symbol. The proposed techniques are presented for OFDM and SC-FDE schemes, and their performances are investigated in terms of error probability and complexity as well as cyclic feature suppression.

The rest of the chapter is organized as follows. Section II provides an overview of blind parameter estimation and synchronization algorithms based on cyclostationary introduced by CP. The CP selection method is presented in Section III while the symbol time randomization technique is described in Section IV. Numerical results are given in Section V, and Section VI concludes the chapter with a final discussion.

## **5.1 Blind Parameter Estimation, Synchronization and Equalization with CP**

Blind receiver design is a very important topic especially for military communications and public safety domain and well investigated in the literature. In this regard, the proposed algorithms targeting to achieve parameter estimation [72, 86–88] and channel identification [90, 98] are mostly utilizing cyclic features (or cyclostationarity) introduced by the CP. If the transmission parameters such as OFDM symbol duration (frame duration for SC-FDE) and CP size, are somehow estimated, blind synchronization in time and frequency can be performed by exploiting the CP. A simple

illustration of the maximum-likelihood (ML) based synchronization is given in Figure 5.1. The synchronization metric providing the sample index where OFDM symbol starts, can be calculated as

$$R(l) = \sum_{n=0}^{N_{CP}-1} s[l-n]s^*[l-n+N_S], \quad (5.1)$$

where  $s[n]$  is the received signal,  $N_{CP}$  is the length of CP and  $N_S$  is the length of the useful portion. Then, the synchronization parameters including the timing position of the symbol,  $\hat{\tau}_0$ , and the frequency offset caused by the mismatch between local oscillators of the transmitter and receiver,  $f_0$ , can be extracted as

$$\hat{\tau}_0 = \arg \max_l \{|R(l)|\}, \quad (5.2)$$

$$f_0 = \frac{1}{2\pi} \angle R(\hat{\tau}_0). \quad (5.3)$$

One may note that, the received signal is distorted after passing through the multipath channel and due to the additive noise. Thus, obtaining synchronization parameters with one symbol is not practical by just performing this method. Moreover, frequency offset causes an extra degradation in the correlation of the repetitive components. Therefore, the metrics given in (2) and (3) should be calculated for a number of symbols and their averaging should be done to achieve a reliable synchronization. After carrying out synchronization and parameter estimation, the effect of multipath channel can easily be fixed with a single tap frequency domain equalization and the data can be decoded.

## 5.2 Cyclic Feature Concealing CP Selection

In Figure 5.2, we illustrate cyclic features for a conventional OFDM signal via the cyclic autocorrelation function (CAF) (likewise possessed by classical SC-FDE signals). As discussed in earlier sections, such features introduced by CP can be exploited for blind signal demodulation and this can enable unauthorized users to eavesdrop the communication by obtaining the transmitted

data. Therefore, suppressing these features is very critical for protecting data against potential eavesdropping attacks. In this section, we present our CP selection method (firstly proposed in [97]) that conceals the CP based cyclic features without degrading spectral efficiency while maintaining the low complexity frequency domain equalization in general. Unlike the classical procedure in CP selection, i.e., picking the last  $N_{CP}$  samples of the time domain symbol (or frame for SC-FDE), we shift the CP selection region towards the next symbol by a positive random variable as shown in Fig. 5.3. Since, the time duration between CP and its selection region varies for each symbol, cyclic features are suppressed and blind decoding of the data becomes much more difficult. Note that, the shifting information of each symbol should also be known by the receiver. For improving security further, guard time between frames, i.e., packets, can also be randomized. Thus, each frame is required to be synchronized individually and the suppressed cyclic features remain useless for the limited number of symbols in a frame.

In order to represent the proposed method analytically, let us define the  $i$ th time domain symbol vector as

$$\hat{\mathbf{x}}^{(i)} = [\mathbf{\Gamma}^{(i)} \mathbf{x}^{(i)}], \quad (5.4)$$

where  $\mathbf{\Gamma}^{(i)}$  is the CP whose selection region is shifted by  $N_{\alpha}^{(i)}$  towards the  $(i+1)$ th data block, and  $\mathbf{x}^{(i)} = [x_1^{(i)}, x_2^{(i)}, \dots, x_N^{(i)}]$  is the useful data part. Assuming  $N_{\alpha}^{(i)}$  takes value between zero and  $N_{CP}$ ,  $\mathbf{\Gamma}^{(i)}$  is defined as

$$\mathbf{\Gamma}^{(i)} = [x_{N-N_{CP}+N_{\alpha}^{(i)}}^{(i)}, x_{N-N_{CP}+N_{\alpha}^{(i)}+1}^{(i)}, \dots, x_N^{(i)}, \hat{x}_1^{(i+1)}, \hat{x}_2^{(i+1)}, \dots, \hat{x}_{N_{\alpha}^{(i)}}^{(i+1)}]. \quad (5.5)$$

In equalization stage, the proposed CP selection mechanism has to be taken into account for maintaining low complexity and zero ISI advantages at the receiver side. Therefore, each symbol is considered with an additional extension of  $N_{\alpha}^{(i)}$  samples from the next time domain symbol as

illustrated in Fig. 5.4. Let us define the extension including time domain samples of the  $l$ th symbol copied from the received signal as  $\mathbf{y}^{(l)} = [y_1^{(l)}, y_2^{(l)}, \dots, y_{N+N_{CP}+N_\alpha}^{(l)}]$ . After CP removal, i.e., removing the first  $N_{CP}$  elements of  $\mathbf{y}^{(l)}$ , frequency domain equalization is performed to estimate the data including the aforementioned extension in frequency domain as

$$\hat{Y}_k^{(l)} = \frac{Y_k^{(l)} H_{kl}^*}{|H_{kl}|^2}, \quad (5.6)$$

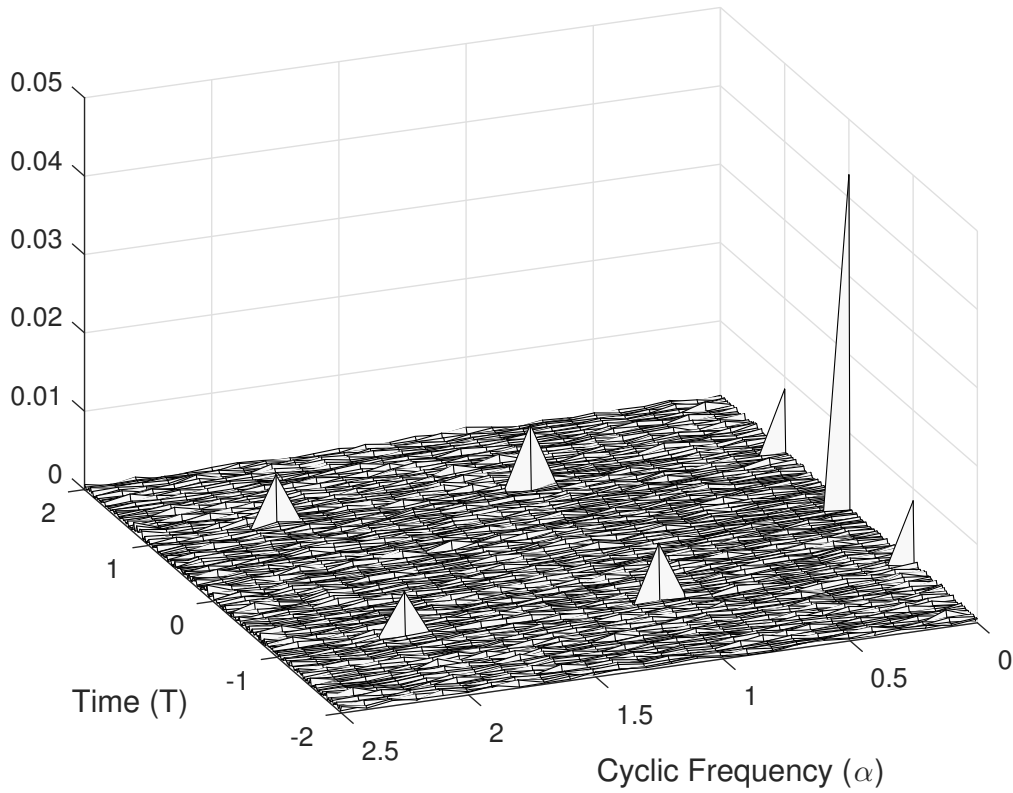


Figure 5.2 Cyclic autocorrelation function (CAF) of a conventional CP-OFDM signal (same as conventional SC-FDE).

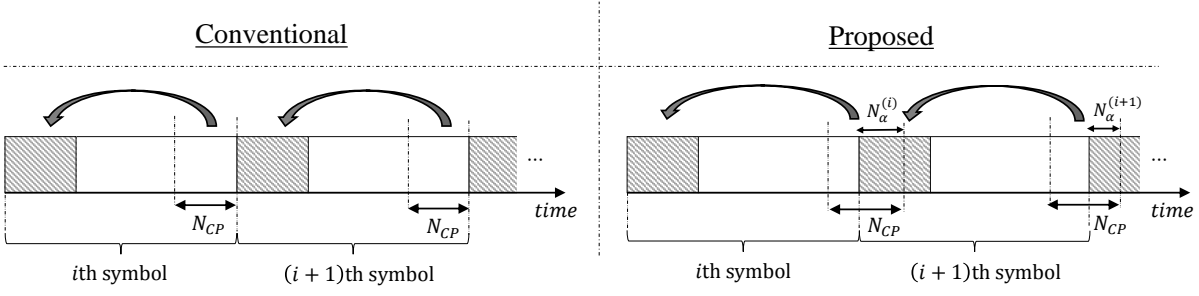


Figure 5.3 Illustration of cyclic feature concealing CP selection.

where  $H_{kl}$  is the frequency response for the  $l$ th symbol, assumed to be known by the receiver, that corresponds to  $k$ th bin in frequency domain, and

$$Y_k^{(l)} = \sum_{n=0}^{N+N_\alpha^{(l)}} y_n^{(l)} e^{-j2\pi kn/(N+N_\alpha^{(l)})}. \quad (5.7)$$

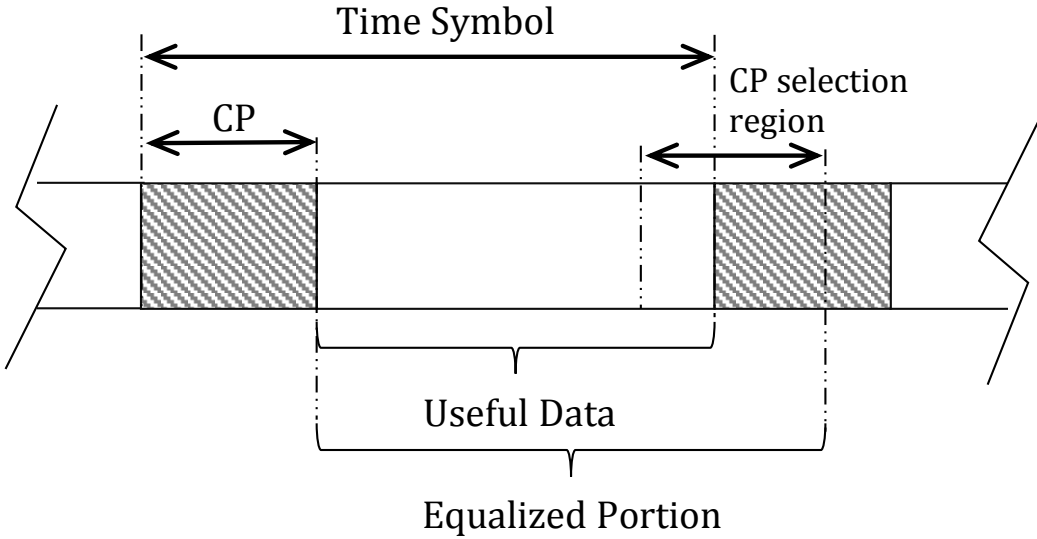


Figure 5.4 Illustration of the equalization part for an OFDM symbol designed with the proposed method.



Since the convolution of  $\mathbf{y}^{(l)}$  with the channel is circular, one-tap frequency domain equalization, given in (6), compensates the multipath channel effect. However, the  $N_\alpha^{(l)}$  – point extension in the  $l$ th symbol still exists and should be removed to obtain the pure data.

The remaining operations including equalization and  $N_\alpha^{(l)}$  – point extension removal are separately given for OFDM and SC-FDE schemes in the following subsections. Then, the effect of proposed structure on their error performance could also be discussed in a clear way.

### 5.2.1 OFDM

Removal of extension after equalization requires symbols to be transformed back to the time domain in OFDM. After doing so and removing the extension, fast Fourier transformation (FFT) of the actual time domain symbol is taken to obtain the estimated elements of the useful data set,  $\mathbf{S}^{(l)}$  as

$$S_k^{(l)} = \sum_{n=0}^N s_n^{(l)} e^{-j2\pi kn/N}, \quad (5.8)$$

where the data set of  $s_n^{(l)}$  selected from the first  $N$  element of the equalized  $\mathbf{y}^{(l)}$  can be defined as  $\mathbf{s}^{(l)} = [\hat{y}_1^{(l)}, \hat{y}_2^{(l)}, \dots, \hat{y}_N^{(l)}]$  and

$$\hat{y}_n^{(l)} = \frac{1}{N + N_\alpha^{(l)}} \sum_{k=0}^{N+N_\alpha^{(l)}} \hat{Y}_k^{(l)} e^{j2\pi nk/(N+N_\alpha^{(l)})}. \quad (5.9)$$

Even though, the time dispersion effect of the channel can easily be compensated and the actual data can be obtained at the expense of a reasonable complexity introduced by an extra FFT/IFFT operation, the proposed technique may result in a degraded BER performance for OFDM. In conventional OFDM, subcarriers are independent of each other. Therefore, in case of a deep fading in a part of the transmission frequency, only the data assigned to the deep faded subcarriers are severely affected from the noise. However, in the proposed method, the number of samples changes through the extension removal process after equalization. In this case, the fading effect cannot be kept only in the corresponding frequencies, inevitably and the enhanced noise af-

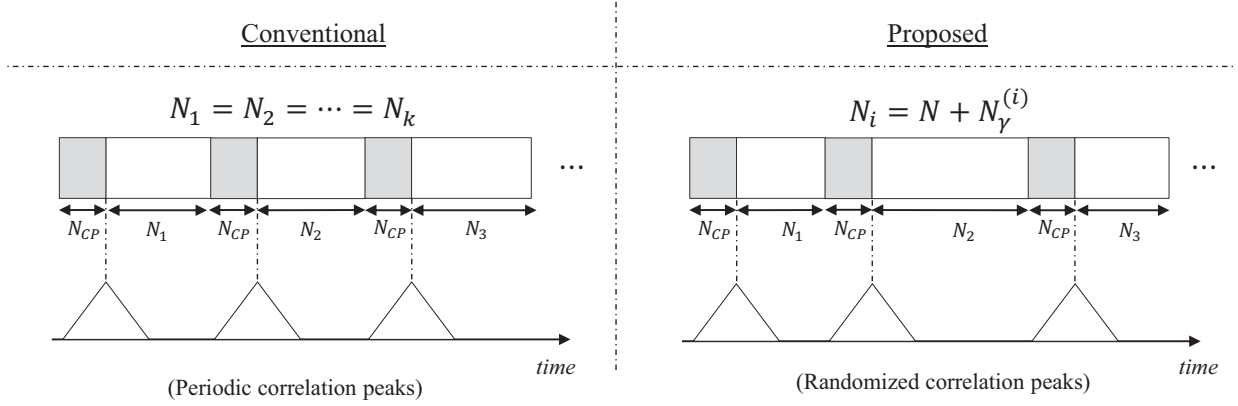


Figure 5.5 Illustration of cyclic feature suppressing symbol time randomization and resulting randomized correlation peaks.

ter equalization contaminates the neighboring subcarriers which would lead a degradation in BER performance.

### 5.2.2 SC-FDE

In SC-FDE schemes, IFFT is applied to the signal for obtaining the transmission data after equalization as

$$\hat{y}_n^{(l)} = \sum_{n=0}^{N+N_\alpha^{(l)}} \hat{Y}_k^{(l)} e^{-j2\pi kn/(N+N_\alpha^{(l)})}. \quad (5.10)$$

Since the random extension exist in the time domain, it can be directly removed from the  $l$ th signal and the useful data can be obtained as  $\tilde{y}_n^{(l)} = [\hat{y}_1^{(l)}, \hat{y}_2^{(l)}, \dots, \hat{y}_N^{(l)}]$ . Note that, unlike OFDM, removal of the redundant part does not require an extra FFT/IFFT and therefore, the proposed technique introduces no additional complexity for SC-FDE. Also, there is nothing to degrade BER performance unless the channel changes through the extension duration.

## 5.3 Cyclic Feature Suppressing Symbol Time Randomization

In order to suppress the cyclic features stemming from periodicity of CPs, we propose a symbol time randomization in this section as illustrated in Fig 5.5. Unlike our first technique, we keep the general structure of CP selection and equalization part the same as the conventional OFDM

and SC-FDE. On the other hand we change the symbol time by a random index for by varying the number of QAM-symbols carried by each symbol. Let us represent  $i$ th time domain symbol as done in Eq. 5.4,

$$\bar{\mathbf{x}}^{(i)} = [\tilde{\mathbf{I}}^{(i)} \quad \tilde{\mathbf{x}}^{(i)}], \quad (5.11)$$

where  $\tilde{\mathbf{x}}^{(i)} = [x_1^{(i)}, x_2^{(i)}, \dots, x_{N+N_\gamma}^{(i)}]$  is the actual data vector with a varying size specified by the discrete random variable  $N_\gamma^{(i)}$  and  $\tilde{\mathbf{I}}^{(i)}$  is the CP selected from the last  $N_{CP}$  bins of  $\tilde{\mathbf{x}}^{(i)}$ . Note that, changing the symbol time is done by changing the number of subcarriers for each symbol. For example, if the symbol time is extended by a positive number assigned as  $N_\gamma^{(i)}$ , more subcarriers are allocated on the given band, i.e., more QAM-symbols are transmitted in parallel during the symbol duration. Therefore, the ratio between the symbol time and number of symbols carried for each symbol remain the same, and this corresponds to have the same spectral efficiency for each symbol. One may note that the ratio between the CP duration and symbol duration is also effective on spectral efficiency. Although, we change this ratio for each symbol in this technique, it will not be affecting the spectral efficiency as long as the mean of  $N_\gamma^{(i)}$  is zero. Note that, the equations of the remaining processes in the transmission and reception are not given for this technique since they are not different than the regular implementation of plain OFDM and SC-FDE.

An important issue to be considered from practical point of view for both techniques is the implementation of FFT/IFFT algorithm. In both methods, the number of FFT/IFFT points are changed, and it will not be a power of two unless the extension amount is as much as the length of one whole symbol. In order to meet the requirement of having a power of two bins for the implementation of FFT algorithm, we perform interpolation and complete the number of bins to the next closest power of two, e.g., if the number of bins in the symbol is 268 after implementing any of two techniques, it is interpolated and up-sampled to have 512 bins. This complementing operation can easily be done by zero padding before taking IFFT and by adjusting the sampling rate at the transmitter and receiver sides, respectively. Therefore FFT/IFFT sizes are doubled for both techniques and implementation complexity becomes  $O(2N \log(2N))$  while it was  $O(N \log(N))$

in classical design. As an exception, implementation of OFDM in CP selection technique requires two extra  $N$ -point FFT/IFFT operations and therefore, a little more complex than the others.

### 5.3.1 PAPR Mitigation for OFDM

Symbol randomization can also be used to obtain various benefits along with the security. Here, we use this technique for PAPR mitigation which is one of the most serious issues in OFDM signals and can be given for  $i$ th symbol as

$$PAPR = \frac{\max\{|\bar{\mathbf{x}}^{(i)}|^2\}}{E\{|\bar{\mathbf{x}}^{(i)}|^2\}}. \quad (5.12)$$

In order to achieve that, rather than using arbitrary numbers generated in a pseudo-random fashion for symbol time randomization,  $N_\gamma^{(i)}$  is selected in such a way that combination of the symbols, for the given search range of  $N_\gamma^{(i)}$ , exhibits the minimum PAPR. The objective function for this can be analytically expressed as

$$\begin{aligned} \bar{N}_\gamma^{(i)} &= \arg \min_{N_\gamma^{(i)}} \{PAPR\} \\ &\text{subject to } N_\gamma^{(i)} \leq N_p, \end{aligned} \quad (5.13)$$

where  $N_p$  is the search range for  $N_\gamma^{(i)}$  and  $\bar{N}_\gamma^{(i)}$  is the optimum variable minimizing the PAPR within the given search range. In this way, we can obtain an extra advantage besides the security at the expense of a searching complexity.

### 5.3.2 Sidelobe Suppression for OFDM

Frequency domain representation of the  $i$ th OFDM signal can be given as

$$S^{(i)}(f) = \sum_N^{k=0} x_k^{(i)} a_k(f), \quad (5.14)$$

while

$$a_k(f) = \int_{-T/2}^{T/2} e^{\frac{j2\pi k}{T_s}} e^{j2\pi ft} dt = \text{sinc}(Tf - T\frac{k}{T_s}) \quad (5.15)$$

where  $T_s$  is the duration for the actual symbol and  $T$  is the symbol time whole OFDM symbol including CP.

In order to represent the out-of-band radiation caused by the sidelobes, we sample the out-of-band region and assign it to the vector  $S_o^{(i)} = [S_o^{(i,0)}, S_o^{(i,1)}, \dots, S_o^{(i,M-1)}]$ . Then we can give the objective function for sidelobe suppression of  $i$ th OFDM signal as

$$\bar{N}_\gamma^{(i)} = \arg \min_{N_\gamma^{(i)}} \left\{ \sum_{m=0}^{M-1} |S_o^{(i,m)}|^2 \right\} \quad (5.16)$$

subject to  $N_\gamma^{(i)} \leq N_p$ .

Then out-of-band radiation can also be suppressed along with PAPR mitigation, either jointly or independently, based on the system requirements.

We should note that the randomization index will be a specific number for each symbol if the given operations for PAPR mitigation and sidelobe suppression are performed. While the transmitter and the receiver could share only one seed number exploiting the CSI and can generate all the other random variables in a pseudo-random manner for regular CP selection and symbol time randomization algorithms, it is not possible when the PAPR mitigation and sidelobe suppression are also taken into account. Therefore, a PAPR mitigating or sidelobe suppressing randomization index should be shared with the receiver for each symbol via a secure channel and this introduces an extra signaling to the system as a trade off.

## 5.4 Numerical Results

We referred to IEEE 802.11 standard for OFDM simulation parameters, and determined the number of subcarriers as 64 in 20 MHz of transmission bandwidth [99]. The modulation type is

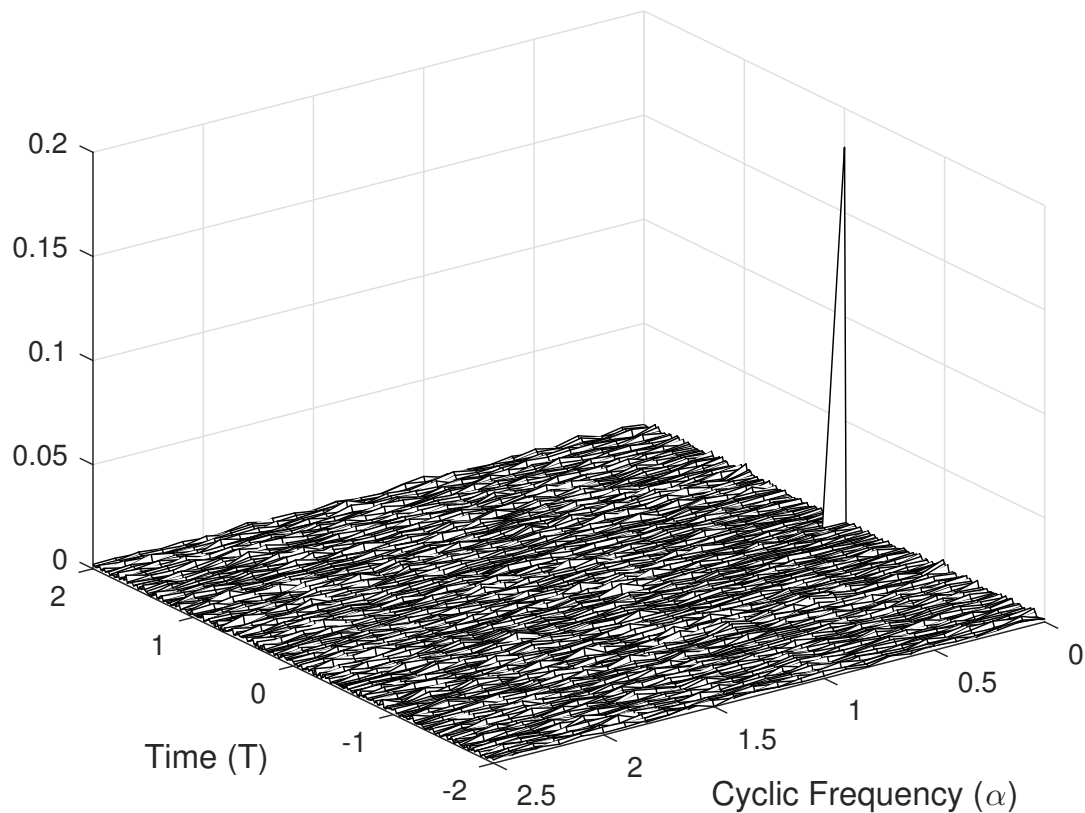


Figure 5.6 CAF for the CP selection and symbol time randomization methods.

chosen as  $M$ -QAM where  $M = 64$  for our simulations. The number of transmitted QAM symbols in an SC-FDE frame is similarly specified as 64, and the transmission bandwidth and modulation are the same as the OFDM signal.

In order to show the performance of both proposed techniques, i.e., CP selection and symbol time randomization, in cyclic feature suppression, CAF of an OFDM signal is given in Figure 5.6 for 100 symbols with  $1/4$  CP rate in a channel and noise free scenario. Since the same result is valid for SC-FDE, it is not given with an extra figure. It is clearly seen that all the peaks except the one at zero index in time and frequency are suppressed with the proposed techniques even without noise and channel effects. Therefore, an adversary cannot perform blind synchronization and other receiver algorithms by exploiting cyclostationary.

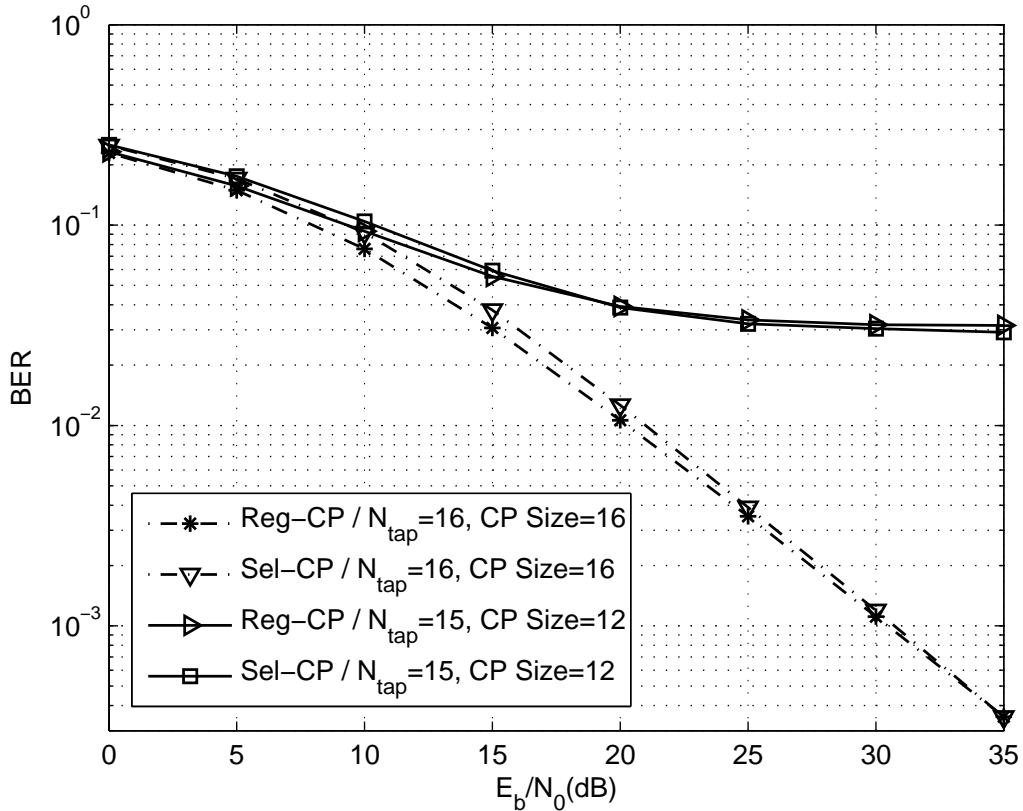


Figure 5.7 BER performance of OFDM with regular CP (Reg-CP) and proposed CP (Sel-CP) selection for different number of channel taps ( $M = 64$ ).

For BER analysis of our CP selection method, we consider multi-path Rayleigh channel with different number of taps. In order to see the effect of ISI in this technique, we also performed simulations for symbols with insufficient CP sizes where the number of channel taps is larger than CP size. On the legitimate receiver side, the multi-path dispersion in the signal can trivially be removed by taking the advantage of CP, as long as the time shifting information in the CP selection is known and the CP size is not smaller than the number of channel taps. However, due to the previously mentioned noise expansion in OFDM, BER performance is a little bit degraded compared to conventional OFDM as seen in Figure 5.7. As expected, this effect is more apparent for low signal-to-noise ratio (SNR) values. On the other hand, when the proposed technique is implemented for SC-FDE, no negative effect is observed on BER performance as given in Figure 5.8. This is because, there is no need of extra FFT/IFFT in redundancy removal for SC-FDE.

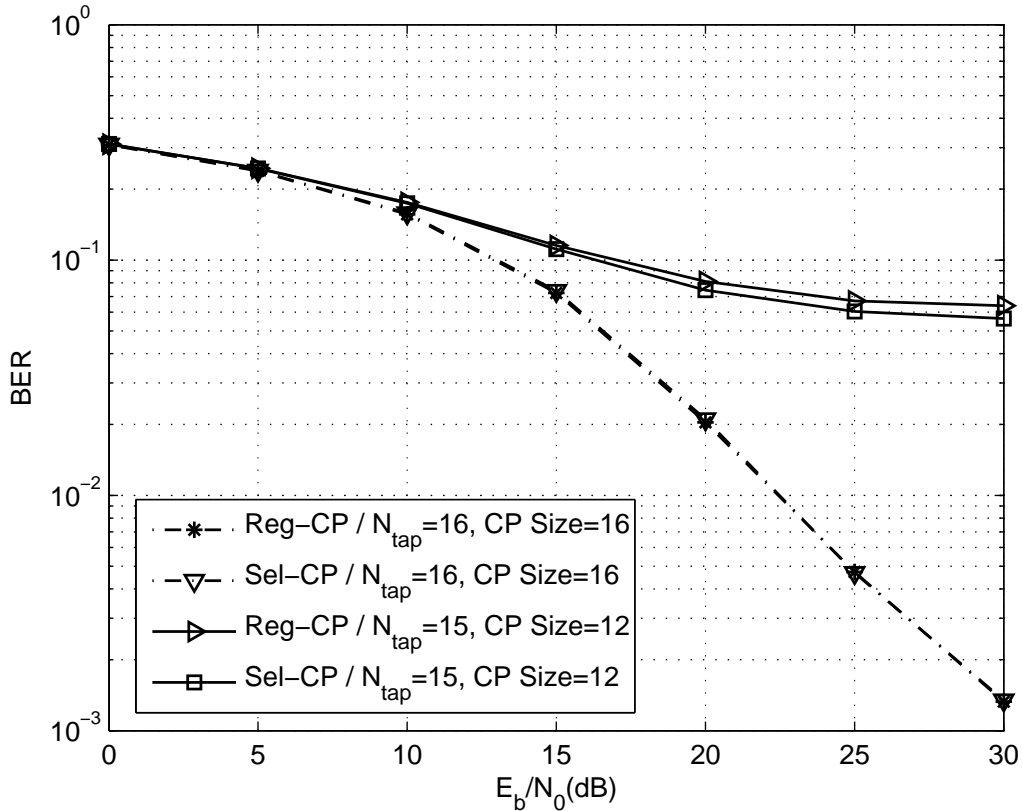


Figure 5.8 BER performance of SC-FDE with regular CP (Reg-CP) and proposed CP (Sel-CP) selection for different number of channel taps ( $M = 64$ ).

Another interesting advantage of the proposed CP selection method is to decrease the effect of ISI in the case of insufficient CP usage. By selecting CP at least partially from the next symbol, symbol duration that we have during the equalization is actually extended. As the effect of ISI due to insufficient CP is depending on the ratio of the interference power and symbol duration, our technique exhibits a better performance than the conventional approach via spreading the interference over a symbol having longer duration.

BER performance of symbol randomization technique is also investigated for ISI-free and ISI introduced, i.e., sufficient and insufficient CP, cases via Monte-Carlo simulations. The signal parameters are specified the same as done for CP selection. The mean of the randomization index,  $N_{\gamma}^{(i)}$ , is also kept as zero, i.e., the expected value of the symbol times generated with symbol randomization technique is the same as the aforementioned regular symbol time. When the tech-



nique is implemented on OFDM signals, BER performances are obtained as given in Figure 5.9. Obviously, BER performances are maintained and the same signal quality is achieved as the regular implementation. This is obviously an expected result since symbol time randomization does not hurt orthogonality at all. Also, since the mean of the randomization index is zero, average ratio between the interference power and symbol power exhibits the same values for insufficient CP cases. The BER results for the SC-FDE signals are also given in Figure 5.10. Similar to OFDM case, the same performances are obtained as the regular SC-FDE signals for both, sufficient and insufficient CP cases.

The simulations are also performed for investigating PAPR mitigation and sidelobe suppression with symbol time randomization technique. In Figure 5.11, complementary cumulative distribution function (CCDF) of PAPR values for different search ranges,  $N_p$ , are given. As clearly seen, even for a very small search range, e.g., when  $N_p$  is 2, our technique achieves around 1 dB mitigation. At the expense of more searching by increasing  $N_p$ , PAPR mitigation performance can be enhanced further. Note that, while searching the optimum randomization index,  $\bar{N}_\gamma^{(i)}$ , symbol size also changes (even if we up-sample it to have a bin number as power of two for implementing FFT algorithm). Therefore, even small values of randomization indexes might make a significant difference in PAPR. In Figure 5.12, out-of-band emissions of OFDM symbols are shown for different  $N_p$ 's. As the edge subcarriers are quite effective on the sidelobes, especially for the close band regions, we see up to 10 dB power reduction for  $N_p=16$ . This much suppression may not be satisfactory to meet the requirements of many systems. However, it will help to reduce the redundancy or disadvantages caused by other sidelobe suppression techniques such as windowing and precoding.

## 5.5 Conclusion

In this chapter, we presented two cyclic feature suppression techniques to provide a covert communication and to improve PHY security against eavesdropping attacks by carrying out cyclic feature suppression for CP based waveforms, OFDM and SC-FDE. The first technique achieves that by pseudo-randomly changing the CP selection region symbol-by-symbol, while the second one randomizes the time of actual symbols and keeps CP size the same for each symbol. The seeds

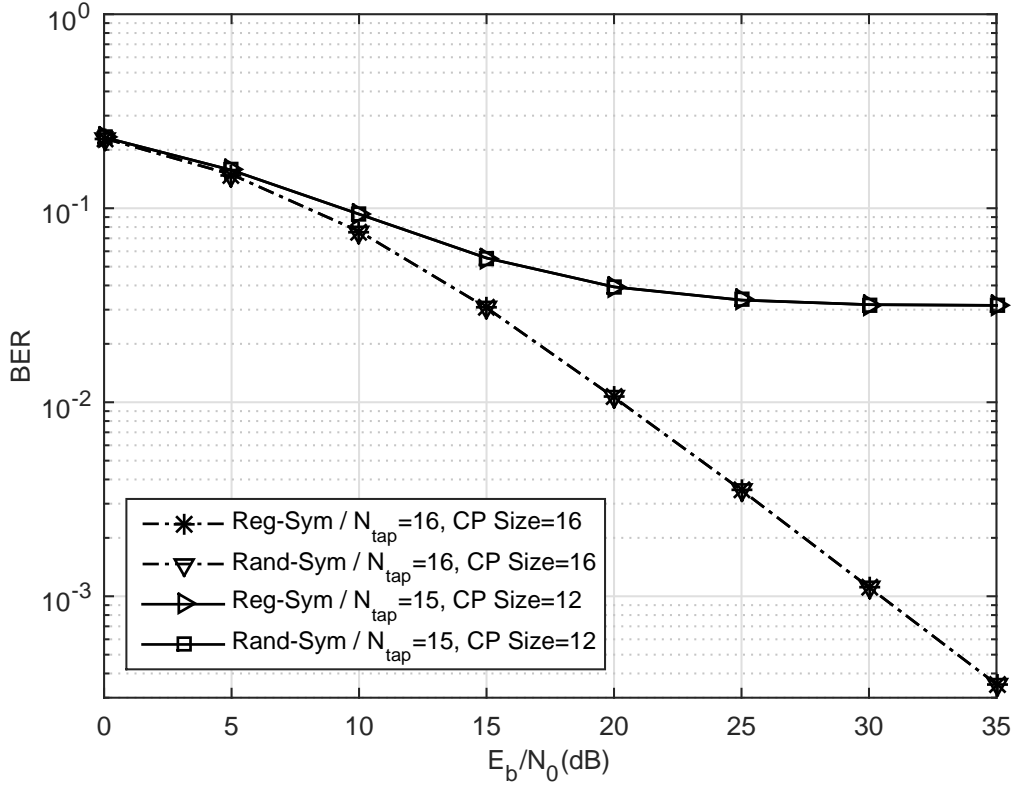


Figure 5.9 BER performance of OFDM with regular symbol generation (Reg-Sym) and time-randomized symbol (Rand-Sym) for different number of channel taps ( $M = 64$ ).

for generating pseudo-random indexes are obtained from the CSI by legitimate users. In this way, cyclic features are securely concealed for a covert communication without any degradation in spectral efficiency. Although, no disadvantage appears for SC-FDE in the first technique in terms of BER, its implementation for OFDM is done at the expense of a little degradation in BER performance due to a modification in equalization. In the second technique, conventional procedure is followed for CP selection and equalization. Thus, the disadvantages of the first technique are removed in terms of performance degradation in OFDM. Also, symbol time randomization is used for PAPR mitigation and sidelobe suppression for OFDM signals as an additional advantage of this technique. Both techniques require doubling the FFT/IFFT sizes and therefore, introducing some complexity in implementation. Only OFDM in CP selection technique needs an extra  $N$ -point FFT/IFFT pair because of the aforementioned modifications and becomes a bit more complex than the others.

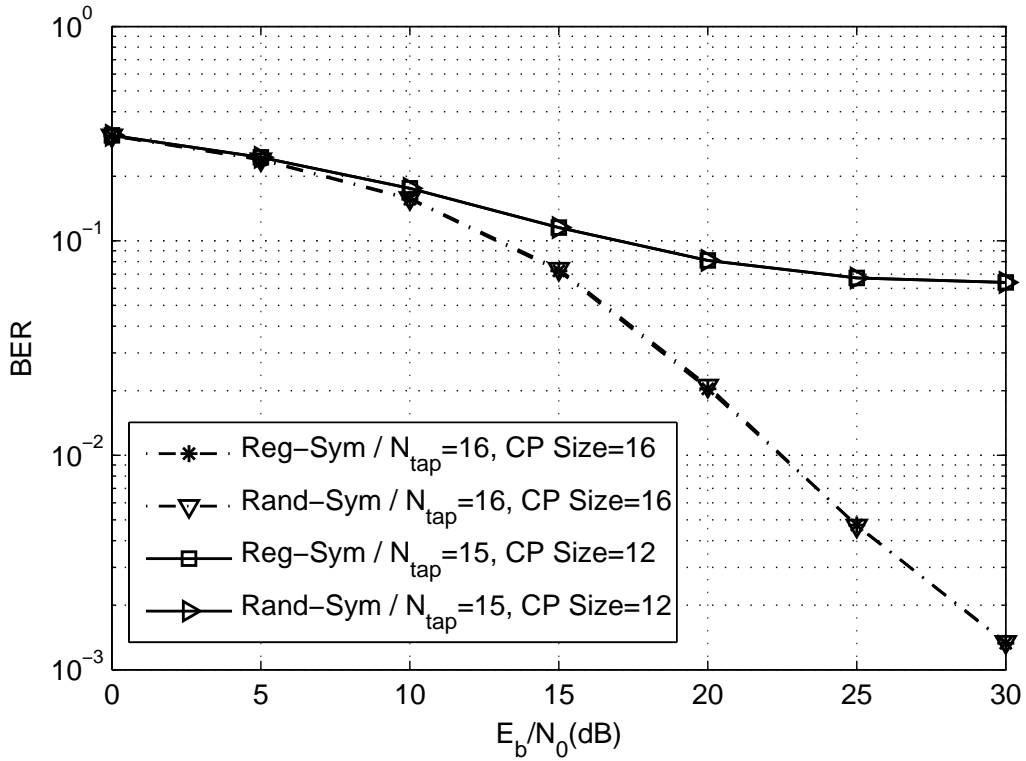


Figure 5.10 BER performance of SC-FDE with regular symbol generation (Reg-Sym) and time-randomized symbol (Rand-Sym) for different number of channel taps ( $M = 64$ ).

Considering the maintenance of conventional equalization, BER performance and complexity, symbol time randomization looks better than CP selection especially for OFDM. Additionally, symbol time randomization offers an extra advantage in PAPR reduction and sidelobe suppression. However, such extra advantages lead to more complexity due to the searching operation for the optimum random index of each symbol. Also, we need to share randomization index for PAPR reduction and sidelobe suppression as it will not be an arbitrary number anymore and cannot be generated in a pseudo-random manner. Another important advantage of "CP selection" upon "symbol time randomization" is that, it reduces the effect of ISI in case of insufficient CP. These are the trade offs of our two methods and should be considered based on the primary requirements of the desired system.

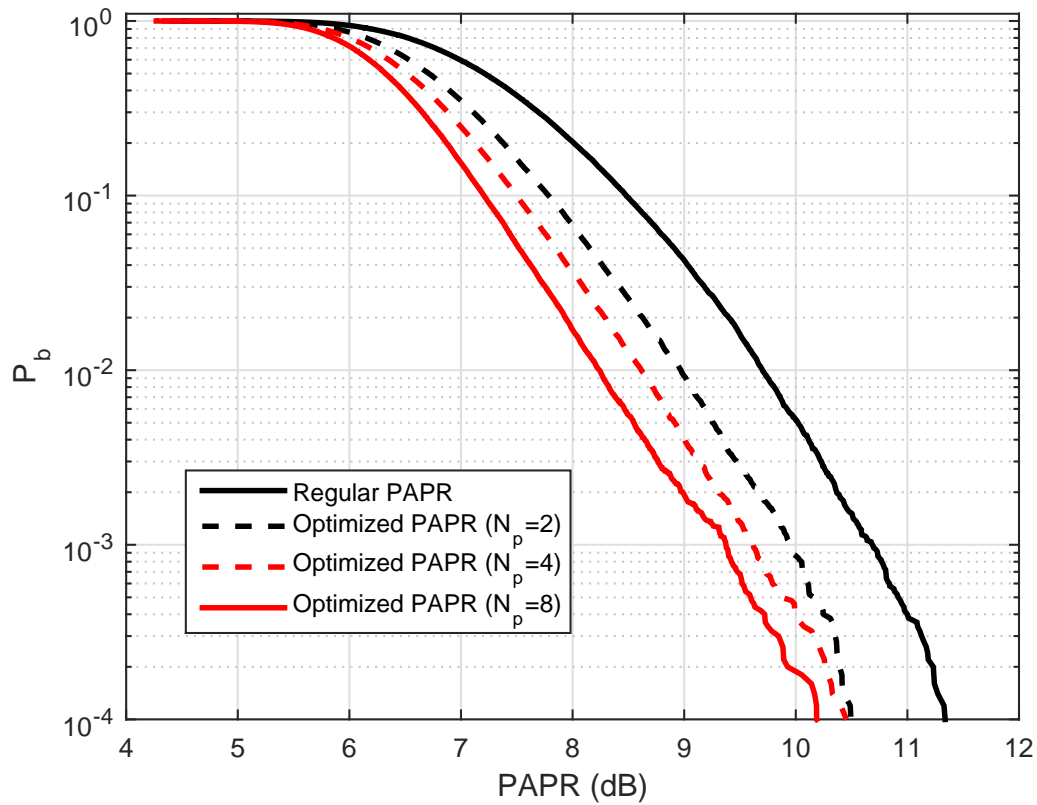


Figure 5.11 CCDF of mitigated PAPR values obtained with symbol time randomization for different search ranges, varying the number of sub-carriers around 128.

## 5.6 Acknowledgment

We thank Murat Karabacak for the technical discussions. This study is supported by Scientific and Technological Research Council of Turkey (TUBITAK). The statements made herein are solely the responsibility of the authors.

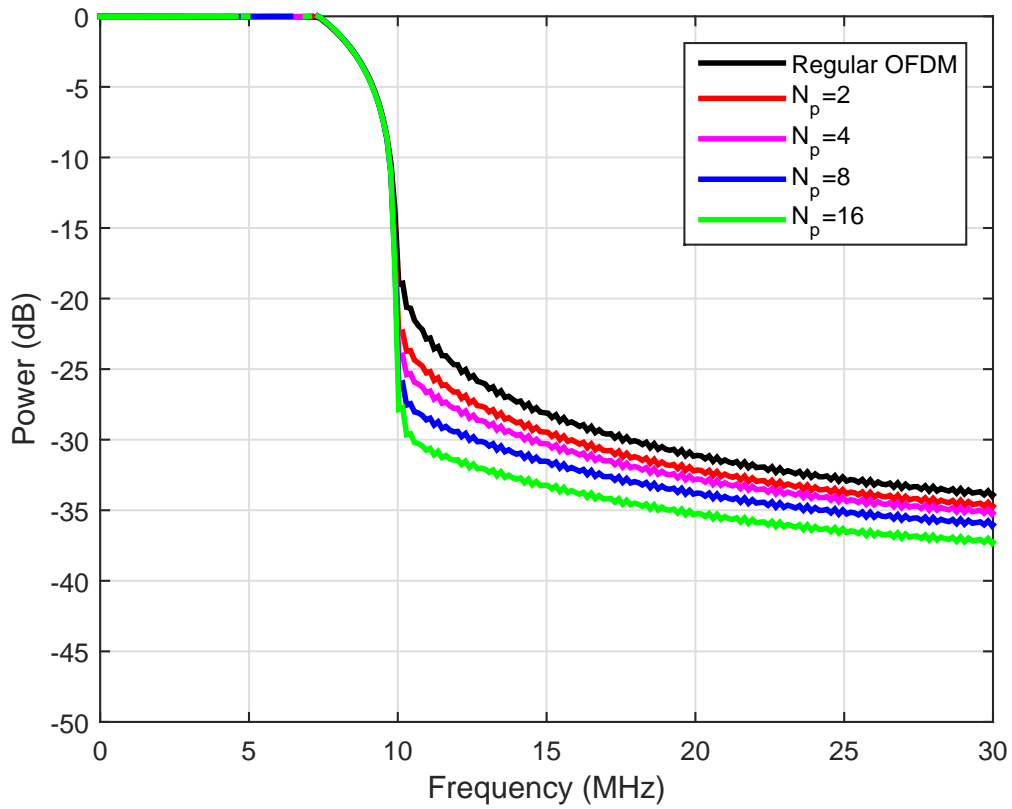


Figure 5.12 Spectrum of sidelobe-suppressed OFDM signals with symbol time randomization for different search ranges, varying the number of sub-carriers around 128.

## CHAPTER 6

# PHYSICAL LAYER SECURITY FOR WIRELESS IMPLANTABLE MEDICAL DEVICES<sup>1</sup>

### 6.1 Introduction

In our vision of pervasive healthcare, implantable medical devices (IMDs), e.g., pacemakers, implantable cardiac defibrillators (ICDs), drug delivery systems and neurostimulators, have a vital importance. They provide a substantial advantage by enabling physicians to manage many diseases [101] with the identification, monitoring, and treatment of patients in anywhere, at anytime [102] and save innumerable lives [103]. Such IMDs have already been deployed in many patients, and their usage is expected to expand in the near future. For example, the number of insulin pump users in 2005 was about 245,000, and the expected growth rate for the insulin pump market is 9% from 2009 to 2016 as reported in [104].

While many IMDs are able to perform complex analyses and sophisticated decision-making algorithms in addition to storing detailed personal medical data, wireless signals conveying critical information need protection from a variety of attacks [105]. Considering the growing utilization of IMDs and increasing security risks, comprehensive techniques against wireless adversaries have emerged as an important requirement to ensure that the patients can use IMDs confidently and without harm. Authentication is critically important, since an adversary may wirelessly change various IMD parameters and cause a dangerous mistreatment of a patient. For example, an insulin pump user might face an overdose attack that may even result in death. In the literature, proposed protection techniques against such attacks can be classified into three main categories; cryptography, anomaly detection, and "friendly" jamming. A review of the literature on these approaches, along

---

<sup>1</sup>This chapter was patented [100] and published in IEEE Computer Aided Modelling and Design of Communication Links and Networks (CAMAD) Conference [75]. Permission is included in Appendix A.

with their comparison is done in [106]. A brief description of these approaches can be given as follows:

- **Cryptography:** Relies on a secret key shared between IMD and the external device. However, cryptography may not be properly deployed if the limitations of IMDs are considered as mentioned in [107]. For example, cryptography-based techniques conflict with the accessibility requirement of IMDs in the case of any emergency, since the closest physician may not have the secret key. Then, required urgent modifications on IMD cannot be done and patients may experience serious problems.
- **Anomaly detection:** Relies on identifying the legitimacy of received commands based on the variance of IMD parameter values that are observed over the time. However, such a mechanism is not agile in adapting new conditions of patients as it requires long time monitoring and data analyzing to achieve a reasonable performance.
- **Friendly Jamming:** This technique attempts to sense the existence of a malicious attack and prevents the reception of illegitimate commands by jamming the IMD with the help of an external device. Although it does not have a direct conflict with IMD requirements, energy efficiency of the external device is a drawback as it performs very complex and power consuming operations, i.e., continuous spectrum sensing and jamming, and may preclude normal IMD operation.

A popular approach in IMD communications and in aforementioned security techniques is the usage of a wearable external device (WED) attached to the patient body. These devices act as a relay between the IMD and the central external node, and provide a substantial advantage in terms of the IMD's energy consumption for signal transmission and processing. In this study, we propose a pre-equalization based wireless communication system between the IMD and the WED in order to improve performance in terms of channel estimation, decrease the processing burden on the IMD and importantly provide authentication at the physical layer. An illustration of the proposed scenario is given in Fig.1. Considering the small distance between the IMD and the WED, the resulting path loss lower than that experienced by the nodes located relatively far away from the

patient. These more distant nodes may be adversaries and our goal is to prevent any adversary (AD) from controlling the IMD. Basically, the IMD sends pilot signals to enable the WED to estimate the channel. By using this estimation, the WED pre-equalizes the data signal that is transmitted to the IMD. Assuming that an adversary cannot be closer to the IMD than the WED, the pilot signals will reach the adversary with much less power and greater dispersion and lead to erroneous channel estimation. Since pre-equalization with such an estimation leads to a significant distortion in the AD's signal, an adversary's attempt to communicate with IMD will fail even if the transmitted signal is extremely powerful. In this way, adversaries trying to control or mislead IMDs from relatively distant locations can be prevented from achieving impersonation attacks.

However, these aforementioned techniques may not ensure security if ADs deploy highly advanced signal processing algorithms or hardware having a very small noise floor. Then, they might still be able to estimate the channel, properly. In case of such scenarios, we also introduce a friendly jamming mechanism to our system. In order to achieve this, we design the pilot signal transmitted by IMD as a "wake-up" signal for WED. If the pilot signal is transmitted upon the request of an unauthorized user, the WED is activated and sends a jammer signal to IMD for preventing it from decoding any AD's signal. This capability is extremely important for the IMDs to retain the ability to treat the patient and resist the AD attack. Any wrong treatment, e.g., high voltage injection for a pacemaker and overdosing of an insulin pump, may result in serious problems including death. Also, since equalization is performed in the WED, the proposed technique works in a power efficient way in terms of processing. Also, since more advanced components can be deployed on WEDs because of its size flexibility as compared to IMD, channel estimation performance can be considerably enhanced.

The chapter is organized as follows. Section II provides the system model for the proposed technique. In Section III, channel effects for WED and AD are presented. Finally, numerical results are given in Section IV, and Section V concludes the chapter.



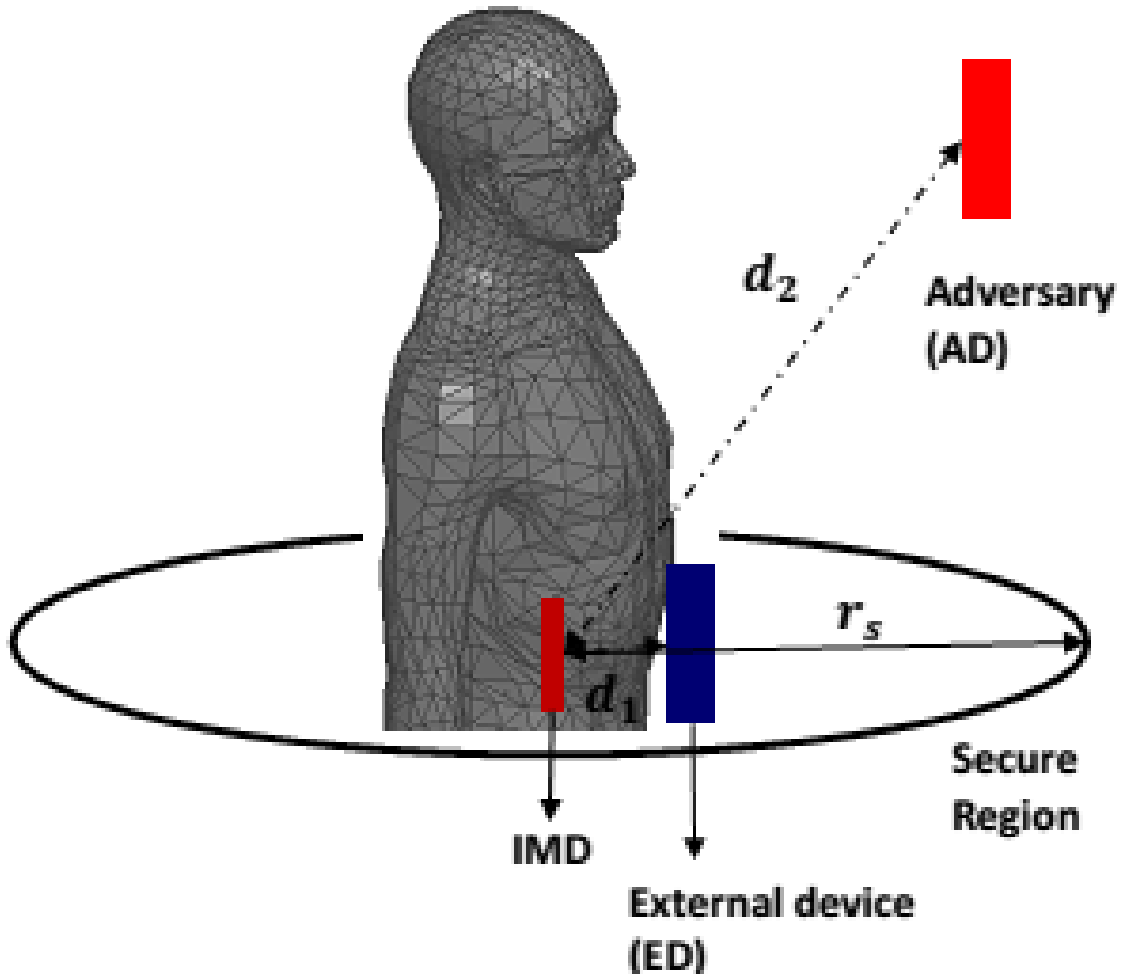


Figure 6.1 Wireless adversaries may perform various malicious attacks and compromise the safety of IMD using patients.

## 6.2 System Model

Channel estimation performed by a WED can be much better than that performed by an IMD because of the greater capabilities of the external device. For example, more advanced device components with a lower noise floor can be used in the design of WEDs and the channel estimation error can be reduced. In this regard, pre-equalization might be a very useful method for IMD communications. As illustrated in Fig. 1, wireless adversaries (AD) may perform various malicious attacks and compromise the safety of IMDs. In our proposed scenario, the IMD transmits a pilot signal,  $p(t)$ , that is used to enable the WED to estimate the channel. Then channel estimation is

performed as

$$h_\epsilon(t) = h(t) + w(t)p^{-1}(t) \quad (6.1)$$

where  $w(t)$  is the additive noise. Note that,  $h_\epsilon$  is defined as a scalar value, i.e, a one-tap channel estimation is performed for pre-equalization considering the non-dispersive medium between IMD and wearable external device (WED). Then, we can give the analytical expression of the baseband signal, transmitted from WED as

$$x(t) = h_\epsilon^{-1} \sum_{n=-\infty}^{\infty} X_n g(t - n\tau_0), \quad (6.2)$$

where  $n$ ,  $g(t)$  and  $\tau_0$  indicate the index of QAM symbol, pulse shaping filter and time spacing between the symbols, respectively. After passing through the linear time-variant channel,  $h(t)$ , received signal including the additive noise can be written as

$$y(t) = \int_{-\infty}^{\infty} h(\tau)x(t - \tau)d\tau. \quad (6.3)$$

Assuming the channel is a one-tap channel due to the small distance between communicating nodes, the received signal can be shown as

$$r(t) = h(t)x(t) + w(t) \quad (6.4)$$

where  $h(t)$  denotes the channel gain as a function of time,  $w(t)$  is the additive noise.

In channel estimation, received pilot symbols are also subject to the channel impairments. Therefore, the estimated channel response can be given as

$$\hat{h} = h + \underbrace{w(t)/P}_\epsilon, \quad (6.5)$$

Table 6.1 Path loss model parameters [1].

Parameter	Parameter Value
$n$	1.48
$d_0$	0.01 m
$P_{0dB}$	39.37 dB

where  $P$  indicates the pilot symbol and  $\epsilon$  stands for the error in channel estimation. Its effect on bit-error-rate (BER) performance should be investigated to identify the secure region around the patient’s body. Considering more sophisticated attacks where ADs are equipped with highly advanced devices, we propose an additional mechanism to ensure authentication. Here, the pilot signal sent by IMD is regarded as a "wake-up" message for the WED. If an AD requests a pilot transmission before sending an unauthorized command to the IMD, the WED activates as soon as IMD sends the pilot signal. Since the WED can easily understand that an unauthorized user made this request, it sends a jamming signal and blocks reception by the IMD. However, the AD may send its signal at the same time with WED and may dominate WED’s command with a very high power. In order to overcome this issue, IMD applies a power threshold criteria not to decode a received message exceeding a certain power level. If the WED sends its jamming signal close to this power level, additional AD signals will likely result in exceeding the pre-determined power threshold and the IMD’s reception will be blocked. In this way, the AD will be disabled from maliciously controlling the IMD.

### 6.3 Channel Models for WED and Adversary

The major effect on a narrow band wireless signal is path loss for in body communications as dispersion in time is generally small compared to the data symbol duration. Also, considering a stationary environment, the frequency dispersion effect of the channel may not need to be taken into account. Note that accounting for dispersion gives us more degrees of freedom to provide security. Therefore, the one-tap technique may be viewed as a worst-case scenario. In order to investigate the channel effect on legitimate and malicious nodes, a path loss channel model obtained as the

function of distance for body-centric communication environment should be used [108, 109]. The general expression for such a model is given as

$$P_{dB} = P_{0dB} + n \left( \frac{d}{d_0} \right) \quad (6.6)$$

where  $d$  is the distance,  $d_0$  is the reference distance and  $P_{0dB}$  is the path loss for reference distance. These parameters for a body model is given in [1] as shown in Table 1. Measurement-based results are also reported in [110, 111] In order to investigate the performance of the users located far away, different channel models might be superposed with the given model. However, we only consider the users nearby the patient. Therefore, only given model will be taken into account.

#### 6.4 Numerical Results

Performance of the proposed technique is presented using MATLAB simulations. Firstly, we investigate the effect of distance between the IMD and other devices on the BER performance. As we mentioned before, a greater distance corresponds to a further path loss. As a device is moving away from the IMD, the power of the received pilot signal become weaker and this will lead to error in channel estimation. A command signal pre-equalized with an erroneous channel estimation will naturally cause a distortion in the signal independent of the signal's SNR. In Fig.2, BER results of a command signal sent from different distances is given, where the SNR of the transmitted signal is specified as 100 dB in order to see the effect of channel estimation error only. As shown in Fig.2, increasing distance of the AD from the IMD and resulting increased channel estimation error dramatically degrade BER performance. For example, if an adversary is located 90 *cm* away from the IMD, more than 1% error probability is experienced for 0 dBm transmission power and -120 dBm noise floor (NF) at the AD.

Considering some scenarios where the AD performs a strong signal processing and uses more advanced hardware having very low noise floors, we also deployed our self-jamming approach to ensure authentication. As mentioned earlier, IMD applies a power-limitation criterion in order to prevent the AD from dominating WED's jamming signal. While determining the WED's jamming

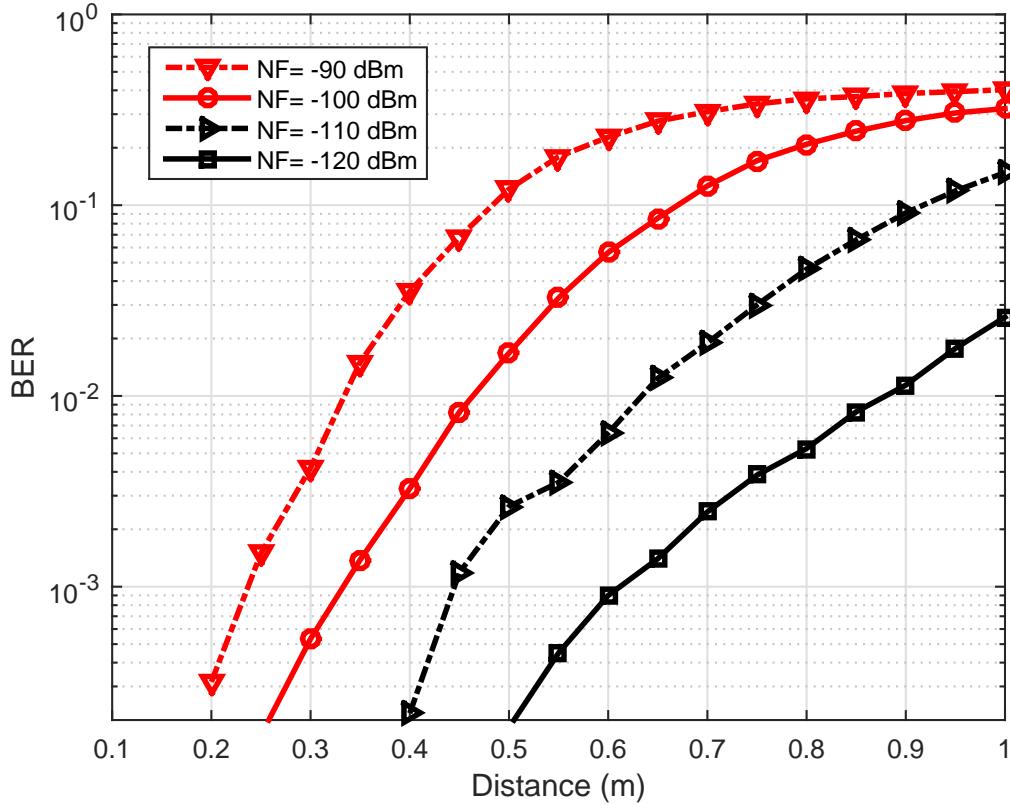


Figure 6.2 BER performance versus distance for different noise floors (NFs).

signal power,  $P_{WED}$ , we used a power threshold  $P_{tr}$  as a metric, i.e.,  $P_{WED}$  is specified in terms of  $P_{tr}$ . Command signals are designed as packets consisting of 150 QPSK symbols and the outage probability of these packets will be used as the performance measure. In Fig. 3, outage probabilities for different jamming powers indicated as  $P_{WED}/P_{tr}$  are given for the AD along with the bit-error probabilities. Note that we assumed that AD has perfect channel estimation and its signal has a 20 dB SNR for this case. Even in such an extreme case, the AD's packets are all distorted when  $P_{WED}$  is 30% of  $P_{tr}$ . Then, we can ensure proper authentication, i.e., blockage of AD, once  $P_{WED}/P_{tr}$  is 0.3 or more.

We also investigate the effect of the proposed technique on the desired communication between the IMD and the WED. The power of the WED's signal is very critical here since IMD stops reception based on the received power. If WED's signal power exceeds  $P_{tr}$  after being combined with

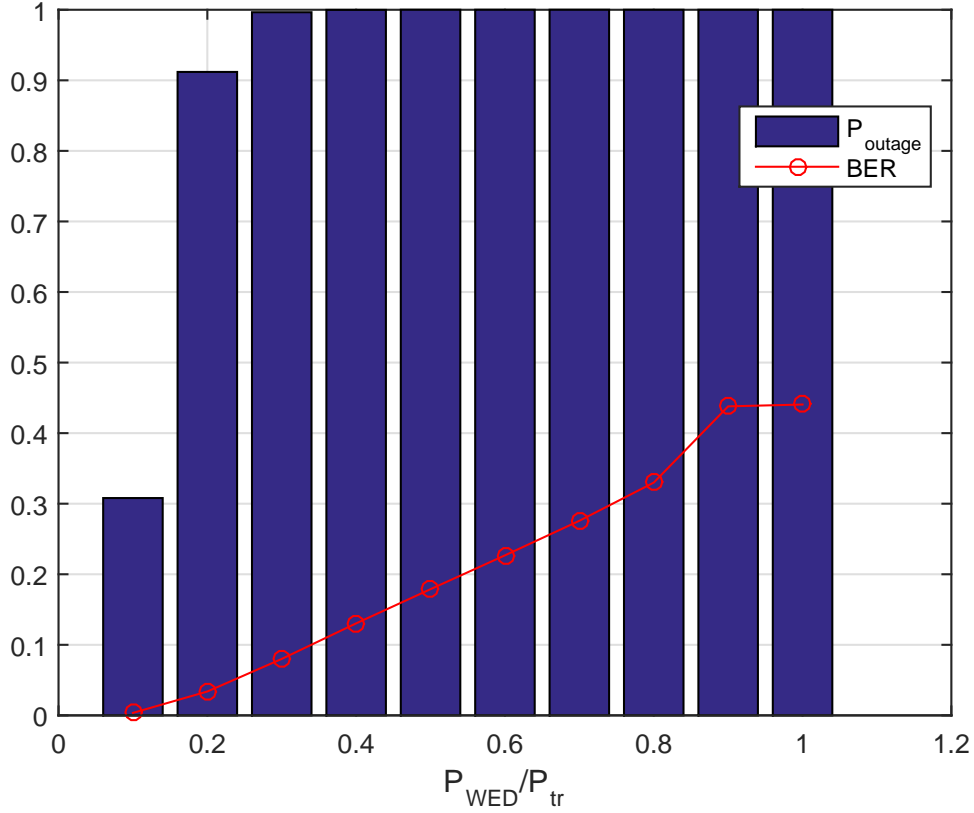


Figure 6.3 Adversary outage probabilities for different jammer signal powers.

noise, legitimate commands will be eliminated as well. In Fig.4, outage probabilities are given as  $P_{outage1}$  and  $P_{outage2}$  for the WED's command with and without proposed technique, respectively. For small power values, outage probability for both cases are almost equal to each other. Here,  $P_{WED}$  is given as 0 dBm and if the  $P_{WED}/P_{tr}$  ratio is 1, the SNR of the received signal is specified as 20 dB, i.e., noise floor of IMD is adjusted for having 20 dB SNR. Then, if  $P_{WED}/P_{tr}$  ratio is 0.1, the SNR becomes 10 dB and the outage probability approaches unity. The proposed technique does not degrade the successful transmission performance of WED unless  $P_{WED}/P_{tr}$  is greater than 0.7. After that level, the probability of blocking the WED packets increases since transmission power gets close to the threshold. Therefore, jamming power of WED  $P_{WED}$  should carefully be selected considering WED's performance and authentication requirements.

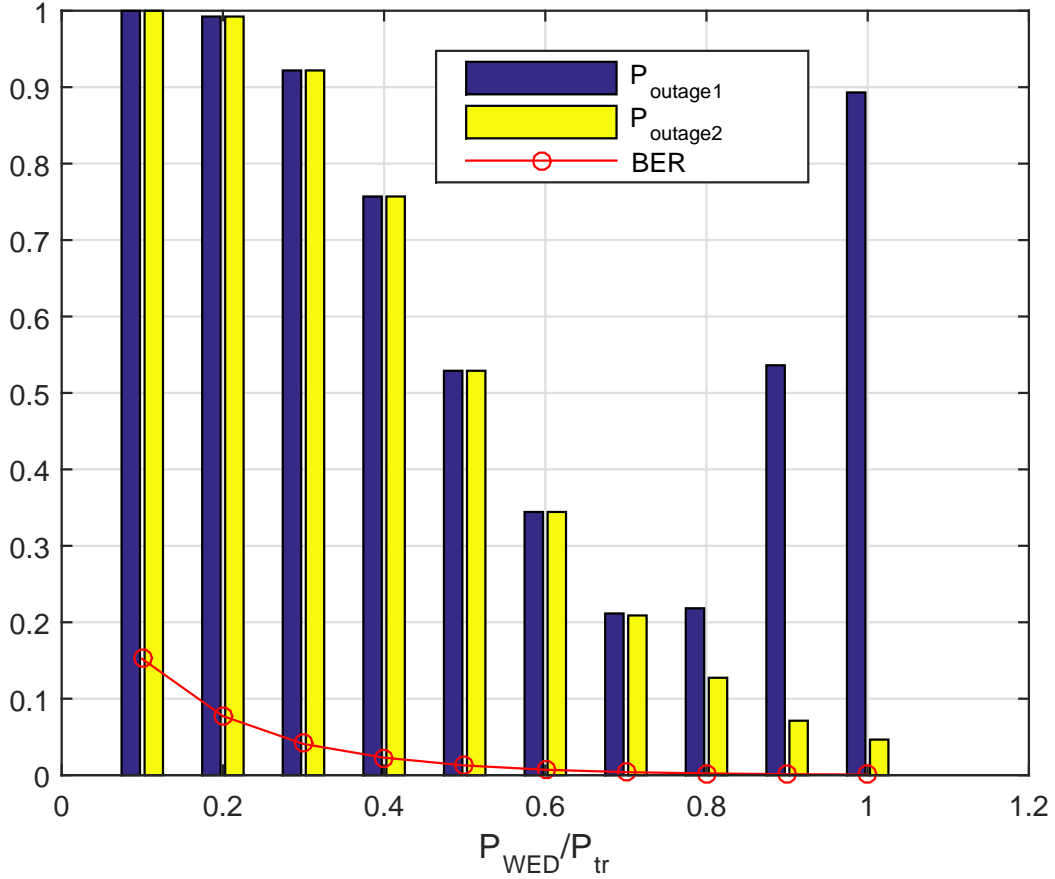


Figure 6.4 Outage probabilities of WED's command with and without proposed technique represented by  $P_{outage1}$  and  $P_{outage2}$ , respectively.

## 6.5 Conclusions

In this study, a physical layer authentication technique based on pre-equalization is proposed for IMDs. Besides authentication, our approach can enhance channel estimation performance by utilizing more advanced hardware and signal processing complexity in the WED because of its external location and not being limited in size as IMDs. Since only path loss was considered for the in vivo channel estimation, including other channel effects, e.g., dispersion in time and frequency will likely enable increase reliability. This will be investigated in our future studies.

## CHAPTER 7

### CONCLUSION AND OPEN ISSUES

In this dissertation, we presented PHY algorithms in waveform design and security for enhancing spectral efficiency and reliability of wireless systems which will be potentially deployed in the near future. Considering different limitations and goals, two algorithms that enhance the characteristics of OFDM-based waveforms in terms of out-of-band emission and peak to average power ratio are provided. The generalization of the proposed schemes along with additional operations such as adjacent channel interference rejection is an open issue and left for the future studies. Considering the increasing heterogeneity of the user requirements we investigated the flexibility aspects of the radio access technologies and provide our proposals for achieving more flexible frames with multiple waveforms and designing advanced numerologies with the novel approaches in the literature. Solid analysis of the proposed methods for future generation scenarios and developing novel approaches beyond the mentioned ones for advanced numerology design are the open issues here.

Practical PHY security methods are also presented for a confidential deployment of wireless technologies. We addressed the eavesdropping problem for OFDM/SC-FDE based broadband systems and impersonation attacks for wireless IMDs. Other security issues for various scenarios should also be investigated while taking the practical limitations into account.



## REFERENCES

- [1] A. F. Demir, Q. H. Abbasi, Z. E. Ankarali, E. Serpedin, H. Arslan *et al.*, “Numerical characterization of in vivo wireless communication channels,” in *IEEE MTT-S International Microwave Workshop Series on RF and Wireless Technologies for Biomedical and Healthcare Applications (IMWS-Bio)*, 2014, pp. 1–3.
- [2] A. Tom, A. Şahin, and H. Arslan, “Suppressing Alignment: Joint PAPR and OOB reduction for OFDM-based systems,” *IEEE Trans. Commun.*, vol. 64, pp. 1100–1109, Mar. 2016.
- [3] Z. E. Ankaralı, B. Peköz, and H. Arslan, “Enhanced OFDM for Enhanced OFDM for 5G RAN G RAN,” *ZTE COMMUNICATIONS*, vol. 15, no. S1, 2017.
- [4] Z. E. Ankaralı, M. H. Yılmaz, M. Hafez, and H. Arslan, “Channel independent physical layer security,” in *IEEE 17th Annual Wireless and Microwave Technology Conference (WAMICON)*, 2016, pp. 1–5.
- [5] J. G. Andrews, S. Buzzi, W. Choi, S. V. Hanly, A. Lozano, A. C. Soong, and J. C. Zhang, “What will 5G be?” *IEEE Journal on Selected Areas in Communications*, vol. 32, no. 6, pp. 1065–1082, 2014.
- [6] “FP7 European Project 318555 5G NOW (5th Generation NonOrthogonal Waveforms for Asynchronous Signalling) 2012. [Online]. Available: <http://www.5gnow.eu/>.”
- [7] “FP7 European Project 317669 METIS (Mobile and Wireless Communications Enablers for the Twenty-Twenty Information Society) 2012. [Online]. Available: <https://www.metis2020.com/>.”
- [8] “FP7 European Project (FP7-ICT-619563) miWaveS (Beyond 2020 Heterogeneous Wireless Networks with Millimeter-Wave Small Cell Access and Backhauling) 2016. [Online]. Available: <http://www.miwaves.eu/>.”
- [9] “Horizon 2020 project (ICT-671660) FANTASTIC-5G (Flexible air interface for scalable service delivery within wireless communication networks of the 5th Generation) 2016. [Online]. Available: <http://fantastic5g.eu/>.”
- [10] Steve Methley, William Webb, Stuart Walker, and John Parker, “5G Candidate Band Study: Study on the Suitability of Potential Candidate Frequency Bands above 6 GHz for Future 5G Mobile Broadband Systems,” Quotient Associates Ltd, Tech. Rep., 2015.
- [11] B. Farhang Boroujeny, “Filter bank multicarrier modulation: A waveform candidate for 5G and beyond,” *Advances in Electrical Engineering*, vol. 2014, 2014.
- [12] A. Sahin, I. Guvenc, and H. Arslan, “A survey on multicarrier communications: Prototype filters, lattice structures, and implementation aspects,” *IEEE Commun. Surveys Tuts.*, vol. 16, no. 3, pp. 1312–1338, 2014.

- [13] F. Hu, *Opportunities in 5G Networks: A Research and Development Perspective*. CRC Press, 2016.
- [14] G. Wunder, P. Jung, M. Kasparick, T. Wild, F. Schaich, Y. Chen, S. Ten Brink, I. Gaspar, N. Michailow, A. Festag *et al.*, “5GNOW: non-orthogonal, asynchronous waveforms for future mobile applications,” *IEEE Commun. Mag.*, vol. 52, no. 2, pp. 97–105, 2014.
- [15] Jialing Li, Erdem Bala, and Rui Yang, “Resource block Filtered-OFDM for future spectrally agile and power efficient systems,” *Physical Communication*, vol. 11, pp. 36–55, jun 2014.
- [16] Ian F. Akyildiz, Shuai Nie, Shih-Chun Lin, and Manoj Chandrasekaran, “5G roadmap: 10 key enabling technologies,” *Computer Networks*, vol. 106, pp. 17 – 48, 2016.
- [17] G. Fettweis, M. Krondorf, and S. Bittner, “GFDM - Generalized Frequency Division Multiplexing,” in *IEEE 69th Vehicular Technology Conference (VTC Spring)*, Apr. 2009, pp. 1–4.
- [18] Rohit Datta, Gerhard Fettweis, Zsolt Kollár, and Peter Horváth, “FBMC and GFDM Interference Cancellation Schemes for Flexible Digital Radio PHY Design,” in *2011 14th Euromicro Conference on Digital System Design*, ser. DSD '11. Washington, DC, USA: Institute of Electrical and Electronics Engineers (IEEE), aug 2011, pp. 335–339.
- [19] “Qualcomm Inc., "Waveform Candidates", 3GPP Standard Contribution (R1-162199), Busan, Korea, April 11-15, 2016.”
- [20] “Huawei, HiSilicon, "5G Waveform: Requirements and Design Principles", 3GPP Standard Contribution (R1-162151), Busan, Korea, April 11-15, 2016.”
- [21] “Huawei, HiSilicon, "f-OFDM scheme and filter design", 3GPP Standard Contribution (R1-165425), Nanjing, China, May 23 - 27, 2016.”
- [22] W. Jiang and M. Schellmann, “Suppressing the out-of-band power radiation in multi-carrier systems: A comparative study,” in *IEEE Global Communications Conference (GLOBECOM)*, 2012, pp. 1477–1482.
- [23] T. Weiss, J. Hillenbrand, A. Krohn, and F. K. Jondral, “Mutual interference in OFDM-based spectrum pooling systems,” in *2004 IEEE 59th Vehicular Technology Conference. VTC 2004-Spring (IEEE Cat. No.04CH37514)*, vol. 4, May 2004, pp. 1873–1877 Vol.4.
- [24] A. Şahin and H. Arslan, “Edge windowing for OFDM based systems,” *IEEE Commun. Lett.*, vol. 15, no. 11, pp. 1208–1211, Sep. 2011.
- [25] S. Brandes, I. Cosovic, and M. Schnell, “Reduction of out-of-band radiation in OFDM systems by insertion of cancellation carriers,” *IEEE Commun. Lett.*, vol. 10, no. 6, pp. 420–422, Jun. 2006.
- [26] D. Qu, Z. Wang, and T. Jiang, “Extended active interference cancellation for sidelobe suppression in cognitive radio OFDM systems with cyclic prefix,” *IEEE Trans. Veh. Technol.*, vol. 59, no. 4, pp. 1689–1695, May 2010.
- [27] I. Cosovic, S. Brandes, and M. Schnell, “Subcarrier weighting: a method for sidelobe suppression in OFDM systems,” *IEEE Commun. Lett.*, vol. 10, no. 6, pp. 444–446, Jun. 2006.
- [28] A. Tom, A. Şahin, and H. Arslan, “Mask compliant precoder for OFDM spectrum shaping,” *IEEE Commun. Lett.*, vol. 17, no. 3, pp. 447–450, Mar. 2013.

- [29] Y. Rahmatallah and S. Mohan, "Peak-To-Average Power Ratio Reduction in OFDM Systems: A Survey And Taxonomy," *IEEE Commun. Surveys Tuts.*, vol. 15, no. 4, pp. 1567–1592, Fourth 2013.
- [30] A. Ghassemi, L. Lampe, A. Attar, and T. A. Gulliver, "Joint sidelobe and peak power reduction in OFDM-based cognitive radio," in *IEEE 72nd Vehicular Technology Conf. (VTC) Fall*, Sep. 2010, pp. 1–5.
- [31] E. Güvenkaya, A. Tom, and H. Arslan, "Joint Sidelobe Suppression and PAPR Reduction in OFDM Using Partial Transmit Sequences," in *IEEE Military Communications Conference (MILCOM)*, Nov 2013, pp. 95–100.
- [32] C. Ni, T. Jiang, and W. Peng, "Joint PAPR Reduction and Sidelobe Suppression Using Signal Cancellation in NC-OFDM-Based Cognitive Radio Systems," *IEEE Trans. Veh. Technol.*, vol. 64, no. 3, pp. 964–972, March 2015.
- [33] A. Tom, A. Şahin, and H. Arslan, "Suppressing alignment: An approach for out-of-band interference reduction in OFDM systems," in *2015 IEEE International Conference on Communications (ICC)*, June 2015, pp. 4630–4634.
- [34] M. Maso, M. Debbah, and L. Vangelista, "A Distributed Approach to Interference Alignment in OFDM-Based Two-Tiered Networks," *IEEE Trans. Veh. Technol.*, vol. 62, no. 5, pp. 1935–1949, Jun 2013.
- [35] M. Maso, S. Lakshminarayana, T. Q. Quek, and H. V. Poor, "A composite approach to self-sustainable transmissions: Rethinking OFDM," *IEEE Trans. Commun.*, vol. 62, no. 11, pp. 3904–3917, Oct. 2014.
- [36] Z. E. Ankarali, A. Sahin, and H. Arslan, "Static Cyclic Prefix Alignment for OFDM-Based Waveforms," in *IEEE Global Communications Conference (GLOBECOM) Workshops*, Dec. 2016.
- [37] A. A. Zaidi, R. Baldemair, H. Tullberg, H. Bjorkegren, L. Sundstrom, J. Medbo, C. Kilinc, and I. Da Silva, "Waveform and Numerology to Support 5G Services and Requirements," *IEEE Commun. Mag.*, vol. 54, no. 11, pp. 90–98, November 2016.
- [38] Z. E. Ankarali and H. Arslan, "Joint physical layer security and PAPR mitigation in OFDM systems," Oct. 25 2016, US Patent 9,479,375.
- [39] Z. E. Ankarali, A. Sahin, and H. Arslan, "Joint Time-Frequency Alignment for PAPR and OOB Suppression of OFDM-Based Waveforms," *IEEE Communications Letters*, 2017.
- [40] Z. E. Ankarali, A. Sahin, and H. Arslan, "Static Cyclic Prefix Alignment for OFDM-Based Waveforms," in *Globecom Workshops (GC Wkshps), 2016 IEEE*. IEEE, 2016, pp. 1–6.
- [41] J. Lofberg, "YALMIP: A toolbox for modeling and optimization in MATLAB," in *IEEE Int. Sym. on Comp. Aided Control Sys. Design*, Sep. 2004, pp. 284–289.
- [42] S. Brandes, I. Cosovic, and M. Schnell, "Reduction of out-of-band radiation in OFDM systems by insertion of cancellation carriers," *IEEE Commun. Lett.*, vol. 10, no. 6, pp. 420–422, Jun. 2006.
- [43] E. Guvenkaya, A. Şahin, and H. Arslan, "N-continuous OFDM with CP alignment," in *IEEE Military Communications Conf. (MILCOM)*, Oct. 2015, pp. 587–592.

- [44] H. Maleki, S. A. Jafar, and S. Shamai, “Retrospective interference alignment over interference networks,” *IEEE J Sel. Topics in Signal Process.*, vol. 6, no. 3, pp. 228–240, 2012.
- [45] M. A. Maddah Ali and D. Tse, “Completely stale transmitter channel state information is still very useful,” *IEEE Trans. Inf. Theory*, vol. 58, no. 7, pp. 4418–4431, Oct. 2012.
- [46] Z. ANKARALI, B. Pekoz, and H. ARSLAN, “Flexible Radio Access Beyond 5G: A Future Projection on Waveform, Numerology & Frame Design Principles,” *IEEE Access*, 2017.
- [47] Luís Carlos Gonçalves, Pedro Sebastião, Nuno Souto, and Américo Correia, “On the Impact of User Segmentation and Behaviour Analysis over Traffic Generation in beyond 4G Networks,” *Trans. Emerging Tel. Tech.*, Feb. 2015.
- [48] X. Zhang, L. Chen, J. Qiu, and J. Abdoli, “On the Waveform for 5G,” *IEEE Commun. Mag.*, vol. 54, no. 11, pp. 74–80, 2016.
- [49] A. A. Zaidi, R. Baldemair, H. Tullberg, H. Bjorkegren, L. Sundstrom, J. Medbo, C. Kilinc, and I. Da Silva, “Waveform and Numerology to Support 5G Services and Requirements,” *IEEE Commun. Mag.*, vol. 54, no. 11, pp. 90–98, November 2016.
- [50] “Number of Smartphone Users in the U.S. 2010-2021,” <https://www.statista.com/statistics/201182/forecast-of-smartphone-users-in-the-us/>.
- [51] “Cisco Visual Networking Index: Global Mobile Data Traffic Forecast Update, 2015-2020 White Paper,” Tech. Rep., 2016.
- [52] J. Wiart, C. Dale, A. V. Bosisio, and A. Le Cornec, “Analysis of the influence of the power control and discontinuous transmission on RF exposure with GSM mobile phones,” *IEEE Trans. Electromagnetic Compatibility*, vol. 42, no. 4, pp. 376–385, 2000.
- [53] W. Webb and R. Steele, “Variable rate QAM for mobile radio,” *IEEE Trans. Commun.*, vol. 43, no. 7, pp. 2223–2230, 1995.
- [54] A. J. Goldsmith and S.-G. Chua, “Variable-rate variable-power MQAM for fading channels,” *IEEE Transactions on communications*, vol. 45, no. 10, pp. 1218–1230, 1997.
- [55] G. J. Pottie, “System design choices in personal communications,” *IEEE Personal Communications*, vol. 2, no. 5, pp. 50–67, 1995.
- [56] Z. Han and K. J. R. Liu, “Rate Adaptation,” in *Resource Allocation for Wireless Networks: Basics, Techniques, and Applications*. Cambridge University Press, Apr. 2008, pp. 75–98.
- [57] F. Khan, “Downlink Access,” in *LTE for 4G Mobile Broadband: Air Interface Technologies and Performance*. Cambridge University Press, Mar. 2009, pp. 20–69.
- [58] L. Hanzo, H. Haas, S. Imre, D. O’Brien, M. Rupp, and L. Gyongyosi, “Wireless Myths, Realities, and Futures: From 3G/4G to Optical and Quantum Wireless,” *Proc IEEE*, vol. 100, no. Special Centennial Issue, pp. 1853–1888, May 2012.
- [59] F. M. Han and X. D. Zhang, “Wireless Multicarrier Digital Transmission via Weyl-Heisenberg Frames over Time-Frequency Dispersive Channels,” *IEEE Trans. Commun.*, vol. 57, no. 6, pp. 1721–1733, Jun. 2009.
- [60] B. Farhang Boroujeny, “OFDM Versus Filter Bank Multicarrier,” *IEEE Sig. Proc. Mag.*, vol. 28, no. 3, pp. 92–112, 2011.

- [61] D. Astely, E. Dahlman, A. FuruskÅdr, Y. Jading, M. LindstrÅm, and S. Parkvall, "LTE: The Evolution of Mobile Broadband," *IEEE Commun. Mag.*, vol. 47, no. 4, pp. 44–51, Apr. 2009.
- [62] H. Holma and A. Toskala, Eds., *LTE for UMTS: Evolution to LTE-Advanced*, 2nd ed. Chichester, West Sussex, United Kingdom: Wiley, 2011.
- [63] N. Guo, *Implementation Aspects of 3GPP TD-LTE*, 2009.
- [64] M. Agiwal, A. Roy, and N. Saxena, "Next Generation 5G Wireless Networks: A Comprehensive Survey," *IEEE Commun. Surv. Tutor.*, vol. 18, no. 3, pp. 1617–1655, thirdquarter 2016.
- [65] "Nokia, Alcatel-Lucent Shanghai Bell, "Guard band arrangement supporting mixed numerology", 3GPP Standard Contribution (R1-1701151), Spokane, U.S.A., January 16 - 20, 2017."
- [66] "NTT DOCOMO, INC., "Text Proposal to TR 38.804 on physical layer aspects", 3GPP Standard Contribution (R1-1700638), Spokane, U.S.A., January 16 - 20, 2017."
- [67] "NTT DOCOMO, INC., "Workplan for Study on NR Access Technology", 3GPP Standard Contribution (R1-1610052), Lisbon, Portugal, October 10 - 14, 2016."
- [68] Robert W. Chang, "Synthesis of Band-Limited Orthogonal Signals for Multichannel Data Transmission," *The Bell System Technical J.*, pp. 1775–1796, Dec. 1966.
- [69] B. Saltzberg, "Performance of an efficient parallel data transmission system," *IEEE Trans. Commun. Technol.*, vol. 15, no. 6, pp. 805–811, Dec. 1967.
- [70] R. van Nee and R. Prasad, *OFDM for Wireless Multimedia Communications*, 1st ed. Norwood, MA, USA: Artech House, Inc., 2000.
- [71] A. A. Nasir, S. Durrani, H. Mehrpouyan, S. D. Blostein, and R. A. Kennedy, "Timing and Carrier Synchronization in Wireless Communication Systems: A Survey and Classification of Research in the Last 5 Years," *EURASIP J. Wirel. Commun. Netw.*, vol. 2016, no. 1, p. 180, 2016.
- [72] H. Ishii and G. W. Wornell, "OFDM blind parameter identification in cognitive radios," in *Proc. IEEE 16th Int. Symp. Personal, Indoor and Mobile Radio Communications*, Berlin, DE, Sep. 2005, pp. 700–705.
- [73] P. D. Sutton, K. E. Nolan, and L. E. Doyle, "Cyclostationary signatures in practical cognitive radio applications," *Selected Areas in Communications, IEEE Journal on*, vol. 26, no. 1, pp. 13–24, 2008.
- [74] S.-H. Fang, J.-Y. Chen, M.-D. Shieh, and J.-S. Lin, "Subspace-based blind channel estimation by separating real and imaginary symbols for cyclic-prefixed single-carrier systems," *Broad-casting, IEEE Transactions on*, vol. 59, no. 4, pp. 698–704, 2013.
- [75] Z. E. Ankarali and H. Arslan, "Cyclic feature suppression for physical layer security," *Physical Communication*, 2016.
- [76] E. Bala, J. Li, and R. Yang, "Shaping spectral leakage: a novel low-complexity transceiver architecture for cognitive radio," vol. 8, no. 3, pp. 38–46, 2013.
- [77] "CMCC, "Discussion and Evaluation on Numerology Design for High Speed Train Scenario", 3GPP Standard Contribution (R1-167107), Gothenburg, Sweden, August 22 - 26, 2016."

- [78] E. Lähetkangas, K. Pajukoski, J. Vihriälä, G. Berardinelli, M. Lauridsen, E. Tirola, and P. Mogensen, "Achieving Low Latency and Energy Consumption by 5G TDD Mode Optimization," in *Proc. IEEE Int. Conf. Communications Workshops*, Sydney, AU, Jun. 2014, pp. 1–6.
- [79] H. Ochiai and H. Imai, "On the Distribution of the Peak-to-Average Power Ratio in OFDM Signals," *IEEE Trans. Commun.*, vol. 49, no. 2, pp. 282–289, Feb. 2001.
- [80] "5G Vision, Requirements, and Enabling Technologies," 5G Forum, Whitepaper V.2.0, Mar. 2016. [Online]. Available: <http://kani.or.kr/5g/whitepaper/5gVision,Requirements,andEnablingTechnologies.pdf>
- [81] A. Sahin and H. Arslan, "Multi-User Aware Frame Structure for OFDMA Based System," in *Proc. IEEE Vehicular Technology Conf.-Fall*, Québec City, QC, Sep. 2012, pp. 1–5.
- [82] A. Şahin, . Güvenç, and H. Arslan, "A Comparative Study of FBMC Prototype Filters in Doubly Dispersive Channels," in *Proc. IEEE Global Communications Conf. Workshops*, Anaheim, CA, Dec. 2012, pp. 197–203.
- [83] A. Sahin and H. Arslan, "The Impact of Scheduling on Edge Windowing," in *Proc. IEEE Global Communications Conf.*, Dec. 2011, pp. 1–5.
- [84] E. Guvenkaya, E. Bala, R. Yang, and H. Arslan, "Time-Asymmetric and Subcarrier-Specific Pulse Shaping in OFDM-Based Waveforms," *IEEE Trans. Veh. Technol.*, vol. PP, no. 99, pp. 1–1, 2014.
- [85] Z. E. Ankaralı, A. Şahin, and H. Arslan, "Intentional-overlapping for multicarrier schemes based on user-specific filters," *Analog Integrated Circuits and Signal Processing*, vol. 78, no. 3, pp. 683–690, 2014.
- [86] L. Zou, "Detection of the guard interval length in OFDM systems," in *Consumer Communications and Networking Conference, 2006. CCNC 2006. 3rd IEEE*, vol. 2. IEEE, 2006, pp. 1048–1051.
- [87] H. Li, Y. Bar Ness, A. Abdi, O. S. Somekh, and W. Su, "OFDM modulation classification and parameters extraction," in *Cognitive Radio Oriented Wireless Networks and Communications, 2006. 1st International Conference on.* IEEE, 2006, pp. 1–6.
- [88] T. Yücek and H. Arslan, "OFDM signal identification and transmission parameter estimation for cognitive radio applications," in *Global Telecommunications Conference, 2007. GLOBECOM'07. IEEE.* IEEE, 2007, pp. 4056–4060.
- [89] W.-L. Chin, "Blind symbol synchronization for OFDM systems using cyclic prefix in time-variant and long-echo fading channels," *Vehicular Technology, IEEE Transactions on*, vol. 61, no. 1, pp. 185–195, 2012.
- [90] C. Shin, R. W. Heath, and E. J. Powers, "Non-redundant precoding-based blind and semi-blind channel estimation for MIMO block transmission with a cyclic prefix," *Signal Processing, IEEE Transactions on*, vol. 56, no. 6, pp. 2509–2523, 2008.
- [91] R. R. Meyer and M. N. Newhouse, "OFDM waveform feature suppression," in *MILCOM 2002. Proceedings*, vol. 1. IEEE, 2002, pp. 582–586.
- [92] H. Hurd, "Stationarizing properties of random shifts," *SIAM Journal on Applied Mathematics*, vol. 26, no. 1, pp. 203–212, 1974.

- [93] S. C. Surender and R. M. Narayanan, "Synchronization for wireless multi-radar covert communication networks," in *Defense and Security Symposium*. International Society for Optics and Photonics, 2007, pp. 65 780U–65 780U.
- [94] X. Wang, P. Ho, and Y. Wu, "Robust channel estimation and ISI cancellation for OFDM systems with suppressed features," *Selected Areas in Communications, IEEE Journal on*, vol. 23, no. 5, pp. 963–972, 2005.
- [95] T. Yucek and H. Arslan, "Feature suppression for physical-layer security in OFDM systems," in *IEEE Military Communications Conference (MILCOM)*, 2007, pp. 1–5.
- [96] M. Bouanen, F. Gagnon, G. Kaddoum, D. Couillard, and C. Thibeault, "An LPI design for secure OFDM systems," in *IEEE Military Communication Conference (MILCOM)*, 2013, pp. 1–6.
- [97] Z. E. Ankarali, M. Karabacak, and H. Arslan, "Cyclic Feature Concealing CP Selection for Physical Layer Security," in *IEEE Military Communications Conference (MILCOM)*, 2014, pp. 485–489.
- [98] R. W. Heath Jr and G. B. Giannakis, "Exploiting input cyclostationarity for blind channel identification in OFDM systems," *Signal Processing, IEEE Transactions on*, vol. 47, no. 3, pp. 848–856, 1999.
- [99] *802.11a-1999 - IEEE Standard for Telecommunications and Information Exchange Between Systems - LAN/MAN Specific Requirements - Part 11: Wireless Medium Access Control (MAC) and physical layer (PHY) specifications: High Speed Physical Layer in the 5 GHz band*, Std.
- [100] Z. E. Ankarali, A. F. Demir, H. Arslan, and R. D. Gitlin, "Physical layer security for wireless implantable medical devices," Aug. 29 2017, US Patent 9,749,086.
- [101] D. T. Halperin, T. S. Heydt Benjamin, B. Ransford, S. S. Clark, B. Defend, W. Morgan, K. Fu, T. Kohno, and W. H. Maisel, "Pacemakers and implantable cardiac defibrillators: Software radio attacks and zero-power defenses," in *IEEE Symposium on Security and Privacy*, 2008.
- [102] K. Malasri and L. Wang, "Securing wireless implantable devices for healthcare: Ideas and challenges," *IEEE Comm. Mag.*, vol. 47.7, pp. 74–80, 2009.
- [103] W. H. Maisel and K. Tadayoshi, "Improving the security and privacy of implantable medical devices," *New England journal of medicine*, vol. 362.13, p. 1164, 2010.
- [104] *Insulin pumps - global pipeline analysis, opportunity assessment and market forecasts to 2016, globaldata. Global Data (2010)*.
- [105] K. Fu, "Inside risks: Reducing risks of implantable medical devices," *Communications of the ACM*, vol. 52.6, pp. 25–27, 2009.
- [106] Z. Ankarali, Q. H. Abbasi, A. F. Demir, E. Serpedin, K. Qaraqe, and H. Arslan, "A comparative review on the wireless implantable medical devices privacy and security," in *EAI 4th International Conference on Wireless Mobile Communication and Healthcare (Mobihealth)*. IEEE, 2014, pp. 246–249.
- [107] S. Gollakota, H. Hassanieh, B. Ransford, D. Katabi, and K. Fu, "They can hear your heartbeats: non-invasive security for implantable medical devices," *ACM SIGCOMM Computer Communication Review*, vol. 41.4, pp. 2–13, 2011.

- [108] A. F. Demir, Z. E. Ankarali, Q. H. Abbasi, Y. Liu, K. Qaraqe, E. Serpedin, H. Arslan, and R. D. Gitlin, "In Vivo Communications: Steps Toward the Next Generation of Implantable Devices," *IEEE Vehicular Technology Magazine*, vol. 11, no. 2, pp. 32–42, 2016.
- [109] A. F. Demir, Z. E. Ankarali, Y. Liu, Q. H. Abbasi, K. Qaraqe, E. Serpedin, H. Arslan, and R. D. Gitlin, "In Vivo Wireless Channel Modeling," *Advances in Body-Centric Wireless Communication: Applications and state-of-the-art. Institution of Engineering and Technology*, pp. 187–211, 2016.
- [110] A. F. Demir, Q. H. Abbasi, Z. E. Ankarali, M. Qaraqe, E. Serpedin, and H. Arslan, "Experimental characterization of in vivo wireless communication channels," in *IEEE Vehicular Technology Conference (VTC Fall)*, 2015, pp. 1–2.
- [111] A. F. Demir, Q. Abbasi, Z. E. Ankarali, A. Alomainy, K. Qaraqe, E. Serpedin, and H. Arslan, "Anatomical Region-Specific In Vivo Wireless Communication Channel Characterization," *IEEE J. Biomedical and Health Informatics*, 2017.



## APPENDICES

## Appendix A: Copyright Permissions

The copyright notices for the use of material in Chapter 1 are below.

**PERMISSION REQUEST**

9/19/2017

To: ZTE Communications,

I am a graduate student at University of South Florida. I am in the process of preparing a dissertation for publication and am seeking permission to include the following material in my publication. A copy of the work is enclosed.

Authors: Zekeriyya Esat Ankarali, Berker Pekoz, Huseyin Arslan  
Title: Enhanced OFDM for 5G RAN  
Publication: ZTE Communications, vol. 15, no. S1  
Date: June 25, 2017  
Content requested: Full paper

The work will be used in the following manner: I would like to include parts of the figures and texts from the requested work in my dissertation to be published. The publication information is as follows: **Title:** Physical Layer Algorithms for Reliability and Spectral Efficiency in Wireless Communications, **Publication type:** dissertation, **Publisher:** University of South Florida, **Publication Date:** Dec. 9, 2017.

Please indicate your approval of this request by signing the letter where indicated below and returning it to me as soon as possible. Your signing of this letter will also confirm that you own the copyright to the above-described material.

Very truly yours,

Zekeriyya Esat Ankarali, Ph.D. candidate


Zekeriyya  
Ankarali

Email: [zekeriyya@mail.usf.edu](mailto:zekeriyya@mail.usf.edu)  
Tel: +1(813)382 4604  
Address: 4202 E Fowler Ave. ENB 118, Tampa, FL, USA, 33613

For copyright owner use:

**PERMISSION GRANTED FOR THE USE REQUESTED ABOVE:**

By: Xinming Huang  
Title: Executive Vice Editor in Chief  
Date: Sept. 25, 2017



## Appendix A (Continued)

11/12/2017

Rightslink® by Copyright Clearance Center



# RightsLink®

Home

Account Info

Help



**Title:** Channel independent physical layer security

**Conference Proceedings:** Wireless and Microwave Technology Conference (WAMICON), 2016 IEEE 17th Annual

**Author:** Z. Esat Ankarali

**Publisher:** IEEE

**Date:** April 2016

Copyright © 2016, IEEE

Logged in as:  
ZEKERIYYA ANKARALI  
Account #:  
3001063876

LOGOUT

### Thesis / Dissertation Reuse

**The IEEE does not require individuals working on a thesis to obtain a formal reuse license, however, you may print out this statement to be used as a permission grant:**

*Requirements to be followed when using any portion (e.g., figure, graph, table, or textual material) of an IEEE copyrighted paper in a thesis:*

- 1) In the case of textual material (e.g., using short quotes or referring to the work within these papers) users must give full credit to the original source (author, paper, publication) followed by the IEEE copyright line © 2011 IEEE.
- 2) In the case of illustrations or tabular material, we require that the copyright line © [Year of original publication] IEEE appear prominently with each reprinted figure and/or table.
- 3) If a substantial portion of the original paper is to be used, and if you are not the senior author, also obtain the senior author's approval.

*Requirements to be followed when using an entire IEEE copyrighted paper in a thesis:*

- 1) The following IEEE copyright/ credit notice should be placed prominently in the references: © [year of original publication] IEEE. Reprinted, with permission, from [author names, paper title, IEEE publication title, and month/year of publication]
- 2) Only the accepted version of an IEEE copyrighted paper can be used when posting the paper or your thesis on-line.
- 3) In placing the thesis on the author's university website, please display the following message in a prominent place on the website: In reference to IEEE copyrighted material which is used with permission in this thesis, the IEEE does not endorse any of [university/educational entity's name goes here]'s products or services. Internal or personal use of this material is permitted. If interested in reprinting/republishing IEEE copyrighted material for advertising or promotional purposes or for creating new collective works for resale or redistribution, please go to [http://www.ieee.org/publications\\_standards/publications/rights/rights\\_link.html](http://www.ieee.org/publications_standards/publications/rights/rights_link.html) to learn how to obtain a License from RightsLink.

If applicable, University Microfilms and/or ProQuest Library, or the Archives of Canada may supply single copies of the dissertation.

BACK

CLOSE WINDOW

Copyright © 2017 [Copyright Clearance Center, Inc.](#) All Rights Reserved. [Privacy statement](#). [Terms and Conditions](#).  
Comments? We would like to hear from you. E-mail us at [customer@copyright.com](mailto:customer@copyright.com)


<https://s100.copyright.com/AppDispatchServlet#formTop>

1/1

## Appendix A (Continued)

The copyright notice for the use of material in Chapter 2 is below.

9/11/2017 Rightslink® by Copyright Clearance Center

  [Home](#) [Account Info](#) [Help](#) 

 **Title:** Joint Time-Frequency Alignment for PAPR and OOB Suppression of OFDM-Based Waveforms  
**Author:** Z. Esat Ankarali  
**Publication:** IEEE Communications Letters  
**Publisher:** IEEE  
**Date:** Dec 31, 1969  
Copyright © 1969, IEEE

Logged in as: ZEKERIYYA ANKARALI  
Account #: 3001063876  
[LOGOUT](#)

### Thesis / Dissertation Reuse

**The IEEE does not require individuals working on a thesis to obtain a formal reuse license, however, you may print out this statement to be used as a permission grant:**

*Requirements to be followed when using any portion (e.g., figure, graph, table, or textual material) of an IEEE copyrighted paper in a thesis:*

- 1) In the case of textual material (e.g., using short quotes or referring to the work within these papers) users must give full credit to the original source (author, paper, publication) followed by the IEEE copyright line © 2011 IEEE.
- 2) In the case of illustrations or tabular material, we require that the copyright line © [Year of original publication] IEEE appear prominently with each reprinted figure and/or table.
- 3) If a substantial portion of the original paper is to be used, and if you are not the senior author, also obtain the senior author's approval.

*Requirements to be followed when using an entire IEEE copyrighted paper in a thesis:*

- 1) The following IEEE copyright/ credit notice should be placed prominently in the references: © [year of original publication] IEEE. Reprinted, with permission, from [author names, paper title, IEEE publication title, and month/year of publication]
- 2) Only the accepted version of an IEEE copyrighted paper can be used when posting the paper or your thesis on-line.
- 3) In placing the thesis on the author's university website, please display the following message in a prominent place on the website: In reference to IEEE copyrighted material which is used with permission in this thesis, the IEEE does not endorse any of [university/educational entity's name goes here]'s products or services. Internal or personal use of this material is permitted. If interested in reprinting/republishing IEEE copyrighted material for advertising or promotional purposes or for creating new collective works for resale or redistribution, please go to [http://www.ieee.org/publications\\_standards/publications/rights/rights\\_link.html](http://www.ieee.org/publications_standards/publications/rights/rights_link.html) to learn how to obtain a License from RightsLink.

If applicable, University Microfilms and/or ProQuest Library, or the Archives of Canada may supply single copies of the dissertation.




[BACK](#)  [CLOSE WINDOW](#)


Copyright © 2017 [Copyright Clearance Center, Inc.](#) All Rights Reserved. [Privacy statement](#). [Terms and Conditions](#).  
Comments? We would like to hear from you. E-mail us at [customer-care@copyright.com](mailto:customer-care@copyright.com)

## Appendix A (Continued)

The copyright notice for the use of material in Chapter 3 is below.

9/11/2017 Rightslink® by Copyright Clearance Center

  [Home](#) [Account Info](#) [Help](#) 

 **Requesting permission to reuse content from an IEEE publication**

**Title:** Static Cyclic Prefix Alignment for OFDM-Based Waveforms  
**Conference Proceedings:** Globecom Workshops (GC Wkshps), 2016 IEEE  
**Author:** Z. Esat Ankarali  
**Publisher:** IEEE  
**Date:** DEC. 2016  
Copyright © 2016, IEEE

Logged in as:  
ZEKERIYYA ANKARALI  
Account #:  
3001063876  
[LOGOUT](#)

### Thesis / Dissertation Reuse

**The IEEE does not require individuals working on a thesis to obtain a formal reuse license, however, you may print out this statement to be used as a permission grant:**

*Requirements to be followed when using any portion (e.g., figure, graph, table, or textual material) of an IEEE copyrighted paper in a thesis:*

- 1) In the case of textual material (e.g., using short quotes or referring to the work within these papers) users must give full credit to the original source (author, paper, publication) followed by the IEEE copyright line ♠ 2011 IEEE.
- 2) In the case of illustrations or tabular material, we require that the copyright line ♠ [Year of original publication] IEEE appear prominently with each reprinted figure and/or table.
- 3) If a substantial portion of the original paper is to be used, and if you are not the senior author, also obtain the senior author's approval.

*Requirements to be followed when using an entire IEEE copyrighted paper in a thesis:*

- 1) The following IEEE copyright/ credit notice should be placed prominently in the references: ♠ [year of original publication] IEEE. Reprinted, with permission, from [author names, paper title, IEEE publication title, and month/year of publication]
- 2) Only the accepted version of an IEEE copyrighted paper can be used when posting the paper or your thesis on-line.
- 3) In placing the thesis on the author's university website, please display the following message in a prominent place on the website: In reference to IEEE copyrighted material which is used with permission in this thesis, the IEEE does not endorse any of [university/educational entity's name goes here]'s products or services. Internal or personal use of this material is permitted. If interested in reprinting/republishing IEEE copyrighted material for advertising or promotional purposes or for creating new collective works for resale or redistribution, please go to [http://www.ieee.org/publications\\_standards/publications/rights/rights\\_link.html](http://www.ieee.org/publications_standards/publications/rights/rights_link.html) to learn how to obtain a License from RightsLink.

If applicable, University Microfilms and/or ProQuest Library, or the Archives of Canada may supply single copies of the dissertation.

[BACK](#)

[CLOSE WINDOW](#)

Copyright © 2017 [Copyright Clearance Center, Inc.](#) All Rights Reserved. [Privacy statement](#). [Terms and Conditions](#).  
Comments? We would like to hear from you. E-mail us at [customer-care@copyright.com](mailto:customer-care@copyright.com)

## Appendix A (Continued)

The copyright notice for the use of material in Chapter 4 is below.

9/11/2017 Rightslink® by Copyright Clearance Center

  [Home](#) [Account Info](#) [Help](#) 

 **Title:** Flexible Radio Access Beyond 5G: A Future Projection on Waveform, Numerology & Frame Design Principles

**Author:** ZEKERIYYA ANKARALI

**Publication:** IEEE Access

**Publisher:** IEEE

**Date:** Dec 31, 1969

Copyright © 1969, IEEE

Logged in as:  
ZEKERIYYA ANKARALI  
Account #:  
3001063876

[LOGOUT](#)

### Thesis / Dissertation Reuse

**The IEEE does not require individuals working on a thesis to obtain a formal reuse license, however, you may print out this statement to be used as a permission grant:**

*Requirements to be followed when using any portion (e.g., figure, graph, table, or textual material) of an IEEE copyrighted paper in a thesis:*

- 1) In the case of textual material (e.g., using short quotes or referring to the work within these papers) users must give full credit to the original source (author, paper, publication) followed by the IEEE copyright line ♦ 2011 IEEE.
- 2) In the case of illustrations or tabular material, we require that the copyright line ♦ [Year of original publication] IEEE appear prominently with each reprinted figure and/or table.
- 3) If a substantial portion of the original paper is to be used, and if you are not the senior author ♦s approval.

*Requirements to be followed when using an entire IEEE copyrighted paper in a thesis:*

- 1) The following IEEE copyright/ credit notice should be placed prominently in the references: ♦ [year of original publication] IEEE. Reprinted, with permission, from [author names, paper title, IEEE publication title, and month/year of publication]
- 2) Only the accepted version of an IEEE copyrighted paper can be used when posting the paper or your thesis on-line.
- 3) In placing the thesis on the author's university website, please display the following message in a prominent place on the website: In reference to IEEE copyrighted material which is used with permission in this thesis, the IEEE does not endorse any of [university/educational entity's name goes here]'s products or services. Internal or personal use of this material is permitted. If interested in reprinting/republishing IEEE copyrighted material for advertising or promotional purposes or for creating new collective works for resale or redistribution, please go to [http://www.ieee.org/publications\\_standards/publications/rights/rights\\_link.html](http://www.ieee.org/publications_standards/publications/rights/rights_link.html) to learn how to obtain a License from RightsLink.

If applicable, University Microfilms and/or ProQuest Library, or the Archives of Canada may supply single copies of the dissertation.

[BACK](#)

[CLOSE WINDOW](#)

Copyright © 2017 [Copyright Clearance Center, Inc.](#) All Rights Reserved. [Privacy statement](#). [Terms and Conditions](#).  
Comments? We would like to hear from you. E-mail us at [customercare@copyright.com](mailto:customercare@copyright.com)

## Appendix A (Continued)

The copyright notices for the use of material in Chapter 5 are below.

10/12/2017 Rightslink® by Copyright Clearance Center





[Account Info](#) [Help](#) 



**Title:** Cyclic feature suppression for physical layer security

**Author:** Z. Esat Ankaralı, Hüseyin Arslan

**Publication:** Physical Communication

**Publisher:** Elsevier

**Date:** Available online 22 September 2016

Copyright © 1969, Elsevier

Logged in as:  
ZEKERIYYA ANKARALI

Account #:  
3001063876

[LOGOUT](#)

### Order Completed

Thank you for your order.

This Agreement between ZEKERIYYA E ANKARALI ("You") and Elsevier ("Elsevier") consists of your order details and the terms and conditions provided by Elsevier and Copyright Clearance Center.

License number	Reference confirmation email for license number
License date	Oct, 12 2017
Licensed Content Publisher	Elsevier
Licensed Content Publication	Physical Communication
Licensed Content Title	Cyclic feature suppression for physical layer security
Licensed Content Author	Z. Esat Ankaralı, Hüseyin Arslan
Licensed Content Date	Available online 22 September 2016
Licensed Content Volume	n/a
Licensed Content Issue	n/a
Licensed Content Pages	1
Type of Use	reuse in a thesis/dissertation
Portion	full article
Format	electronic
Are you the author of this Elsevier article?	Yes
Will you be translating?	No
Title of your thesis/dissertation	Physical Layer Algorithms for Reliability and Spectral Efficiency in Wireless Communications
Expected completion date	Nov 2017
Estimated size (number of pages)	150
Requestor Location	ZEKERIYYA E ANKARALI 4202 E. Fowler ave ENB 118  TAMPA, FL 33620 United States Attn: ZEKERIYYA E ANKARALI
Publisher Tax ID	98-0397604
Billing Type	Invoice
Billing address	ZEKERIYYA E ANKARALI 4202 E. Fowler ave ENB 118  TAMPA, FL 33620 United States Attn: ZEKERIYYA E ANKARALI
Total	0.00 USD

<https://s100.copyright.com/AppDispatchServlet>

1/2

## Appendix A (Continued)

11/13/2017

Rightslink® by Copyright Clearance Center



RightsLink®

Home

Account Info

Help



**Title:** Cyclic Feature Concealing CP Selection for Physical Layer Security

**Conference Proceedings:** Military Communications Conference (MILCOM), 2014 IEEE

**Author:** Z. Esat Ankaral

**Publisher:** IEEE

**Date:** Oct. 2014

Copyright © 2014, IEEE

Logged in as:  
ZEKERIYYA ANKARALI  
Account #:  
3001063876

LOGOUT

### Thesis / Dissertation Reuse

**The IEEE does not require individuals working on a thesis to obtain a formal reuse license, however, you may print out this statement to be used as a permission grant:**

*Requirements to be followed when using any portion (e.g., figure, graph, table, or textual material) of an IEEE copyrighted paper in a thesis:*

- 1) In the case of textual material (e.g., using short quotes or referring to the work within these papers) users must give full credit to the original source (author, paper, publication) followed by the IEEE copyright line © 2011 IEEE.
- 2) In the case of illustrations or tabular material, we require that the copyright line © [Year of original publication] IEEE appear prominently with each reprinted figure and/or table.
- 3) If a substantial portion of the original paper is to be used, and if you are not the senior author, also obtain the senior author's approval.

*Requirements to be followed when using an entire IEEE copyrighted paper in a thesis:*

- 1) The following IEEE copyright/ credit notice should be placed prominently in the references: © [year of original publication] IEEE. Reprinted, with permission, from [author names, paper title, IEEE publication title, and month/year of publication]
- 2) Only the accepted version of an IEEE copyrighted paper can be used when posting the paper or your thesis on-line.
- 3) In placing the thesis on the author's university website, please display the following message in a prominent place on the website: In reference to IEEE copyrighted material which is used with permission in this thesis, the IEEE does not endorse any of [university/educational entity's name goes here]'s products or services. Internal or personal use of this material is permitted. If interested in reprinting/republishing IEEE copyrighted material for advertising or promotional purposes or for creating new collective works for resale or redistribution, please go to [http://www.ieee.org/publications\\_standards/publications/rights/rights\\_link.html](http://www.ieee.org/publications_standards/publications/rights/rights_link.html) to learn how to obtain a License from RightsLink.

If applicable, University Microfilms and/or ProQuest Library, or the Archives of Canada may supply single copies of the dissertation.

BACK

CLOSE WINDOW

Copyright © 2017 [Copyright Clearance Center, Inc.](#) All Rights Reserved. [Privacy statement](#). [Terms and Conditions](#).  
Comments? We would like to hear from you. E-mail us at [customer@copyright.com](mailto:customer@copyright.com)

<https://s100.copyright.com/AppDispatchServlet#formTop>




1/1




## Appendix A (Continued)

The copyright notice for the use of material in Chapter 6 is below.

9/11/2017 Rightslink® by Copyright Clearance Center

  [Home](#) [Account Info](#) [Help](#) 

 **IEEE**  
Requesting permission to reuse content from an IEEE publication

**Title:** Physical layer security for wireless implantable medical devices

**Conference Proceedings:** Computer Aided Modelling and Design of Communication Links and Networks (CAMAD), 2015 IEEE 20th International Workshop on

**Author:** Z. Esat Ankarali

**Publisher:** IEEE

**Date:** Sept. 2015

Copyright © 2015, IEEE

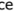
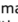
Logged in as:  
ZEKERIYYA ANKARALI  
Account #:  
3001063876

[LOGOUT](#)

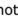
### Thesis / Dissertation Reuse

**The IEEE does not require individuals working on a thesis to obtain a formal reuse license, however, you may print out this statement to be used as a permission grant:**

*Requirements to be followed when using any portion (e.g., figure, graph, table, or textual material) of an IEEE copyrighted paper in a thesis:*

- 1) In the case of textual material (e.g., using short quotes or referring to the work within these papers) users must give full credit to the original source (author, paper, publication) followed by the IEEE copyright line  2011 IEEE.
- 2) In the case of illustrations or tabular material, we require that the copyright line  [Year of original publication] IEEE appear prominently with each reprinted figure and/or table.
- 3) If a substantial portion of the original paper is to be used, and if you are not the senior author, also obtain the senior author's approval.

*Requirements to be followed when using an entire IEEE copyrighted paper in a thesis:*

- 1) The following IEEE copyright/ credit notice should be placed prominently in the references:  [year of original publication] IEEE. Reprinted, with permission, from [author names, paper title, IEEE publication title, and month/year of publication]
- 2) Only the accepted version of an IEEE copyrighted paper can be used when posting the paper or your thesis on-line.
- 3) In placing the thesis on the author's university website, please display the following message in a prominent place on the website: In reference to IEEE copyrighted material which is used with permission in this thesis, the IEEE does not endorse any of [university/educational entity's name goes here]'s products or services. Internal or personal use of this material is permitted. If interested in reprinting/republishing IEEE copyrighted material for advertising or promotional purposes or for creating new collective works for resale or redistribution, please go to [http://www.ieee.org/publications\\_standards/publications/rights/rights\\_link.html](http://www.ieee.org/publications_standards/publications/rights/rights_link.html) to learn how to obtain a License from RightsLink.

If applicable, University Microfilms and/or ProQuest Library, or the Archives of Canada may supply single copies of the dissertation.

[BACK](#)

[CLOSE WINDOW](#)

Copyright © 2017 [Copyright Clearance Center, Inc.](#) All Rights Reserved. [Privacy statement](#). [Terms and Conditions](#).  
Comments? We would like to hear from you. E-mail us at [customer-care@copyright.com](mailto:customer-care@copyright.com)

## Appendix B: List of Acronyms

3GPP	Third generation partnership project
AD	Adversary
AF	Ambiguity function
AMC	Adaptive modulation and coding
AS	Alignment Signal
AWGN	Additive white Gaussian noise
BER	Bit-error rate
BS	Base station
CAF	Cyclic autocorrelation function
CCDF	Complementary cumulative distribution function
CCI	Canceling carrier insertion
CFO	Carrier frequency offset
CIR	Channel impulse response
CP	Cyclic Prefix
CPA	CP Alignment
CSI	Channel state information
DL	Downlink
DoF	Degrees-of-freedom
DSSS	Direct sequence spread spectrum
eMBB	Enhanced mobile broadband
FBMC	Filter bank multicarrier
FFT	Fast Fourier transform
FH	Frequency hopping
FMT	Filtered multitone
GF	Gaussian filter

## Appendix B (Continued)

ICI	Inter carrier interference
IFFT	Inverse fast Fourier transform
IMD	Implantable medical device
INI	Inter numerology interference
IoT	Internet of things
ISI	Inter symbol interference
JTFA	Joint time/frequency alignment
LTE	Long Term Evolution
MIMO	Multiple-input multiple-output
ML	Maximum likelihood
mmWave	Millimeter wave
mMTC	Massive machine type communications
MSE	Mean square error
NF	Noise floor
NR	New Radio
NSF	National science foundation
OFDMA	Orthogonal frequency-division multiple access
OFDM	Orthogonal frequency-division multiplexing
OOBE	Out-of-band emission
PA	Power amplifier
PAPR	Peak-to-average power ratio
PDP	Power delay profile
PHY	Physical Layer
PTS	Partial transmit sequence
QAM	Quadrature amplitude modulation

## Appendix B (Continued)

GFDM	Generalized frequency division multiplexing
ICD	Implantable cardiac defibrillator
RAT	Radio access technology
RAN	Radio access network
RB	Resource block
RC	Raised cosine
RRC	Root raised cosine
RSS	Received signal strength
s-CPA	Static CP alignment
SC-FDE	Single carrier-frequency domain equalization
SC-FDMA	Single carrier-frequency division multiple accessing
SIR	Signal-to-interference ratio
SISO	Single-input single-output
SLM	Selective mapping
SNR	Signal-to-noise ratio
TDD	Time division duplexing
TUBITAK	Scientific and technological research council of Turkey
UE	User equipment
UFMC	Universal filtered multi tone
UL	Uplink
URLLC	Ultra reliable and low latency communications
UWB	Ultra wide band
WED	Wireless external device
WBAN	Wireless body area network

## **ABOUT THE AUTHOR**

Zekeriyya Esat Ankaralı was born in Konya, Turkey. He received his B.S. degree from the department of Control Engineering from Istanbul Technical University in Istanbul, Turkey in 2011 and M.Sc. degree from University of South Florida in Tampa, Florida in 2013. He was with Texas A&M University at Qatar during the summer season in 2013 and 2014.

He has been working towards his Ph.D. degree as a Graduate Research Assistant in the department of Electrical Engineering, University of South Florida in Tampa, Florida since 2013. His research interests are waveform design, wireless body area networks, and physical layer security.